Joint Industry Project for Objective Tropical Cyclone Reanalysis: Final Report
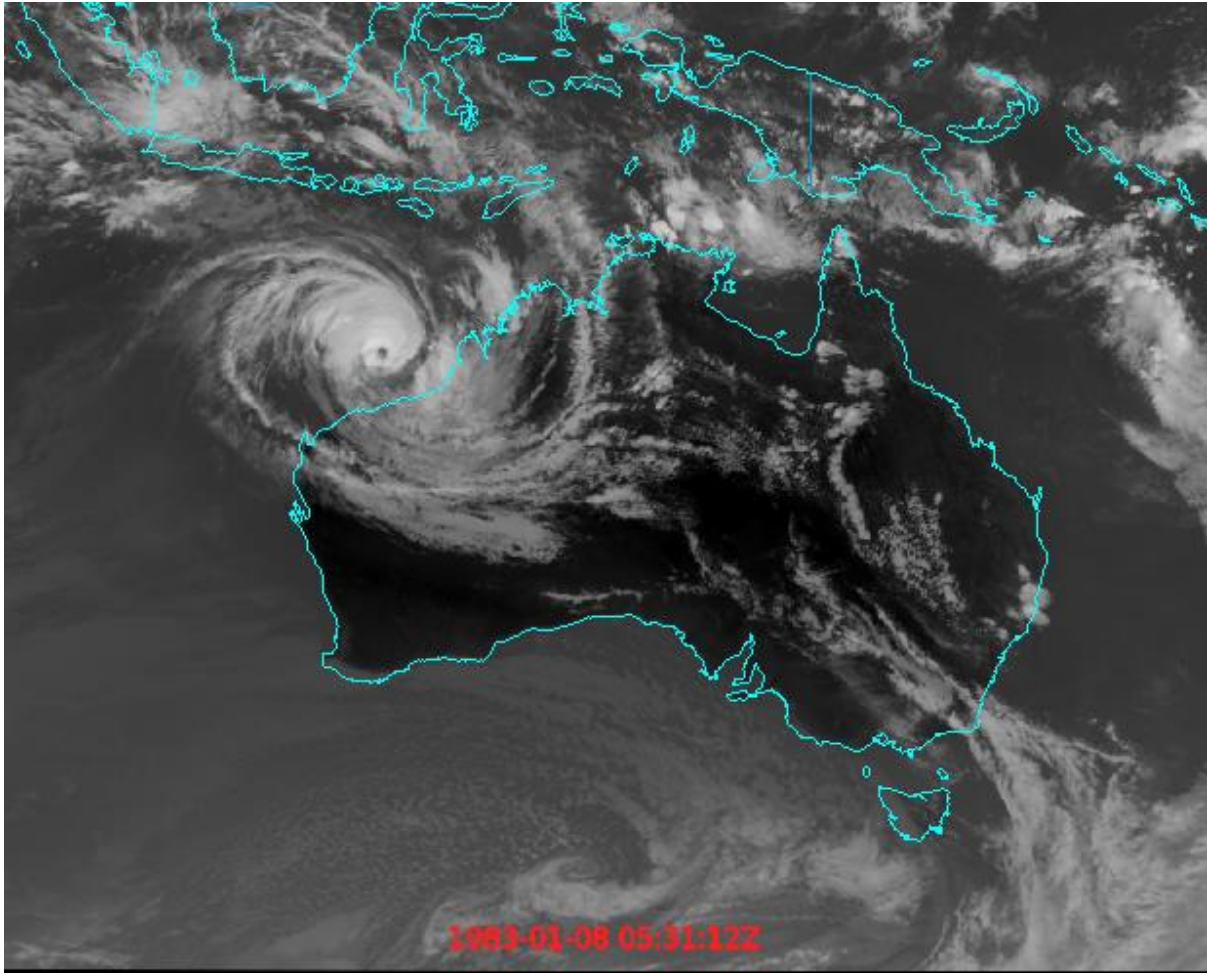

Image: Renavigated infrared image showing Tropical Cyclone Jane off the northwest coast, 0531 UTC 8 January 1983.

Bureau of Meteorology

7 September 2018

Revision History

Date	Version	Description/Changes	Author
25/07/2018	V0.4	Initial draft	Joe Courtney joe.courtney@bom.gov.au
24/08/2018	V0.9	Draft for formal review	Joe Courtney and Andrew Burton
28/08/2018	V1.0	Update to CP	Joe Courtney and Andrew Burton
7/09/2018	V1.3	Revision of summary and conclusions	Joe Courtney and Andrew Burton

Approvals

Date	Version	Approved by
24/08/2018	V0.9	A. Burton
7/09/2018	V1.3	A. Burton

Partners

The Commonwealth of Australia as represented by the Bureau of Meteorology

NERA (National Energy Resources Australia)

Shell Australia Pty Ltd

Woodside Energy Ltd

Chevron Australia Pty Ltd

Acronyms

ADT	Advanced Dvorak Technique
ASCAT	Advanced Scatterometer
BT	Best Track database (BoM)
BoM	Bureau of Meteorology
CI	Dvorak Current Intensity number. Directly relates to V_m.
CIMSS	Cooperative Institute for Meteorological Satellite Studies (University of Wisconsin)
CIRA	Cooperative Institute for Research in the Atmosphere (Colorado State University)
CKZ	Courtney-Knaff-Zehr wind pressure relationship
CP	Central Pressure
DAV	Deviation Angle Variance technique for wind radii dataset by UNSW
ERA-interim	ECMWF reanalysis dataset
FT	Final T. number in the Dvorak Technique
Knaff	Wind radii dataset, using IR; named after author J. Knaff (CIRA)
Lok	BoM wind radii dataset, using ERA, ACCESS-TC and BT; after author C. Lok.
MET	Model Expected T. number in the Dvorak Technique
MTCSWA	Multiplatform TC Surface Wind Analysis (from CIRA)
NATL	North Atlantic basin
NE, SE, SW, NW	Northeast, southeast, southwest and northwest (quadrants)
MAE	Mean Average Error
OTCR-JIP	Objective Tropical Cyclone Reanalysis – Joint Industry Project
P_e	Environmental pressure
PMW	Passive MicroWave
POCI	Pressure of outer closed isobar
QC	Quality Control
QSCAT	Quick Scatterometer
R34, R48, R64	Radius of 34 kn (gales); Radius of 48 kn (storm-force); Radius of 64 kn (hurricane-force)
ROCI	Radius of Outer Closed Isobar
RMW	Radius of Maximum Winds
RMSE	Root Mean Square Error
TCWC	Tropical Cyclone Warning Centre
UNSW	University of New South Wales
V_m	Maximum sustained (10-minute average) wind
WPR	Wind Pressure Relationship

Contents

Executive Summary

Purpose

The Objective Tropical Cyclone Reanalysis - Joint Industry Project (hereafter "the Project") aims to improve the quality of historical tropical cyclone (TC) data to enhance understanding of the risk profile for new and existing offshore infrastructure.

Objectives

The initial objectives of the Project were to produce a TC database for the Australian region (southern hemisphere between longitudes 90 and 160°E) covering the period from 1981 onwards, that has the following attributes:

1. provides a complete record of position, intensity and wind structure (eye size, radius to maximum winds, radius to gales, storm and hurricane force winds in quadrants);
2. has improved homogeneity compared to the existing Australian TC Database (BT);
3. is fit-for-purpose for use in the assessment of historical TC risk in the Australian region; and
4. demonstrates an objective TC reanalysis methodology that can be applied globally.

Outcomes

The Project had partial success with achieving the first two objectives. A new record of TC intensity (as measured by maximum wind (V_m) and central pressure (CP)) was created for the period post-January 1989. This new intensity dataset has improved homogeneity compared to the existing best track (BT) record (Objective 2). However, the project was unable to provide a complete objective record for wind structure parameters for the same period (Objective 1). The project was also unable to produce a reliable TC database for periods before January 1989, due to a high proportion of missing or poorly navigated imagery in the early satellite record.

The resulting dataset is suitable for some risk analyses (Objective 3), but the absence of a reliable extended dataset for wind structure parameters will limit its application without the use of alternative sources of data for wind structure parameters.

The Project has successfully demonstrated a methodology that can be applied globally (Objective 4). The methodology used, and lessons learnt in the project will be shared with the global community via the publication of a scientific paper.

Two other significant benefits have arisen from the Project. Firstly, the creation of a quality controlled satellite image dataset will make it easier to engage in future work with objective algorithms in the Australian region.

Secondly, close examination of the BT record over the course of the Project has:

- facilitated a better understanding of the strengths and weaknesses of the BT record,
- documented (for the first time) periods of reliable record for specific parameters, and
- generated ideas for future work to improve the BT record.

The methodology used in the Project is transferable to other TC affected regions and could be scaled up to produce a global objective analysis. It is hoped that the publication of the scientific paper will encourage others to engage in similar projects in other parts of the globe, thus advancing the science of objective analysis of TCs.

Summary of results

The highest quality dataset is the BT for the limited period from July 2003 to December 2016 (hereafter abbreviated to 2003–2016) for both intensity and structure. Although there remains further work that can be done to improve this period of the BT record, consideration of the factors affecting the BT, and the available independent validation, suggests that this is the most accurate TC record available for the region. Homogeneity across this period is generally good, though for central pressure it improves from 2007 onwards and further work can be done to validate some of the outlying gale radius (R34) estimates.

In general, the quality of the objective techniques for both intensity and structure are of a lower quality than the BT 2003–2016 estimates.

The objective estimates for intensity correspond well with the BT 2003–2016, when the algorithm can use passive microwave data (PMW) as an input. For the period prior to 2003 when PMW data is unavailable, the intensity algorithm has a low bias. The causes of this low bias in the estimates made without PMW data (hereafter "non-PMW" estimates) are known. Systematic corrections were made to the non-PMW objective estimates to produce an extended (1989–2016) homogeneous dataset of maximum wind (V_m) that has sufficient accuracy to be considered for use where a larger homogeneous sample size is valued over a shorter more accurate period of record. An associated record of central pressure (CP) using the Courtney-Knaff-Zehr (CKZ) wind pressure relationship was created.

Disappointingly, the objective algorithms for estimating TC size (as measured by the radius of gales (R34), radius of 48 kn (R48) and radius of 64 kn winds (R64)) were found to lack sufficient skill to enable extension of the reliable period of record.

As noted above, the quality of the objective techniques prior to 1989 is limited by the proportion of missing or poorly navigated satellite imagery in the 1981–1988 period.

Recommendations regarding the best data source for each parameter for different periods of the record are summarised in Table 18.

Impact and value

With the support of the project partners, the Bureau of Meteorology has decided to make the project deliverables freely available in order to maximise the impact and value of this work to the oil and gas sector and the broader community. Ultimately the impact and value of the project will be measured by the degree to which it:

- advances the science of objective TC analysis, both directly and by informing future studies,
- is used by the oil and gas sector in the generation of synthetic tropical tracks for criteria estimation,
- encourages further collaboration across the oil and gas sector.

1. Introduction

Accurate information on return period of extreme wind and waves is an important input into infrastructure design in tropical cyclone (TC) affected regions. This requires reliable and consistent TC position, intensity and structure data over a sufficient length of record. The Australian Tropical Cyclone Best Track database (BT) has records back to 1909 of varying quality. The inherently subjective nature of determining these characteristics has meant it is difficult to quantify the consistency of the record. The current process for recording TC characteristics is regarded as the highest quality using advanced satellite capabilities, comprehensive parameters and more standardised methodology.

Objective techniques to estimate intensity and structure have been developed that produce systematic and reproducible results. TC intensity has historically relied upon the application of the Dvorak Technique (Dvorak, 1984, Dvorak 1995. Velden et al. 2006), either subjectively by the TC analyst or via the Advanced Dvorak Technique (ADT). Objective techniques to estimate wind radii include the Deviation Angle Variation (DAV), an IR technique described in Knaff et al. (2016) (hereafter referred to as 'Knaff') and a combined model output developed at the Bureau of Meteorology (hereafter referred to as 'Lok'). These offer the opportunity to generate estimates over the historical satellite record that remove the subjectivity associated with the BT. These outputs can be compared to BT estimates to assess for reliability and homogeneity suitable for use in infrastructure design applications.

Until now an obstacle in running objective satellite algorithms, has been the lack of a high-quality satellite archive. Significant effort has been required to produce a quality controlled historical satellite imagery dataset that minimises navigation and calibration errors.

The following project deliverables were specified in the research agreement:
- Database of tropical cyclones in the Australian region (southern hemisphere between longitudes 90 and 160°E), covering the period from June 1981 to July 2016, that includes objective estimates of intensity (maximum 10-minute wind and minimum pressure) and wind structure (Eye size, Radius to Maximum Winds, and radius to 64, 48 and 34 knot 10-minute winds in quadrants).
- Report outlining the characteristics of the new tropical cyclone dataset in comparison to the official Bureau of Meteorology Australian Tropical Cyclone Database.
- Scientific paper to be submitted to a reputable peer-reviewed journal detailing the project methodology and results.

This report provides:
- details of an improved satellite archive since 1981;
- descriptions of the existing TC best track (BT) database;
- the process to create datasets of intensity and wind radii; and
- analyses of the quality of the resulting datasets (project deliverables).

2. Satellite data availability and quality control

The initial part of the project aimed to provide a consistently formatted, long, high quality time series of infrared (1981–2015) and visible (1989–2015) observations from sensors on board

geostationary satellites of the TC project target area from the Bureau of Meteorology's digital archive, having corrected these observations for navigational and, where practicable, calibration issues.

For early missions (e.g. pre-1999) the primary issue is the availability of digital data sets (esp. pre-1987). In addition, all missions suffer from navigation issues (early missions having greater uncertainty) and calibration issues (early missions having poorer records of calibration changes and instrument events).

Detailed descriptions of the satellites and the process to improve the data set are provided in Appendix 2. Table 1 shows the frequency of images available per day by satellite mission while Fig. 1 shows the frequency of missing images used for both the ADT and DAV techniques. These show that the percentages of 'good' images was significantly lower in the 1981–1988 period than in the subsequent era. Indeed, the percentage was just 67 per cent in 1984. For example, *Quenton* (198384_03U) had only one image for analysis between 0827 UTC 28 November and landfall some 36 h later. During this stage *Quenton* developed an eye that was not detected by ADT. For this case the adjustment of ADT V_m (not shown) follows BT V_m.

Any objective technique using the 1981–1988 era of satellite imagery will be compromised because of this issue. The 'rules' to subjectively adjust ADT using interpolation will bias towards BT, however the adjustments only apply at stronger intensities. Further details on satellite quality control and availability are comprehensively discussed in Appendix 2.

Table 1. Satellite imagery summary 1981–2016.

| Satellite	Period	Image availability per day (dates given in year/Julian day)
GMS-1 and GMS-2	1981_1984	8
GMS-3	1984–1989	8 until 1987/058; 13 from 1987/059 to 1989/004. 28 after 1989/005
GMS-4	1989–1995	28
GMS-5	1995–2003	28 til 2001/184; 16 after 2001/18
MTSAT1	2005–2015	24-32
MTSAT2	2013–2015	32
HIMAWARI	2015–	48 for analysis (though available every 10 minutes.)
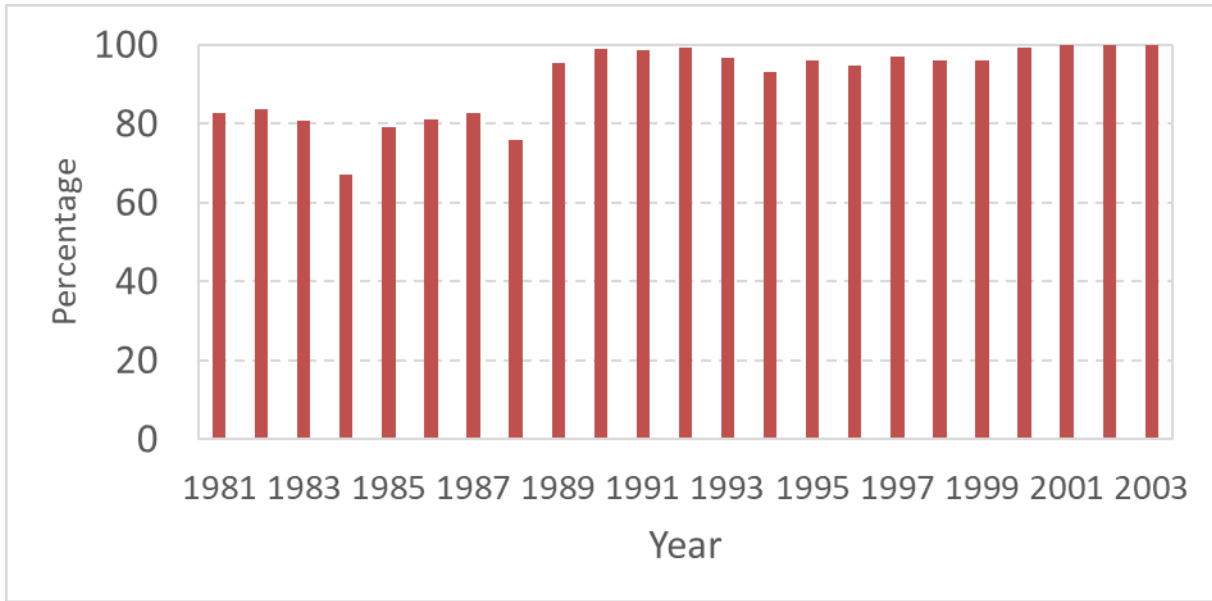
Figure 1. Percentage of 'good images' in the GMS era 1981-2003. The number of available images increased from 13 to 28 per day on 5 January 1989.

3. The Australian Tropical Cyclone Best Track archive

Operational estimates of position, intensity and structure are made under time constraints and without being able to assess the entire TC life cycle. Following each TC event, a reanalysis is performed to determine the most appropriate scientific estimates. These are available at standard times at least every six hours and sometimes at higher resolution typically when close to land.

The accuracy of the BT has been reviewed at various times (e.g. Holland, 1981, Lourensz 1977, Trewin 2008). Since 2005 there has been an ongoing effort to enhance the BT. The following improvements have been made: removed typographical errors and other internal inconsistencies, added extra fixes, merged, added and removed complete systems, corrected for the variations in applying WPRs and 1-minute to 10-minute maximum wind conversions, corrections arising from comparisons with JTWC and the 'Woodside' reanalysis dataset (Harper et. al. 2008), and reanalyses using microwave imagery and reviews of Dvorak estimates. Further changes have occurred during the course of this project with further amendments flagged as a result of this study. This study used the BT as extracted on 20 December 2017.

Further details on the BT are discussed in Appendix 3.

4. Advanced Dvorak Technique (ADT)

4.1 Background

The Advanced Dvorak Technique (ADT) utilizes infrared imagery to estimate TC intensity based upon principles similar to the Dvorak Technique (Velden et al 1988; Olander and Velden, 2007). The inherent subjective nature of the Dvorak technique means the success is dependent upon the skill of the analyst and the procedures being used at the time. ADT sought to alleviate many of the limitations found within the Dvorak Technique. The ADT utilizes an objective TC centre determination scheme and cloud pattern determination logic to remove the subjectivity aspect from the intensity estimation process. It also can be applied to all phases of the TC lifecycle; something that previous objective schemes could not do. Finally, the ADT makes use of statistical analysis results obtained from a sample of more than ten years of North Atlantic (NATL) TCs, along with a significant sample of West and East Pacific TCs, covering the entire spectrum of TC intensities to derive a regression-based intensity value estimate for various phases of the TC lifecycle.

Further information and real-time and archive ADT estimates are available at: Cooperative Institute for Meteorological Satellite Studies (CIMSS) TC ADT web page: http://tropic.ssec.wisc.edu/real-time/adt/adt.html

The technique has some known deficiencies.

1. Covered centre patterns: plateau effect. For the Dvorak embedded centre pattern, ADT applies a ceiling of 55 kn (CI of less than 4.0) until an eye emerges.

2. The technique can significantly underestimate the intensity if it does not resolve an eye. This is particularly the case for very small ('pinhole') eyes or if the centre positioning is offset from the eye.

3. In the early stages of development there is a high degree of variability in the convective patterns in IR imagery and the corresponding surface wind speeds. Hence, there is inherent difficulty in objectively analysing intensities of less than 35 kn.

4. ADT does not provide V_m estimates when the centre is over land.

In addition, missing images will affect ADT results. This is most significant for the 1980s when there were prolonged periods of missing images as discussed in Section 2.

To overcome the first two issues, PMW input is included in the technique which can improve the ADT output as shown in Fig. 2 for TC *Gwenda* (1999). However, unlike the geostationary satellites that take regular IR imagery, PMW imagery is only available from polar orbiting satellites providing occasional coverage on an irregular schedule.

The ADT technique was run on non-PMW and PMW modes and separated into two different eras, 1981–2003 and 2003–2016 (starting with TC *Epi* in June 2003 was the first TC in the latter era).
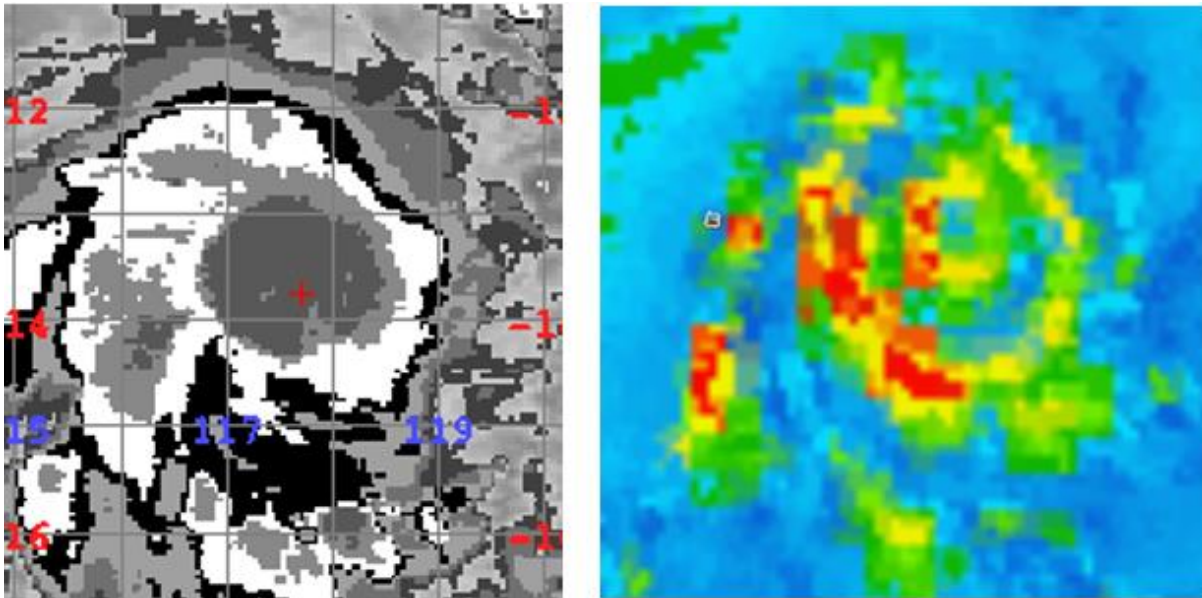
Figure 2 a. TC *Gwenda* (199899_13U) 5 April 1999, enhanced IR image at 18 UTC (left) and 85GHz SSMI (microwave) image at 1309UTC (right) indicating an eye.
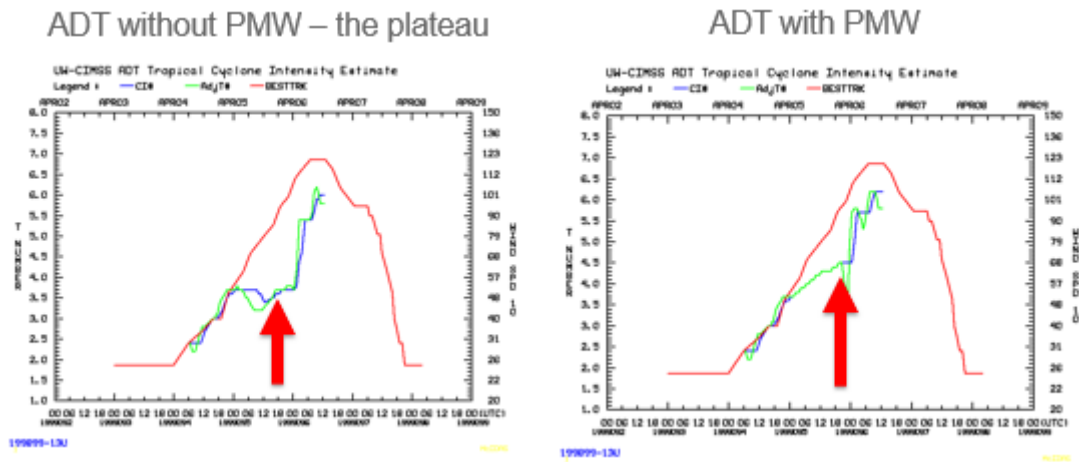
Figure 2 b. Intensity plot for TC *Gwenda* (1999), V_m ADT (blue line) against V_m BT (red line) showing the plateau effect without PMW (left) and the improvement with PMW (right). The BT is higher, the analyst having the benefit of seeing an eye later emerge on IR imagery.

4.2 ADT non-PMW Results

For non-PMW ADT there was a bias of 3.3 kn (V_m BT higher than V_m ADT) for 2003–2016 and 8.8 kn for 1981–2003, and a Mean Average Error (MAE) of 9.3 kn (2003–2016), 11.1 kn (1989–2003) and 11.5 kn (1981–1988). A summary of the statistics is included in Table 3. The scatterplots of BT and ADT non-PMW shown in Fig. 3 a (2003–2016) and Fig. 3 b (1981–2003) show the high bias (BT greater than ADT) being most pronounced when the BT is between 55-110 kn. Nevertheless, it is encouraging that ADT does match BT at the extreme end of the scale above 110 kn.
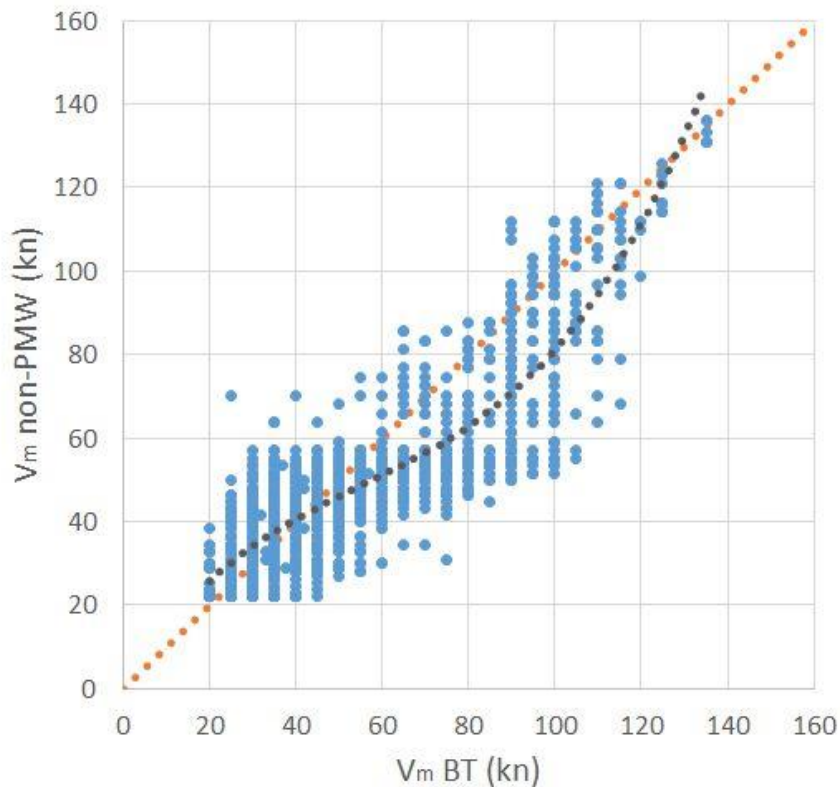
Figure 3 a. Scatterplot of V_m BT against V_m ADT non-PMW for 2003–2016. The correlation was 0.75.
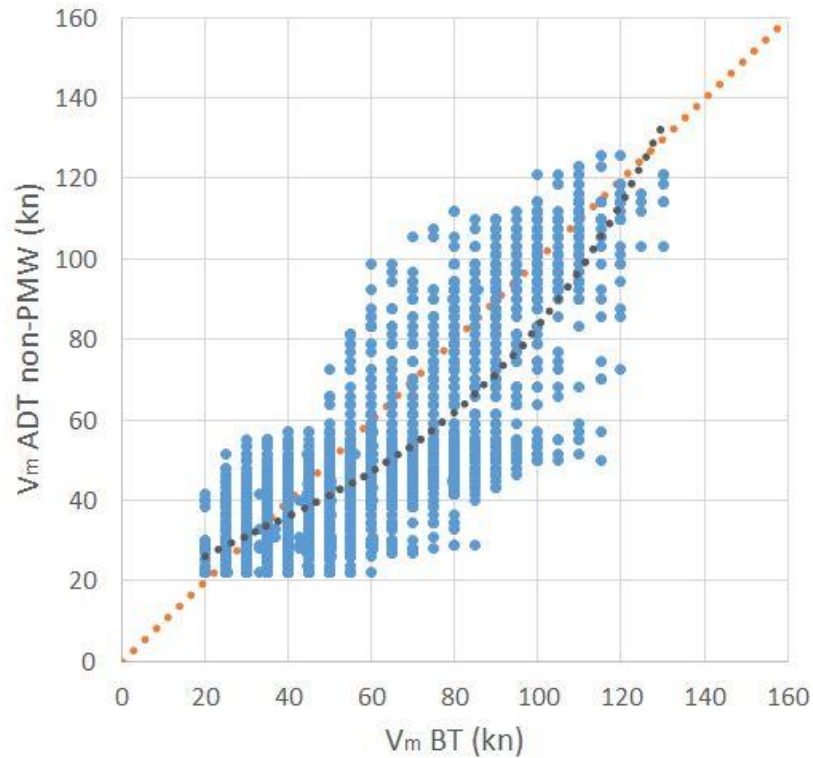
Figure 3 b. As in a. but for 1981–2003. The correlation was 0.69

4.3 ADT PMW

PMW ADT for the 2003–2016 period shows excellent agreement with the BT, the bias being just -0.2 (V_m BT only slightly lower than V_m ADT) and a MAE of 8.0 kn. This provides confidence in the PMW ADT technique. The bias is 5.1 for 1989-2003, with an of 9.8 kn (1989–2003). A summary of the statistics is included in Table 2. The scatterplot of BT and ADT PMW shown in Figs 4 a (2003–2016) and 4 b (1981–2003) indicates the high bias (BT greater than ADT) when BT is between 55-120 kn remains for the 1981–2003 period but is greatly reduced in the 2003–2016 period. The correlation is 0.8 for the ADT PMW 2003–2016 data.

Table 2. Statistics for ADT non-PMW and PMW

|	non-PMW			ADT PMW		
	1981–1988	1989–2003	2003–2016	1981–1989	1989–2003	2003–2016
Mean Bias (kn)	8.8	7.1	3.3	-	5.1	-0.2
Median Bias (kn)	7.0	5.0	0.9	-	3.5	-0.1
RMSE (kn)	15.4	15.1	12.8	-	13.2	10.5
MAE (kn)	11.5	11.1	9.3	-	9.8	8.0
No. samples	1363	4068	2316	-	4071	2309
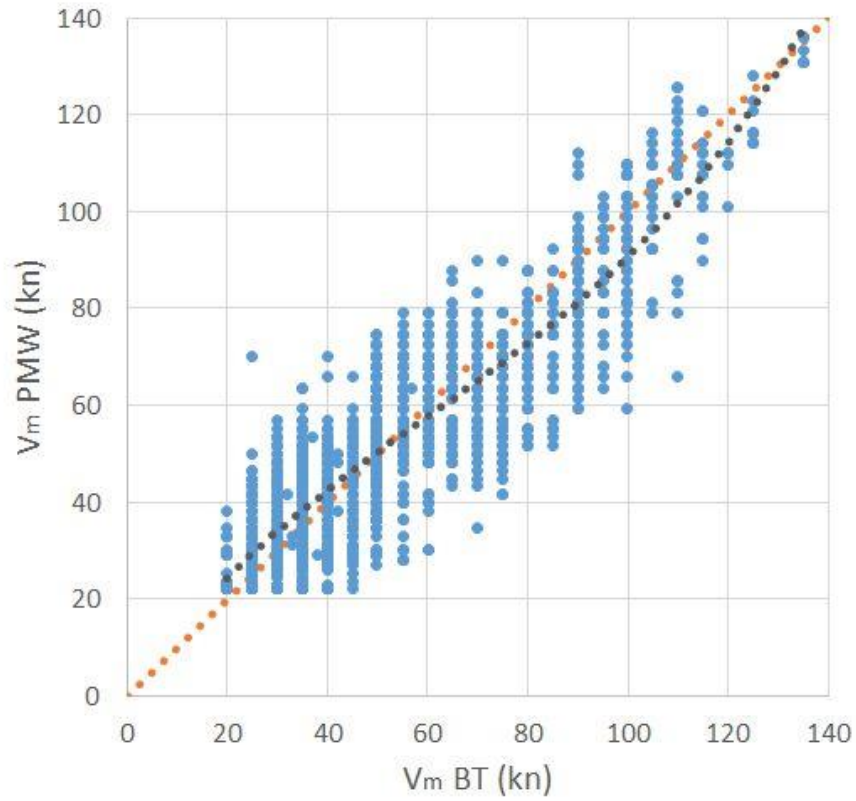
Fig 4 a. Scatterplot of V_m BT against V_m ADT PMW for 2003–2016. The correlation was 0.80.
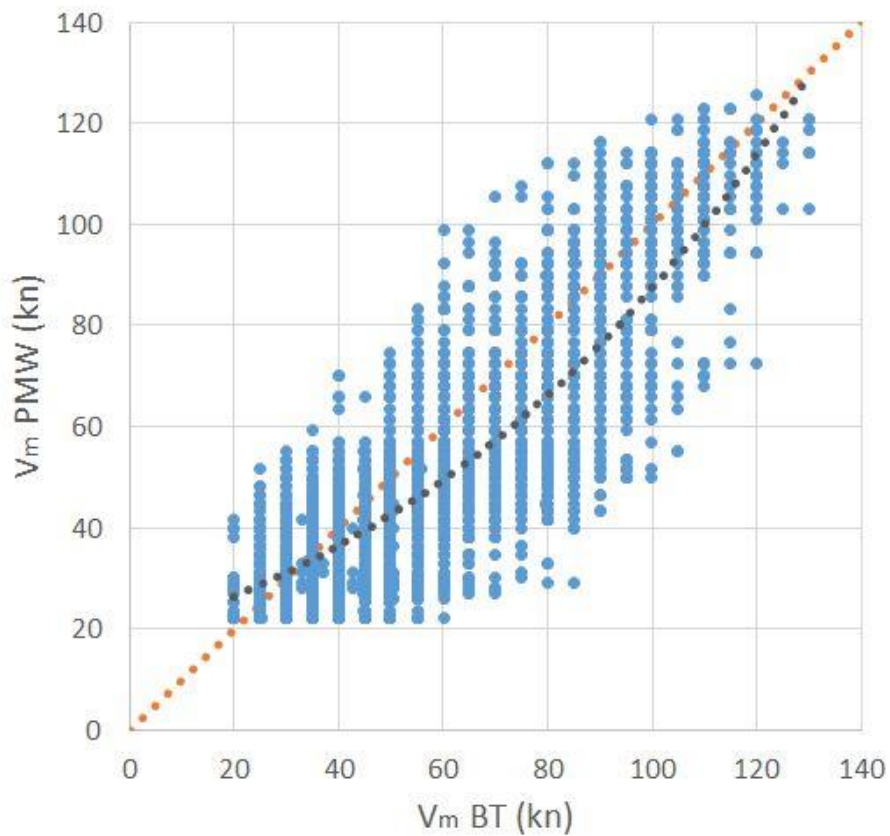

Figure 4 b. As in a. but for 1981–2003. The correlation was 0.72.

4.3.1 Analysis of significant differences BT ADT PMW 2003–2016

Despite the improvements in ADT with PMW there are cases where ADT may still underestimate the intensity. Between 2003 and 2016 there were 12 events where V_m ADT PMW was at least 20 kn less than the BT as listed in Table 3. For all but one of these cases the BT V_m was in the range of 75-85 kn (CI=4.5-5.0 range) when typically, the Dvorak pattern is Embedded Centre. The greatest difference was 40.8 kn during TC *Kara* (2007*)*. While there are several cases where the answer is ambiguous there are compelling grounds to accept or at least strongly bias towards the BT intensity. For example, TCs *Clare, Glenda, Heidi* and *Lua*, are strongly influenced by observations, while others such *as Jana, Nicholas, Kate* and *Nathan* have strong microwave signatures. For *Kara* the BT intensity of 100 kn was based upon a pin-hole eye being observed on Vis imagery that followed a period of rapid intensification. An eye was only resolved on ADT for three images (raw T no.=5.8). The true intensity is difficult to confirm but it is known that ADT will struggle in these cases and BT is likely to be superior. In many of these cases ADT is not influenced by PMW. For a few cases such as *Fay* and *Wati*, the answer is less obvious, although in both cases a lack of PMW input may have hindered ADT, while the BT may be at the upper end of the likely range because of the use of embedded centre pattern and possibly weakening rates.

There weren't any cases when the ADT V_m was higher than BT by more than 20 kn. The greatest was +15 kn during *Alenga* when V_m ADT was at 90 kn.

Table 3. Differences of at least 20 kn between the V_m BT and V_m ADT PMW 2003–2016.

TC	TC ID	Max diff. V_m BT-ADT PMW (kn)	V_m BT (kn)	Comment
Jana	200304_01	21.4	85	BT influenced by microwave eye on TMI.
Fay	200304_08	33.4	75	Between peaks (eye), ADT dropped significantly without PMW, possible BT a bit high.
Clare	200506_05	25.2	75	Observations support BT.
Glenda	200506_14	20.8	80	Observations support BT.
Wati	200506_17	33.4	85	No PMW for ADT then; possible BT a little high.
Kara	200607_13	40.8	100	Pinhole eye after rapid intensification, not resolved on ADT. True intensity difficult but BT likely ok.
Nicholas	200708_11	24.8	80	ADT weakening between peaks. Microwave suggests BT more likely.
Heidi	201112_07	28.6	75	Observations support BT
Lua	201112_16	29.8	85	Observations support BT
Narelle	201213_05	21.4	85	During developing stage towards an eye pattern (100 kn). ADT slower to intensify until an eye emerges.
Kate	201415_04	31.6	85	Post ADT-eye, periodic eye for BT and no microwave influence of ADT so ADT likely too low
Nathan	201415_17	25.2	75	BT biased to microwave eye, no PMW for ADT.

4.3.2 1981–2003 differences

The bias is considerably higher for the period 1981-2003 than for the 2003–2016 period for several reasons:

i.   The microwave influence was less because there were less sensors in that era, see Fig. 5. Microwave sensors improved during this period in terms of quality. The period from about 2003 onwards has the combination of the best sensors and frequent image sampling. In the 1980s there were essentially no improvement in the dataset because of PMW and this only improved gradually during the 1990s.

ii. The BT used the Dvorak 12-h weakening rule instead of the post 2003 guideline to use a 6-h rule which likely maintained the intensity slightly higher during the weakening phase of each TC.

iii. In the 1980s and 90s analysts were more likely to use the embedded centre pattern to arrive at an intensity of 80 kn. Since the early 2000s Dvorak analysts use more discretion and often discount DT estimates using the embedded centre pattern especially for the early stages of development.
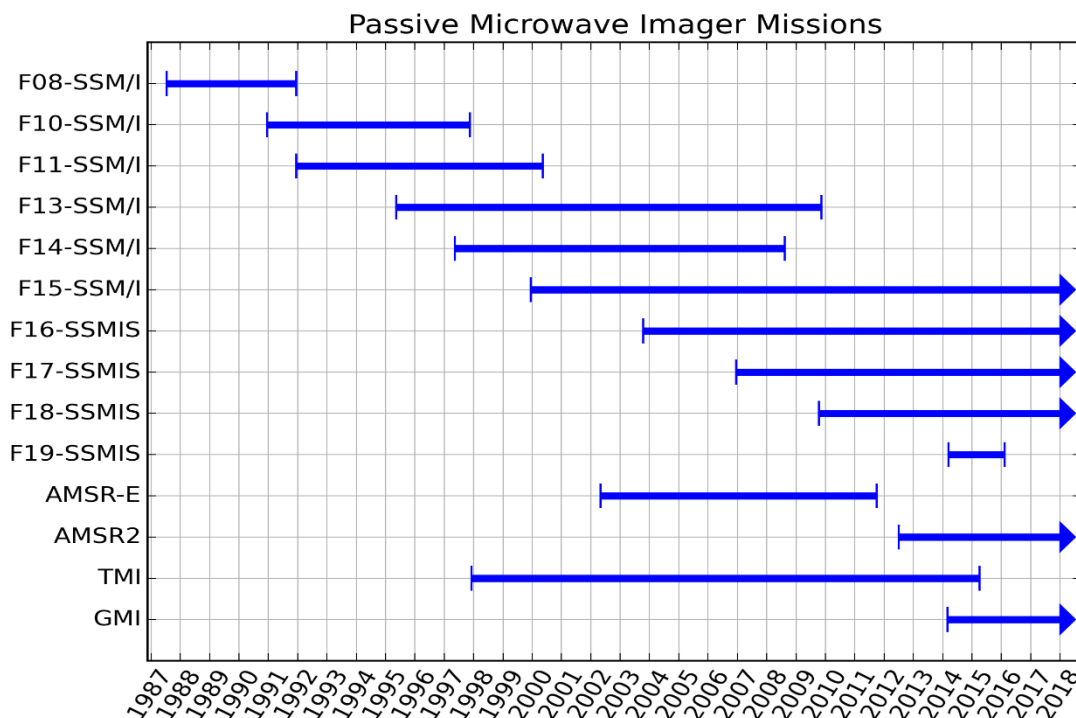
Figure 5. Timeline of PMW imager missions between 1987 and 2018. Image courtesy CIMSS.

4.4 Adjustments to the ADT non-PMW V_m dataset

To enable a consistent dataset from 1981 to 2016, systematic corrections were applied to reduce the bias of the non-PMW ADT V_m (compared to BT V_m) for the 2003–2016 period to zero. The same corrections were applied the earlier era. Theoretically any resultant bias (adjusted ADT V_m compared to BT) in the 1981–2003 period would indicate a combination of potential bias in the BT and the influence of changes in satellite imagery availability. The adjustment approach was to treat the known deficiencies of the non-PMW ADT data and in effect mimic the effect of PMW on ADT.

As discussed in section 4.1 the major deficiency of the non-PMW ADT dataset is the 'plateau effect'. The non-PMW ADT dataset was adjusted to overcome the 'plateau effect' and to address missing

data either because of missing images or for over land. For the plateau effect there were three separate categories investigated.

4.4.1   Missing eye peaks

There were many cases when the CI (BT) was at least 90 kn (CI=5.5) but at that time the CI (ADT) was less than 57 kn (CI=4.0). As all of these cases are when the eye is evident for BT (or observations available), but not on ADT, it is clear that ADT is underestimating the intensity. There was a total of 17 cases, 13 in the 1981–2003 period and four for 2003–2016 where this applied to the peak intensity. For these cases the V_m (ADT) is adjusted to be the same value as that from the BT from 55 kn onwards. An example is *Barry* in 1996 as shown in Fig. 6. The listing of events is provided in Table 4.
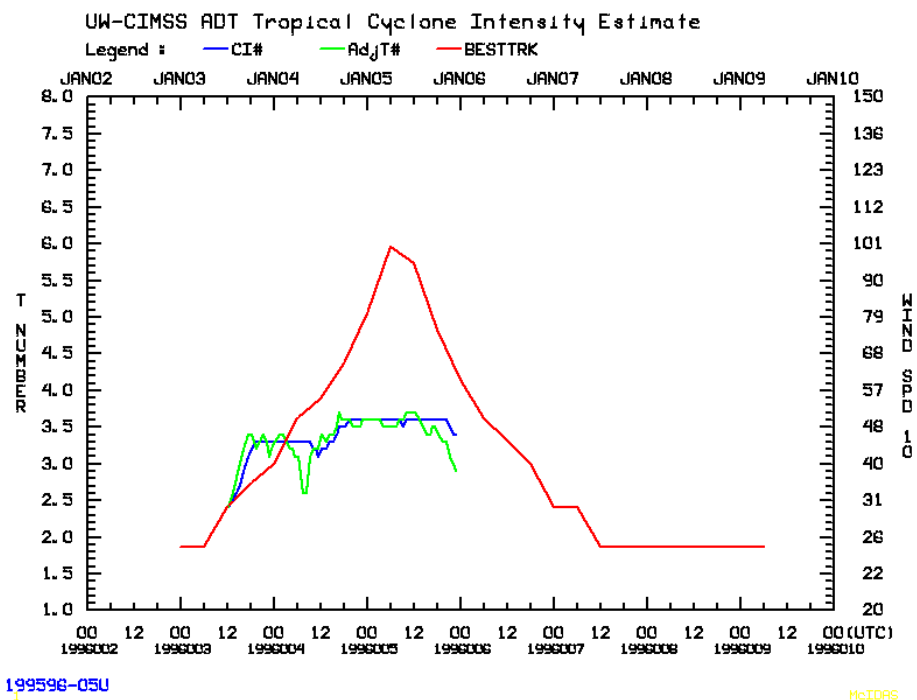
Figure 6. Intensity plot non PMW-ADT Vs BT for *Barry* 1996, showing the BT peak at 6.0 but the ADT did not get beyond the 3.5 plateau.

Table 4. Cases when BT V_m at least 90 kn (CI>=5.5) and ADT less than 57 kn (CI<4.0).

Name	ID	Date/Time (UTC)	Original ADT peak V_m (kn)	BT V_m (kn)	Fixes altered	Comments
Olga	198081_13U	06:00 10/04/1981	57	95	00Z 9/04/1981 - 06Z 13/04/1981	ADT missing many images at time of peak
Quenton	198384_03U	06:00 29/11/1983	30	90	12Z 28/11/2983 - 03Z 30/11/1983	Missing most images
Bobby	198384_14U	18:00 18/02/1984	75	95	00Z 18/02/1984 - 12Z 23/02/1984	Many missing images; ADT

						peak when weakening.
Billy-Lila	198586_14U	12:00 10/05/1986	55	90	03Z 8/05/1986- 00Z 13/05/1986	
Elsie	198687_05U	06:00 25/02/1987	55	100	03Z 23/02/1987 - 15Z 26/02/1987	Many missing images.
Ivor	198990_10U		57	90	00Z 18/03/1990 – 18Z 20/03/1990	
Jane	199192_10U	12:00 14/04/1992	66	110	18Z 09/04/1992 –06Z 17/04/1992	
Bobby	199495_02U	09:00 24/02/1995	53	105	03Z 22/02/1995 – 00Z27/02/1995	Reanalysis confirms.
Barry	199596_05U	06:00 05/01/1996	50	100	12Z 4/01/1996 –00Z 07/01/1996	
Kirsty	199596_12U	19:00 11/03/1996	75	100	07Z 10/03/1996 –13Z 12/03/1996	Reanalysis confirms. Pardoo 938 hPa.
Pancho	199697_09U	07:00 01/02/1997	52	95	10Z 29/01/1997 – 04Z 05/02/1997	2nd peak west of 90°E.
Elaine	199899_11U	22:00 17/03/1999	52	90	22Z 18/03/1999 -13Z 19/03/1999	
Dianne	200102_07U	18:00 08/04/2002	52	90	00Z 08/04/2002 – 18Z 10/04/2002	
Kara	200607_13U	06:00 26/03/2007	59	100	18Z 25/03/2007 - 06Z 27/03/2007	First of two peaks. Pinhole eye.
Bianca	101011_12U	00:00 28/01/2011	55	95	06Z 27/01/2011 -12Z 28/01/2011	ADT peak 77 kn later.
Rusty	201213_10U	00:00 27/02/2013	59	90	12Z 25/02/2012 – 06Z 28/02/2012	High confidence. PMW confirms.
Lam	201415_13U	12:00 19/02/2015	53	100	12Z 18/02/2015 – 00Z 20/02/2015	Landfalling severe TC.

4.4.2.   Eye cases with poor rates of intensification

In addition to missing eye peaks, there are cases where ADT resolves an eye, but has a low bias during the prior period of intensification. An example is Monty (2004) as shown in Fig. 7.

Adjustments were made to ADT during the developing phase when ADT was less than 57 kn (CI=4.0) but later ADT increases abruptly when an eye pattern is observed. There was a total of 69 cases, 47 between 1981 and 2003 and 22 between 2003 and 2016 as listed in Table 5. For these cases the ADT was adjusted using the BT intensities until such time as BT reached ADT.
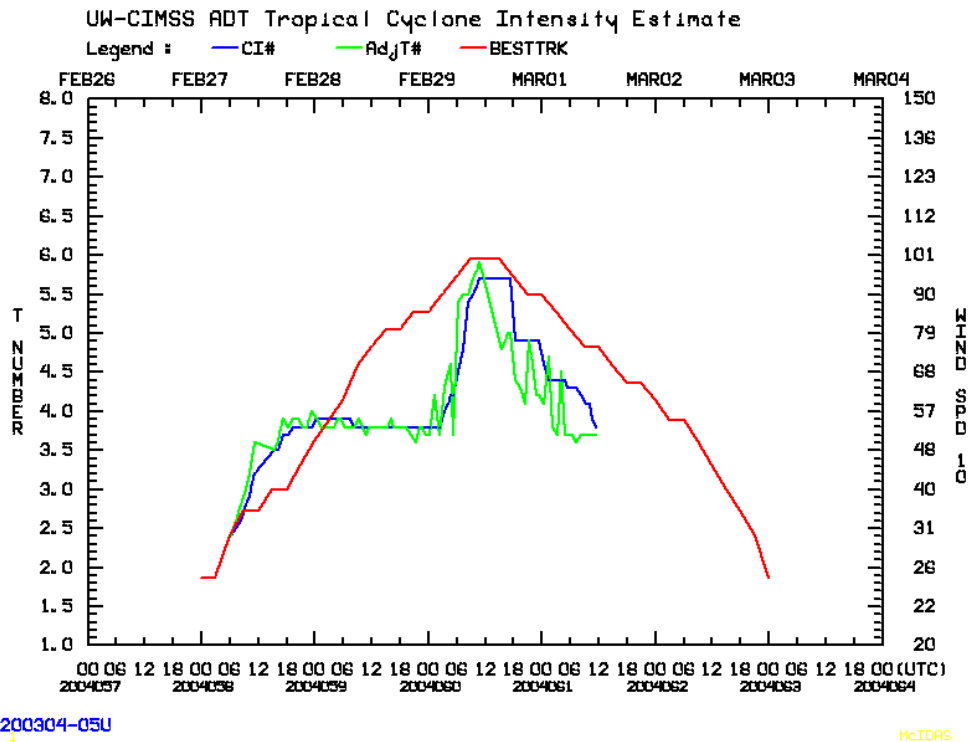
Figure 7. Non PMW-ADT Vs BT for *Monty* (2004) showing the ADT plateau during developing stage.

Table 5. Cases adjusted for plateau cases during developing stages when BT at least 75 kn (CI=4.8) and ADT < 57 kn (CI=4.0) and then subsequently ADT increased.

Name	ID	Fixes altered	Comments
Chris	198182_05U	06Z 08/01/1982 – 00Z 10/01/1982	ADT truncated at 90°E, estimates extended 24h.
Dominic	198182_15U	12Z 06/04/1982 – 06Z 8/04/1982	Many missing images including near peak.
Kathy	198384_21U	00Z 21/03/1984 – 23Z 23/03/1984 (not continuous)	Developing stage - missing images may be an influence. Weakening over land. Similar peak 120 kn.
Jacob	198485_09U	00Z 18/02/1985 – 00Z 22/02/1985	BT Peak comes before ADT peak.
Sandy	198485_14U	00Z 21/03/1985 – 00Z 22/03/1985; 12-18Z 22/03/1985	Missing images early on. Adjust for spurious single ADT between ADT peaks.
Victor	198586_11U	00-12Z 04/03/1986	Minor changes during development but many missing images requiring interpolation.
Namu	198586_15U	06-18Z 19/05/1986	Briefly during developing stage.

Gwenda	198788_03U	00Z 10/02/1988 – 00Z 12/02/1988	ADT affected by missing images.
Kirrily	198889_04U	18Z 07/02/1989 – 00Z 09/02/1989	Developing stage.
Ned	198889_08U	12Z 27/03/1989 – 06Z 28/03/1989	Developing stage.
Aivu	198889_09U	12-18Z 02/04/1989	Developing stage.
Orson	198889_10U	12Z 19/04/1989 – 00Z 20/04/1989	Developing stages and over land values.
Alex	198990_11U	12Z 16/03/1990 – 06Z 18/03/1990	Developing stage.
Joy	199091_02U	06Z 21/12/1990 – 00Z 23/12/1990	Developing stage.
Errol	199091_07U	06Z 25/03/1991 – 00Z 26/03/1991	Developing stage.
Marian	199091_08U	12Z 11/04/1991 - 06Z 13/04/1991	Developing stage.
Graham	199192_01U	18Z 02/12/1991 – 18Z 04/12/1991	Developing stage and inserting for missing ADT fixes.
Harriett	199192_05U	06Z 27/02/1992 – 12Z 01/03/1992	Developing stage and inserting for missing ADT fixes.
Ian	199192_06U	00Z 28/02/1992 – 00Z 29/02/1992	Developing stage.
Neville	199192_09U	18Z 07/04/1992 – 12Z 08/04/1992	Developing stage.
Oliver	199293_04U	00-12Z 06/02/1992	Briefly in developing stage.
Rewa	199394_02U	12Z 31/12/1993 – 06Z 02/01/1994; 00Z 14/01/1994 – 06Z 16/01/1994	Developing stages for both peaks and some missing fixes.
Theodore	199394_07U	00Z 24/02/1994 – 00Z 25/02/1994	Developing stage and some missing fixes.
Sharon	199394_08U	12Z 14/03/1994 – 12Z 15/03/1994	Developing stage.
Annette	199495_01U	12Z 15/12/1995 – 06Z 16/12/1995; 00Z 17/12/1994 – 00Z 18/12/1994; 09Z 18/12/1994- 06Z 20/12/1994.	Adjust during both developing stages and added final over land series.
Chloe	199495_05U	09Z 5/04/1995 – 12Z 06/04/1995	Developing stage.
Agnes	199495_06U	12Z 17/04/1995 – 18Z 18/04/1995	Developing stage.
Frank	199596_03U	19Z 08/12/1995 – 19Z 09/12/1995	Developing stage.
Jacob	199596_10U	13Z 02/02/1996 – 01Z 05/02/1996	Developing stage.
Olivia	199596_14U	22Z 07/04/1996 – 19Z 11/04/1996	Developing stage, peak and add over land values.

Melanie	199697_02U	22Z 02/11/1996 – 10Z 04/11/1996	Developing stage. Break in BT as it is west of 85E near peak intensity. No data included for 5-6 Nov.
Drena	199697_08U	06Z 04/01/1997 – 06Z 05/01/1997	Developing stage.
Pancho	199697_09U	19Z 20/01/1997 – 22Z 24/01/1997	Development to first peak
Rhonda	199697_13U	04Z 13/05/1997 – 07Z 14/05/1997	Developing stage to peak intensity.
Selwyn	199798_03U	22Z 27/12/1997	Briefly during developing stage.
Katrina	199798_04U	12Z 08/01/1998 – 18Z 09/01/1998; 18Z 12/01/1998 – 06Z 15/01/1998.	Developing stages of both peaks. Some uncertainty about the between stage near 160°E when BT only decreases to 65 kn and ADT weakens to 42 kn.
Tiffany	199798_05U	22Z 24/01/1998 – 04Z 27/01/1998	Developing stage.
Thelma	199899_03U	00-03Z 07/12/1998	Briefly in developing stage.
Vance	199899_10U	16Z 18/03/1999 – 19Z 20/03/1999; 06Z 22/03/1999-13Z 23/03/1999.	Developing stage. Use BT peak. Add over land values.
Frederic	199899_12U	07Z 28/03/1999 - 10Z 30/03/1999	Developing stage.
Gwenda	199899_13U	07Z 05/04/1999 – 22Z 07/04/1999.	Developing and weakening over land. Peak intensity average of BT and ADT.
Norman	199900_07U	16Z 01/03/2000 – 22Z 02/03/2000	Developing stage.
Paul	199900_11U	10Z 13/04/1996 – 10Z 15/04/1996	Developing stages.
Rosita	199900_12U	16Z 17/04/2000 – 13Z 19/04/2000; 19Z 19/04/2000 – 22Z 20/04/2000	Developing to ADT peak, then over land.
Chris	200102_04U	16Z 03/02/2002 – 16Z 05/02/2002;	Developing, then over land.
Fiona	200203_02U	00Z 06/02/2003 – -18Z 11/02/2003	Developing and peak. ADT peaked then weakened before BT peak even though several ADT rawT 5.3-6.0.
Inigo	200203_07U	06-18Z 02/04/2003	Developing stage.
Monty	200304_05U	06Z 28/02/2004-00Z 03/03/2004	Developing phase through weakening over land. Note: observations for BT.
Fay	200304_08U	09Z 18/03/2004 – 12Z 28/03/2004	Adjust all of 18/09Z to end – supported by PMW (112 kn first peak and 95 kn 2nd peak) including over land at end of track.
Oscar	200304_11U	12Z 24/03/2004 – 12Z 25/03/2004	Developing stage.
Ingrid	200405_07U	12Z 06/03/2005-12Z 06/03/2005; 06Z 09/03/2005–00Z 10/03/2005; 03Z 13/03/2005 –	Three peaks. Adjust in developing stages and over land. Additional adjustment for Qld crossing when ADT underestimates 20Z 09/03/2005 (55 Vs 95BT).

		00Z 15/03/2005; 12Z 15/03/2005 – 21Z 16/03/ 2005	
Kerry	200405_10U	00-12Z 09/01/2005	Adjust during development. Weakening not changed.
Bertie	200506_01U	06Z 21/11/2005 – 00Z 22/11/2005	Developing.
Glenda	200506_14U	09Z 27/03/2006 – 06Z 31/03/2006	Developing; over land. Note: prior to landfall obs. indicate higher than ADT.
Larry	200506_15U	06Z 18/03/2006 – 12Z 19/03/2006	Developing; to ADT peak, then over land.
Floyd	200506_16U	06Z 23/03/2006 – 18Z 24/03/2006	Developing and peak.
Monica	200506_22U	00Z 21/04/2006 – 06Z 26/04/2006	Developing; over land. Peak similar.
George	200607_11U	12Z 07/03/2007 – 00Z 10/03/2007	Developing; over land. Peak similar.
Pancho	200708_20U	06Z 26/03/2008 – 18Z 27/03/2008	Developing. Peak similar.
Hamish	200809_17U	06Z 06/03/2009 – 06Z 07/03/2009;	Developing, as supported by PMW. Weakening not adjusted.
Ilsa	200809_18U	00Z 19/03/2009 – 06Z 19/03/2009; 06Z 20/03/2009- 00Z 23/03/2009	Adjust a few during developing, as supported by PMW. Weakening not adjusted.
Laurence	200910_01U	00 15/12/2009 – 12Z 18/12/2009; 00Z 20/12/2009 – 06Z 23/12/2009.	Adjust development to two peaks (ADT max) and over land, noting peaks similar.
Zelia	201011_10U	18Z 15/01/2011 – 00Z 17/01/2011	Developing; peak increased to 100 kn.
Yasi	201011_14U	00Z 1/02/2011 – 18Z 01/02/2011; 18Z 02/02/2011- 12Z 03/02/2011	Development, and over land. Peak unchanged.
Narelle	201213_05U	12Z 9/01/2013 – 12Z 11/01/2013	Developing. Peak similar.
Ita	201314_15U	06Z 9/04/2014 – 18Z 10/04/2014	Developing and over land. Mostly BT
Marcia	201415_14U	00Z 19/02/2015 – 18Z 20/02/2015	Developing; over land. Peak similar.
Olwyn	201415_16U	12Z 12/03/2015 – 00Z 13/03/2015	Adjustment to developing stage (ADT peak) and over land.
Ikola	201415_19U	06Z 06/04/2015 – 06Z 07/04/2015	Adjustment to developing stage to peak.

4.4.3.   Other Plateau cases (ADT < 57 kn) for BT peak at 65-80 kn

For ADT plateau cases when BT intensities in the range of 65-80 kn there is less confidence in the BT requiring a different action. The Dvorak pattern for intensities between 75-85 kn may be embedded centre or an eye pattern. Unfortunately, there isn't sufficient information in the historical BT record to know which pattern has been used. For BT eye patterns there is greater confidence in these intensities whereas for embedded centre, it is suggested there might be high bias for cases prior to about 2004, as discussed in section 4.3.2. Embedded centre patterns will typically indicate a DT=5.0 (V_m=80-85 kn) but since about 2004, there has been greater discretion to estimate V_m in the 65- 85 kn range for these cases with addition influences from microwave patterns and objective microwave guidance. A reanalysis of a subset of these cases indicated that if an embedded centre pattern with a DT=5.0 continues for at least 12 h there is greater confidence that the intensity does reach a CI of 5.0 (80 kn).

There were 74 cases in this general category, 53 between 1981 and 2003 and 21 between 2003 and 2016 as shown in Table 6. An example of this is *Hubert* in 1985 shown in Fig. 8.

For these cases a more complex set of rules applied. Adjustment commenced when the difference between ADT and BT V_m was 10 kn or more when ADT reached 45 kn or when BT was at least 55 kn. The adjustment used the average BT and ADT. Adjusted values increased at a similar rate to the BT, then increasing to the BT once the BT plateaued or peaked. This had the effect of delaying the onset of peak intensity, typically by 6-12 h. The initial point of weakening was brought forward 6 h for cases prior to 2004, and then weakening occurred at the same rate as BT until ADT is reached or until the intensity falls to 30 kn.
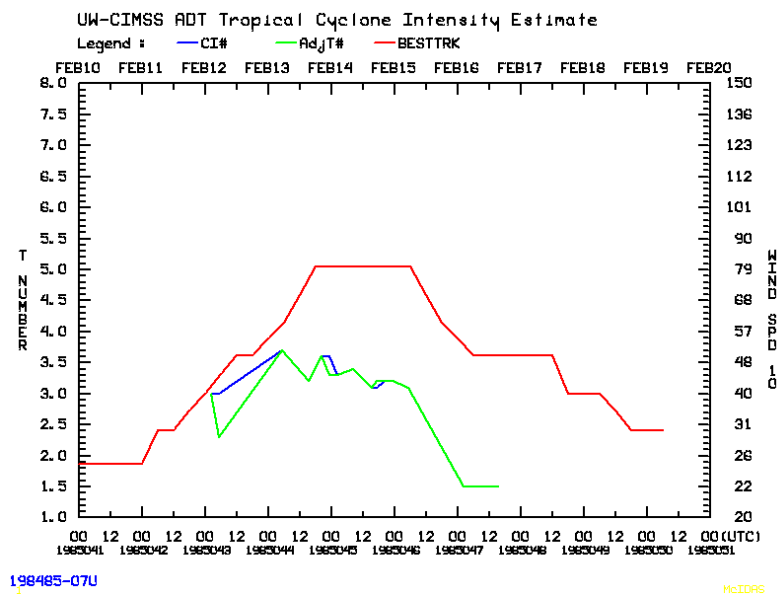

Figure 8. Intensity plot Non PMW-ADT Vs BT for *Hubert* 1985, showing the BT peak at 5.0 but the ADT did not get beyond the 3.5 plateau.

Table 6. Listing of cases where BT peak at 65-85 kn (CI=4.3 -5.3) and ADT < 57 kn (CI < 4.0).

Name	ID	Fixes altered	Comments
Freda	198081_11U	12Z 04/03/1981 – 00Z 07/03/1981	2nd peak adjustment. Peak east of 160°E.
Max	198081_12U	05Z 13/03/1981 – 18Z 17/03/1981	Increase towards BT; same peak (85 kn).
Paddy	198081_14U	18Z 25/05/1981 – 12Z 28/05/1981	Increase towards BT; same peak (65 kn).
Ian	198182_13U	12Z 03/03/1982 – 18Z 08/03/1982	Increase towards BT; same peak; and insert over land values.
Elinor	198283_03U	12Z 13/02/1983 – 06Z 16/02/1983; 00Z 20/02/1983 – 06Z 22/02/1983	Adjustments applied to two developing phases. Missing fixes inserted.
Lena	198283_05U	18Z 05/04/1983 – 06Z 06/04/1983	Missing images. Adjusted to 65 kn (BT peak at landfall).
Monty	198283_07U	06Z 25/04/1983 – 18Z 27/04/1983	Some missing images. Adjusted to 65 kn BT peak.
Grace	198384_09U	12Z 15/01/1984 – 12Z 19/01/1984	Many missing images. Use BT.
Willy	198384_11U	00Z 07/02/1984 – 18Z 09/02/1984	Many missing images. Use BT.
Ingrid	198384_15U	18Z 22/02/1984 – 12Z 24/02/1984	Many missing images. Adjusted to 65 kn BT peak.
Jim	198384_18U	00-18Z 09/03/1984	Some missing images. Adjusted to 65 kn.
Daryl	198384_19U	00Z 12/03/1984 – 06Z 13/03/1984	ADT truncated when Daryl moves west of 90°E on 13th so subsequent intensification not included.
Emma	198485_01U	18Z 09/12/1984 – 21Z 11/12/1984	Some missing images. Adjusted to 65 kn BT peak.
Hubert	198485_07U	12Z 13/02/1985 – 18Z 18/02/1985	Adjust towards BT noting ADT cuts out to west of 90°E.
Isobel	198485_08U	06Z 16/02/1985 – 18Z 17/02/1985	Missing images.
Lindsay	198485_13U	12Z 08/03/1985 – 00Z 11/03/1985	Adjust towards BT and insert over land values.
Margot	198485_16U	18Z 12/04/1985 – 12Z 20/04/1985	Adjust towards BT (same peak 85 kn).
Nicholas	198586_01U	06Z 01/12/1985 – 12Z 06/12/1986	Adjust to BT. Reanalysis confirms BT peak (85 kn).
Winifred	198586_06U	00Z 31/01/1986 – 00Z 02/02/1986	Adjusted to BT (BT supported by observations) and insert over land values
Rhonda	198586_07U	09Z 19/02/1986 – 16Z 20/02/1986	Adjusted to 65 kn BT peak. Some missing images.
Manu	198586_13U	06Z 24/04/1986- 18Z 25/04/1986	Adjusted to 65kn. No missing images.
Connie	198687_01U	12Z 18/01/1987 – 12Z 20/01/1987	Adjusted to BT (BT supported by observations) and insert over land values
Jason	198687_04U	12Z 12/02/1987 – 18Z 13/02/1987	Some missing images and multiple landfalls. Adjustment to peak 70 kn at landfall.

Frederic	198788_02U	21Z 30/01/1988 – 18Z 01/02/1988	Adjust to peak 80 kn.
Charlie	198788_04U	00Z 29/02/1988 – 12Z 01/03/1988	Adjustments to be similar to BT and insert over land values. Observations support BT.
Ilona	198889_01U	09Z 15/12/1988 – 12Z 18/12/1988	Adjustments to be similar to BT and insert over land values. Observations support BT.
Felicity	198990_02U	06Z 15/12/1989 – 06Z 16/12/1989	Eye emerged on imagery at landfall. Adjusted to BT.
Elma	199091_06U	18Z 27/02/1991 – 00Z 03/03/1991	Adjusted to 70 kn BT peak.
Daman	199192_04U	18Z 16/02/1992 - 00Z 20/02/1992	Adjusted to 70 kn BT peak. Adjusted higher as it became extra-tropical.
Nina	199293_02U	12Z 24/12/1992 – 00Z 27/12/1992; 00Z 31/12/1992- 00Z 01/01/1993.	Adjusted to BT on basis of reanalysis (eye at landfall). Over land values included. Also Developing phase for 2nd peak.
Adel	199293_08U	06-18Z 14/05/1993	Developing to landfall 60kn.
Naomi	199394_01U	12Z 16/12/1993 – 06Z 18/12/1993	Peaks prior to landfall; Peak 75 kn.
Pearl	199394_04U	18Z 11/01/1994 – 06Z 19/01/1994	Missing images at start so ADT much less than BT. Initial peak had raw ADT eye. IR has eye 12-17 Jan.
Quenton	199394_05U	12Z 25/01/1994 – 18Z 27/01/1994	Adjust towards BT (same peak); eye on imagery. Some missing images 25, 27 Jan.
Vivienne	199394_10U	21Z 07/04/1994 - 12Z 10/04/1994	Adjust towards BT. Peak 80 kn.
Violet	199495_03U	06Z 04/03/1995 - 00Z 08/03/1995	Adjust to peak 80 kn.
Warren	199495_04U	06Z 05/03/1995 - 06Z 06/03/1995	Adjust to peak 70 kn and insert over land values.
Gertie	199596_04U	19Z 18/12/1995 - 01Z 23/12/1995	Adjust to BT peak 75 kn and insert over land values.
Hubert	199596_06U	22Z 07/01/1996 - 04Z 11/01/1996	Adjust towards BT. Peak 75 kn. ADT cuts out west of 90°E.
Celeste	199596_07U	00Z 27/01/1996 – 06Z 28/01/1996	Observations and radar influence peak of 70kn higher than Dvorak.
Fergus	199697_05U	00Z 26/12/1996 – 06Z 28/12/1996	Adjust towards BT. Peak 80 kn.
Rachel	199697_07U	01Z 06/01/1997 – 22Z 08/01/1997	Adjusted to 70 kn BT peak then over land.
Justin	199697_12U	06Z 16/03/1997 – 12Z 20/03/1997	Adjusted to BT for peak 80 kn (eye on imagery). Observations support BT. Over land values inserted.
Victor	199798_07U	04Z 12/02/1998 – 10Z 13/02/1998	Modified towards BT peak 85 kn. Eye on imagery and seen on raw ADT.
Alison	199899_02U	16Z 8/11/1998 – 22Z 10/11/1998	Adjustments towards BT.
Billy	199899_04U	13Z 03/12/1998 – 13Z 05/12/1998	Adjusted to 65 kn
Damien	199899_07U	07Z 22/01/1999 – 04Z 26/01/1999	Considerable adjustment towards BT (same peak 85 kn).
Kirrily	199900_03U	10Z 28/01/2000 – 10Z 30/01/2000	Adjust towards BT.

Leon	199900_04U	04Z 05/02/2000 – 16Z 07/02/2000	Adjust towards BT (same peak 75 kn).
Tessi	199900_09U	12Z 02/04/2000 – 00Z 03/04/2000	Adjusted to 65 kn.
Abigail	200001_06U	12Z 26/02/2001 - 06Z 27/02/2001	Adjusted to 60 kn at landfall.
Walter	200001_07U	22Z 03/04/2001 – 04Z 07/04/2001	Adjust towards BT (same peak 80 kn).
Claudia	200102_05U	00-06Z 12/02/2002	Adjusted to 65 kn at 160°E.
Erica	200203_05U	18Z 11/03/2003 – 06Z 12/03/2003	Developing phase until moves east of 160°E.
Jana	200304_01U	06Z 08/12/2003 - 12Z 11/12/2003	Adjust similar to BT (same peak 85 kn).
Debbie	200304_02U	09Z 19/12/2003 – 00Z 21/12/2003	Adjusted to 65 kn BT peak then over land values.
Harvey	200405_05U	00Z 07/02/2005 – 18Z 7/02/2005	Adjusted to BT for developing to landfall then over land. Adjustments consistent with PMW ADT.
Willy	200405_08U	18Z 10/03/2005 – 06Z 13/03/2005	Adjusted to BT. Adjustments consistent with PMW ADT.
Adeline	200405_09U	12Z 04/04/2005 – 12Z 05/04/2005	Adjusted to BT. Adjustments consistent with PMW ADT.
Clare	200506_05U	00Z 09/01/2006 – 18Z 10/01/2006	Adjust to BT.
Wati	200506_17U	00Z 21/03/2006 – 18Z 24/03/2006	Adjust to BT.
Jacob	200607_12U	12Z 09/03/2007 – 12Z 10/03/2007	Adjust to 65kn.
Guba	200708_03U	18Z 15/11/2007 – 06Z 17/11/2007	Adjust to 65 kn BT peak.
Nicholas	200708_11U	06Z 15/02/2008 – 06Z 18/02/2008	Adjust to BT
Magda	200910_06U	18Z 20/01/2010 - 12Z 22/01/2010	Adjust to 70 kn BT peak.
Ului	200910_09U	00Z 19/03/2010 – 18Z 20/03/2010	Development to 2nd peak at landfall.
Abele	201011_02U	12-18Z 02/12/2010	Adjust to 70 kn BT peak.
Heidi	201112_07U	12Z 11/01/2012 – 15Z 12/01/2012	Developing to landfall then over land. Observations support BT.
Lua	201112_16U	12Z 15/03/2012 – 06Z 18/03/2012	Developing to landfall then over land.
Freda	201213_03U	06-12Z 29/12/2012	Adjustment to last few BT fixes near 160°E.
Victoria	201213_17U	18Z 09/04/2013 – 18Z 10/04/2013	Adjustment to developing and initial weakening.
Zane	201213_18U	06Z 30/04/2013 – 00Z 01/05/2013	Adjust to 65 kn BT peak.
Jack	201314_16U	12Z 19/04/2014 – 06Z 21/04/2014	Adjustment to developing and initial weakening.
Nathan	201415_17U	06Z 18/03/2015 – 00Z 21/03/2015	Three landfalls. Adjustment to development to highest peak at 90 kn and missing values over land.

4.4.4.   Missing V�m (ADT) values

Many fixes have missing ADT estimates because of missing images and for when the position was located over land. This presents issues which required manual intervention to preserve continuity of realistic estimates on a case by case basis.

As discussed in Section 2, the percentages of 'good' images was significantly lower in the 1981–1988 period than in the subsequent era. Indeed, the percentage was just 67 per cent in 1984. For some individual cases such as *Quenton* (198384_03U) there was only one image for analysis between 0827 UTC 28 November and landfall some 36 h later (see Fig. 9 a). During this stage *Quenton* developed an eye.

While the record becomes more complete during the 1990s, there is still the occasional event that has a considerable amount of missing data. For example, *Daryl* (199596_01U) only had 4 ADT fixes matching BT ones, for the entire period between 16-25 November 1995 (see Fig. 9 b). In that case the ADT Vₘ were consistent with BT, so interpolation followed BT values. Any objective technique using the 1981–1988 era of satellite imagery will be compromised because of this issue.

ADT does not provide estimates when the TC moves over land. To preserve usefulness of the dataset, values have been estimated using a combination of BT and last ADT values. In some cases, an inland decay model can be used but because of the variations in terrain and track, each case had to be considered individually. For example, the intensity characteristics over land can vary from not weakening quickly in the case of a TC tracking over land near the coast preserving the inflow of moist air to weakening rapidly in the case of it tracking quickly over mountainous terrain.

These cases present additional issues for estimates of the wind radii (see Section 5).
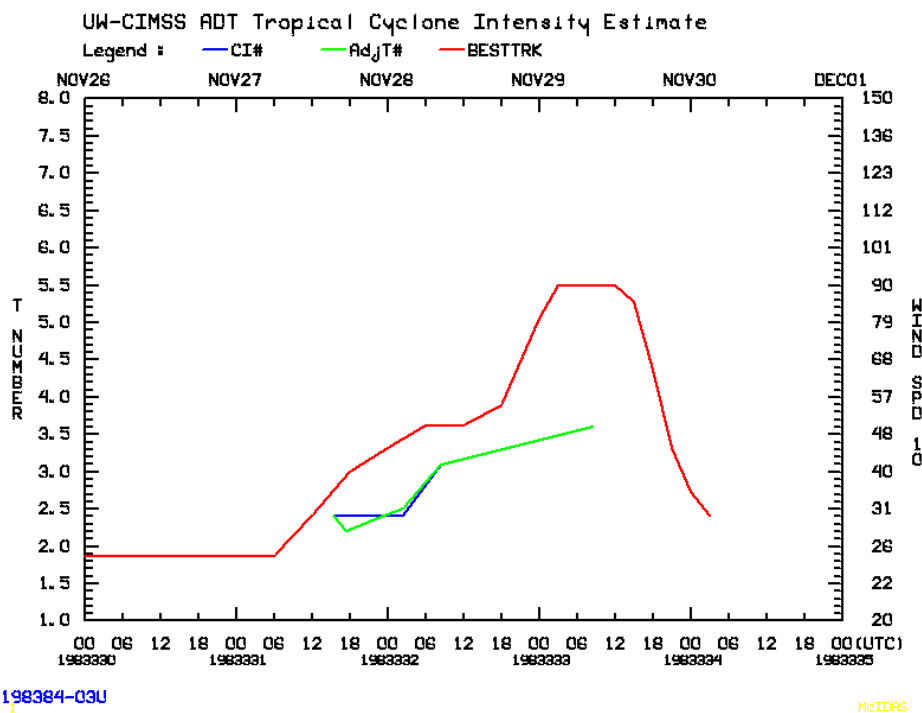

Figure 9 a. *Quenton* 198384_03U. There was only one image for analysis between 0827 UTC 28 November and landfall some 36 h later. During this stage Quenton developed an eye.
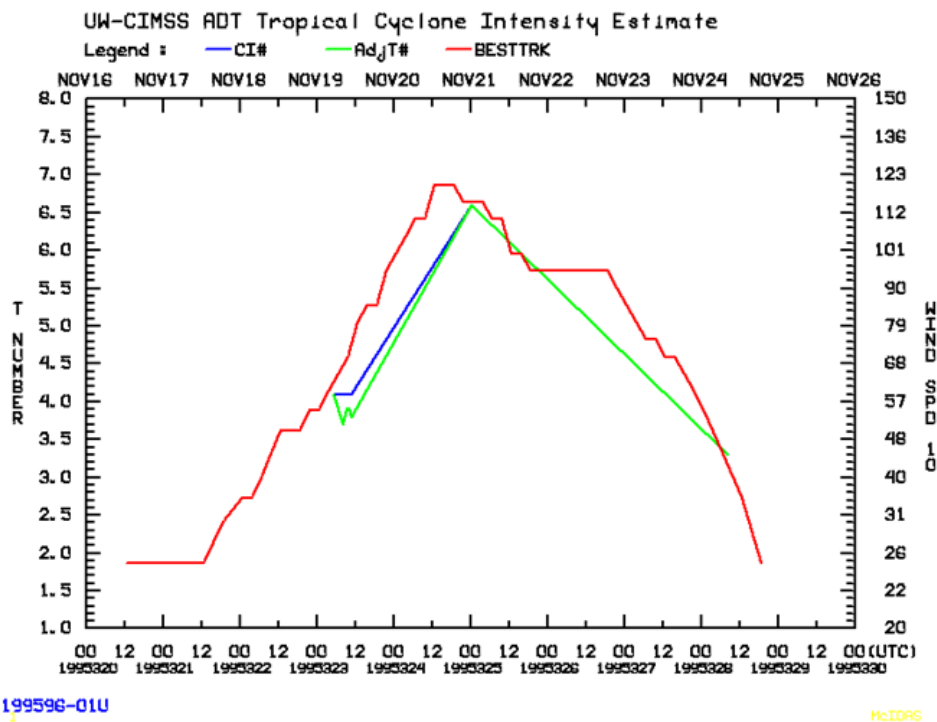
Figure 9 b. *Daryl* (199596_01U) only had 4 ADT fixes matching BT ones, for the entire period between 16-25 November 1995 yet the intensity profile was remarkably similar to the BT.

4.5 Analysis of results

In total there were 33.6 per cent of fixes requiring insertion of a value or alteration to the purely objective ADT V_m value. This included:

- 7.7 per cent were adjusted because the positions were over land and ADT V_m was set to 0.
- 11.5 per cent of fixes did not have an ADT V_m value, requiring an estimate to be inserted by interpolation or extrapolation. Typically, this was because the IR satellite imagery was missing especially for the 1981–1988 period.
- 14.4 per cent of cases that had the ADT V_m estimate adjusted using the rules described in Section 3.4. A total of 97 per cent of these adjustments were at least 5 kn.

These adjustments to the non-PMW ADT dataset reduced the mean bias for the 2003–2016 period from 3.3 kn to 0.1 kn (median is 0.0) as shown in Table 7. The scatterplot of adjusted non-PMW ADT V_m against BT V_m in Fig. 10 a shows a marked improvement from the scatter plot of unadjusted values in Fig. 3 a. MAE was reduced from 9.3 kn to 5.3 kn and correlation improved from 0.75 to 0.89.

The bias for the 1981-2003 period was 3.2 kn. This was separated further to the 1981–1988 period which had a lower quality satellite dataset, and 1989-2003 period.

Table 8 shows the bias statistics for each period, stratified by intensity. The adjusted ADT V_m is higher than BT for weak cases to about 50kn and then higher for strong systems from 65 kn (Fig. 10a and Table 8). The bias is higher for the 1981–2003 period than the reference 2003–2016 period

indicating there may be a high bias in the BT for the earlier era, however some of this is likely due to missing imagery.

Table 9 is a list of 32 TCs that have differences of at least 30kn between the BT and adjusted non-PMW ADT (hereafter simply "adjusted V_m") datasets. Reanalysis of these events would be required to assess whether the BT record requires updating.

Table 7. Bias statistics for ADT V_m datasets against BT.

	V_m bias (kn)			
	1981–2003	1981–1988	1989–2003	2003-–2016
BT - adj. non PMW ADT	2.8	4.2	2.1	**0.1**
BT – non-PMW ADT	7.5	8.8	7.1	**3.3**
BT - PMW ADT	6.0	-	5.1	**-0.2**

Table 8. Bias statistics for V_m ADT datasets against BT by intensity.

|	V_m Bias (BT- adj. ADT) 20032016					
	All V_m	<=30 kn	35-45 kn	35-60 kn	65+kn	80+ kn
Mean Bias (kn)	0.06	-3.80	-1.10	0.78	3.21	3.57
Median Bias (kn)	0.00	-1.06	0.00	0.13	0.00	0.00
RMSE (kn)	8.35	7.64	8.76	8.40	9.03	9.83
MAE (kn)	5.62	5.02	7.03	6.38	4.74	5.21
No. samples	2557	745	768	1294	618	370
	V_m Bias (BT- adj. ADT) 1989 - 2003					
	All V_m	<=30 kn	35-45 kn	35-60 kn	65+kn	80+ kn
Mean Bias (kn)	2.30	-2.06	2.18	4.27	1.55	1.03
Median Bias (kn)	0.09	-0.06	2.19	4.86	0.00	0.00
RMSE (kn)	8.85	6.00	7.94	9.80	8.60	7.85
MAE (kn)	6.05	3.85	6.31	7.42	4.98	4.62
No. samples	4619	878	1434	2435	1306	849
	V_m Bias (BT- adj. ADT) 1981 - 1988					
	All V_m	<=30 kn	35-45 kn	35-60 kn	65+kn	80+ kn
Mean Bias (kn)	4.05	-0.86	3.40	5.67	4.73	4.35
Median Bias (kn)	2.94	-0.06	3.99	5.01	0.09	0.00
RMSE (kn)	9.47	5.47	7.85	9.96	10.94	10.63
MAE (kn)	6.19	3.33	5.96	7.29	6.23	5.84
No. samples	2324	492	597	1253	579	331
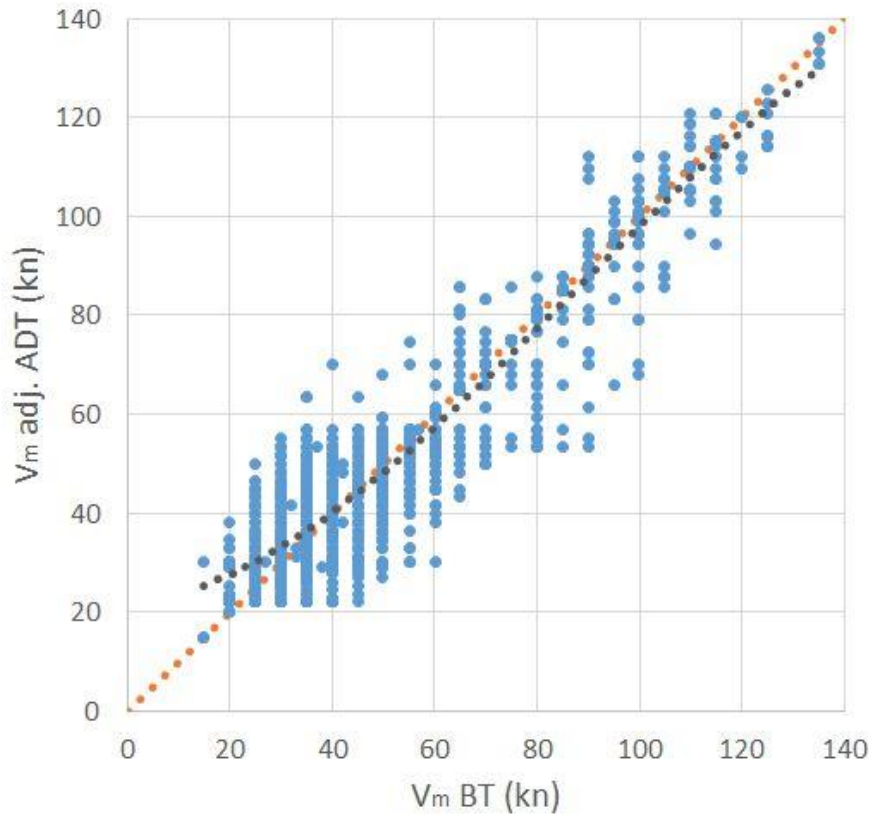
Figure 10 a. Scatterplot of v_m BT against adjusted ADT 2003–2016. The correlation was 0.89.
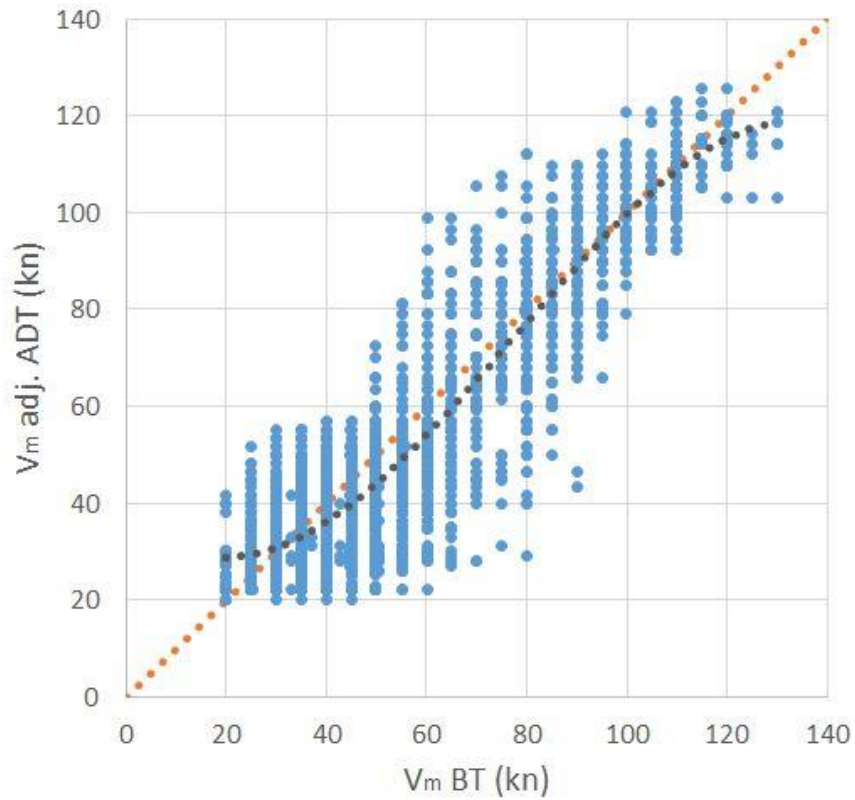

Figure 10 b. Scatterplot of v_m BT against adjusted ADT 1981–2003. The correlation was 0.88.
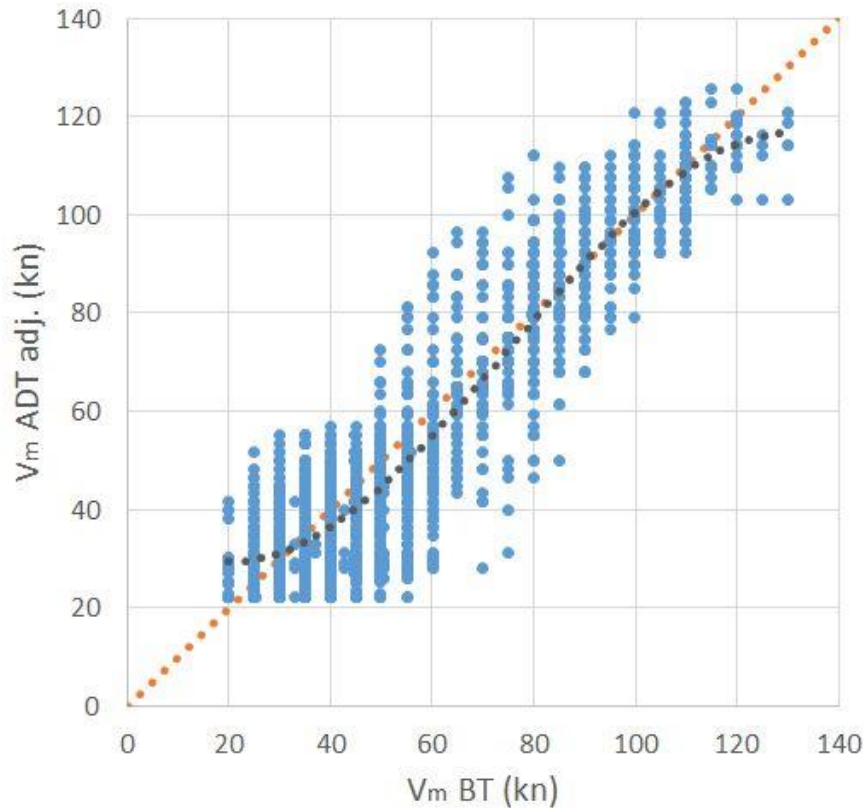
Figure 10 c. Scatterplot of **v**$_m$ BT against adjusted ADT 1989-2003. The correlation was 0.90.

Table 9. Differences of at least 30 kn between the V$_m$ BT and adjusted V$_m$ ADT 1981-2016.

NAME	DISTURBANCE ID	Date/Time (UTC)	BT DVK CI	BT V$_m$ (kn)	Adj. ADT V$_m$	Diff. BT-Adj.	Comments
NEIL	198081_10U	3/03/1981 12:00	4.5	65	30	35	Weakening stage. BT has prolonged period where CI greater than FT, for reanalysis.
PADDY	198081_14U	27/05/1981 12:00	4.5	65	29	36	During weakening.
BERNIE	198182_14U	4/04/1982 18:00	4.5	70	105	-35	
JANE	198283_01U	7/01/1983 12:00	4	60	98.8	-39	
ELINOR	198283_03U	28/02/1983 0:00	4.5	90	43.2	47	V$_m$ from obs. - Lihou Reef E 90-100 kn; higher than from reanalysed CI;
NAOMI	198283_06U	28/04/1983 6:00	5	80	29	51	
FERDINAND	198384_17U	4/03/1984 8:00	4	60	29	31	
LANCE	198384_22U	8/04/1984 23:00		60	22	38	Intensifying sub-tropical low; max

							winds on southern side
FRANK	198485_02U	26/12/1984 0:00	5	80	40	40	
ISOBEL	198485_08U	19/02/1985 6:00	4	60	30	30	
VICTOR	198586_11U	7/03/1986 18:00	4	60	29	31	
KAY	198687_06U	13/04/1987 18:00	4	60	29	31	
FELICITY	198990_02U	17/12/1989 18:00	1.5	55	22	33	Weak satellite signature but observed strong winds in southwest quadrant enhanced by strong ridge to south. Gales may only be in western quadrants
KELVIN	199091_05U	25/02/1991 12:00	3	60	30	30	V_m influenced by obs higher than suggested by CI; Willis Is reports 65 kn
BETSY	199192_03U	14/01/1992 6:00	3.5	60	29	31	V_m from synoptic charts; higher than CI
FRAN	199192_08U	11/03/1992 18:00	4.5	75	36.4	39	Max wind from reanalysed CI; pressure lower as large size and RMW
NINA	199293_02U	1/01/1993 0:00	5	80	48	32	
POLLY	199293_05U	26/02/1993 18:00	4.5	75	105	-30	
SHARON	199394_08U	16/03/1994 0:00	5	80	112	-32	
JUSTIN	199697_12U	10/03/1997 0:00	3	60	28	32	V_m influenced by obs; higher than CI suggests; strong monsoonal flow
KATRINA	199798_04U	16/01/1998 12:00	5	80	49.8	30	
CATHY	199899_05U	26/12/1998 7:00	4	60	29	31	
NORMAN	199900_07UU	3/03/2000 10:00	4.5	75	108	-33	
CHRIS	200102_04U	4/02/2002 4:00	4.5	75	44.8	30	
LARRY	200506_15U	19/03/2006 0:00	5	90	53.4	37	
FLOYD	200506_16U	25/03/2006 6:00	5.5	90	53.4	37	
GLENDA	200506_14U	30/03/2006 0:00	5.5	100	70.2	30	

HAMISH	200809_17U	7/03/2009 6:00	6	110	79	31	
ULUI	200910_09U	20/03/2010 12:00	4.5	80	46.4	34	
DYLAN	201314_07U	30/01/2014 9:00	3	60	30	30	Flinders Reef reports 58 kn.
KATE	201415_04U	27/12/2014 18:00	5	85	53.4	32	
QUANG	201415_21U	1/05/2015 6:00		40	70.2	-30	

4.5.1 Accumulated Cyclone Energy (ACE)

The Accumulated Cyclone Energy (ACE) is a measure to express the energy used by a TC over its lifetime (Bell et al., 2000). The ACE is calculated by summing the squares of V_m (at least 34 kn), at six-hour intervals. The ACE of a season is the sum of the ACEs for each TC and considers the number, strength, and duration of all the TCs in the season. The number is divided by 10,000 to make them more manageable. The unit of ACE is 10^4 kt^2, and for use as an index the unit is assumed.

$$ACE = 10^{-4} \Sigma V_m^{\ 2}$$

ACE is used to better reflect TC activity and hence is an appropriate index to compare the different V_m datasets.

The comparison of ACE using the original BT V_m and the adjusted ADT V_m in Fig. 11 a shows a general strong correlation, but the ACE (BT V_m) being higher than that from ad. ADT V_m. Outliers include Justin 1997, 20.1 (BT) Vs 10.7 (adj. ADT); *Katrina* 1998, 22.4 (BT) Vs 15.9 (adj. ADT); *Kelvin* 1991, 8.6 (BT) Vs 1.6 (adj. ADT); *Betsy* 1992, 7.3 (BT) Vs 1.0 (adj. ADT); *Elinor* 1983, 38.7 (BT) Vs 30.6 (adj. ADT); *Errol* 1982, 5.0 (BT) Vs 0.3 (adj. ADT) and *Naomi* 1983, 6.2 (BT) Vs 1.5 (adj. ADT) highlighted in Fig. 11 b. The years from 1983-86, 1991-92 and 1997 exhibit the highest differences. The above outliers contribute greatly to these differences in those years. These cases warrant further investigation.

The time series of annual differences in ACE in Fig. 11 c would suggest a trend, having the greatest differences in the earlier dataset.

Across the entire dataset the ACE from BT was greater than that from adj. ADT by 12.6 per cent. Splitting this across periods, the percentage differences for 1981–1988, 1989–2003 and 2004–2016 are 21.8, 14.1 and 3.9 per cent respectively. This reflects the combined effects of adjusted V_m being on the low side in the earlier era and BT V_m being on the high side for weakening cases.
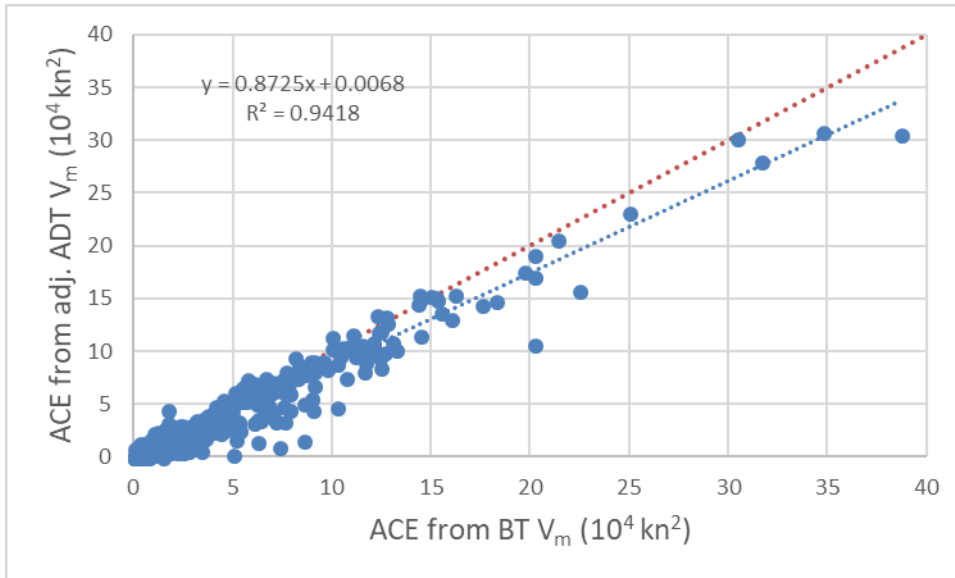
Fig. 11 a. Comparison of ACE derived from BT V_m against VT adjusted V_m ADT.
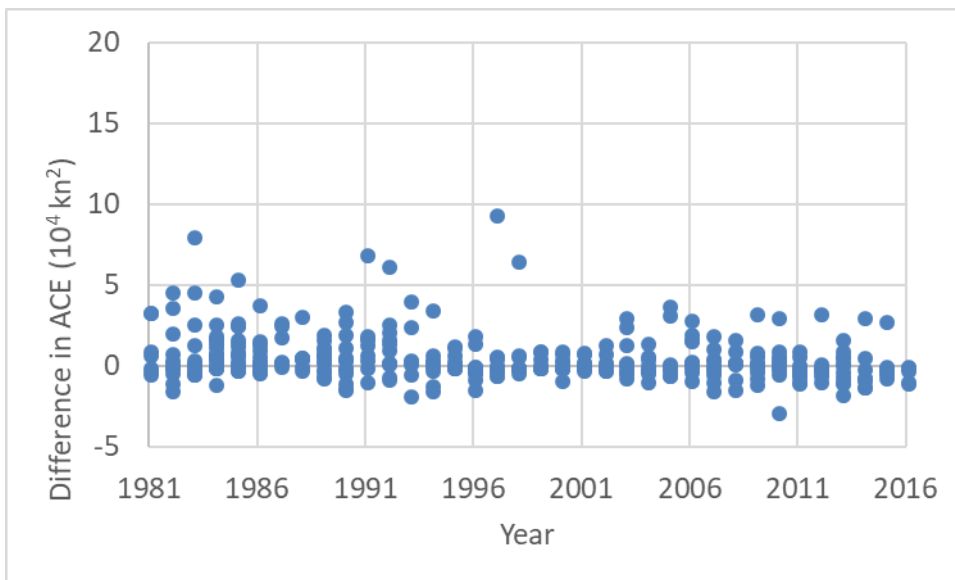
Fig. 11 b. Differences in ACE from BT V_m against adjusted V_m ADT by year.
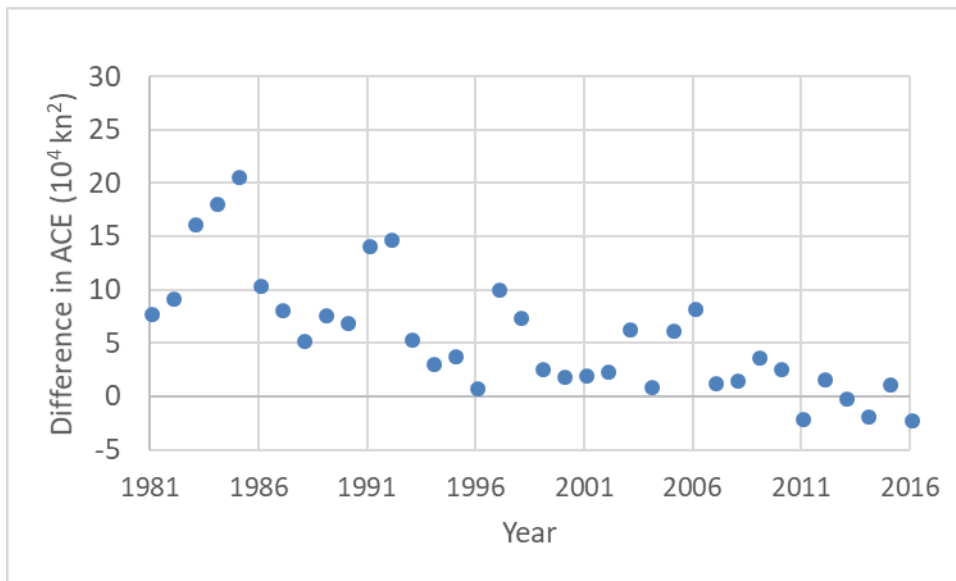
Fig. 11 c. Total annual differences in ACE from BT V_m against adjusted V_m ADT.

4.5.2 Analysis of Peak V_m

The comparison of peak intensity for each TC using the original BT V_m and the adjusted ADT V_m in Fig. 12 a shows a strong correlation (0.88). The difference analysis in Fig 12 b indicates that for TCs to 45 kn peak, the adjusted ADT is higher than BT but for 55-70 kn peak intensity the BT is stronger. These results are consistent with Table 8 and Fig. 10. A consequence of this is that there are less severe TCs (peak more than 64 kn) in the adjusted ADT dataset than the BT. Fig. 12 c show that these differences are scattered throughout the record but are most prominent in the 1981–1986 period. As discussed earlier in this Section, this points to the influence of ADT being too low (the plateau effect) especially when the satellite record was at its weakest in the 1980s.
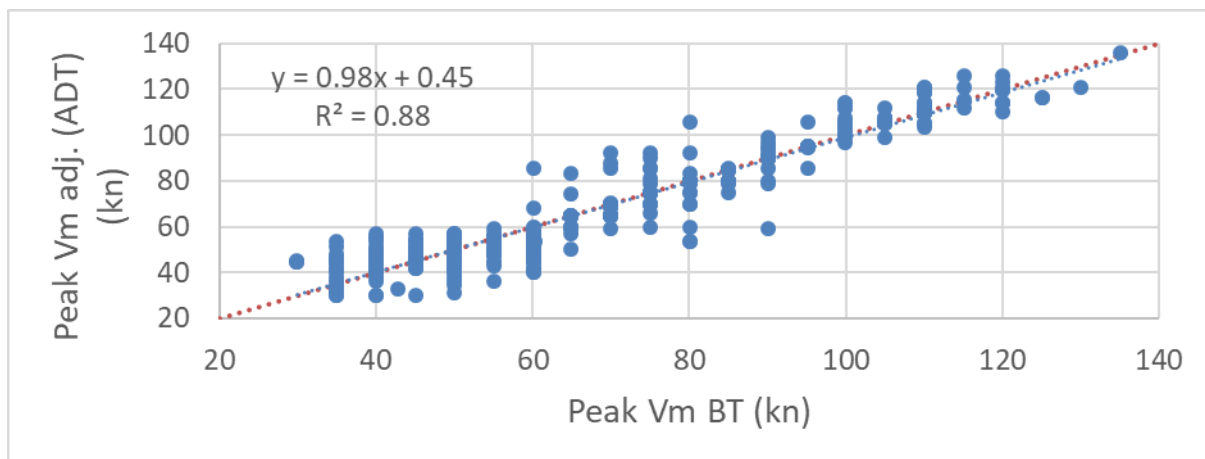

Figure 12 a. Scatterplot of the peak v_m, BT against adjusted ADT 1989-2016.
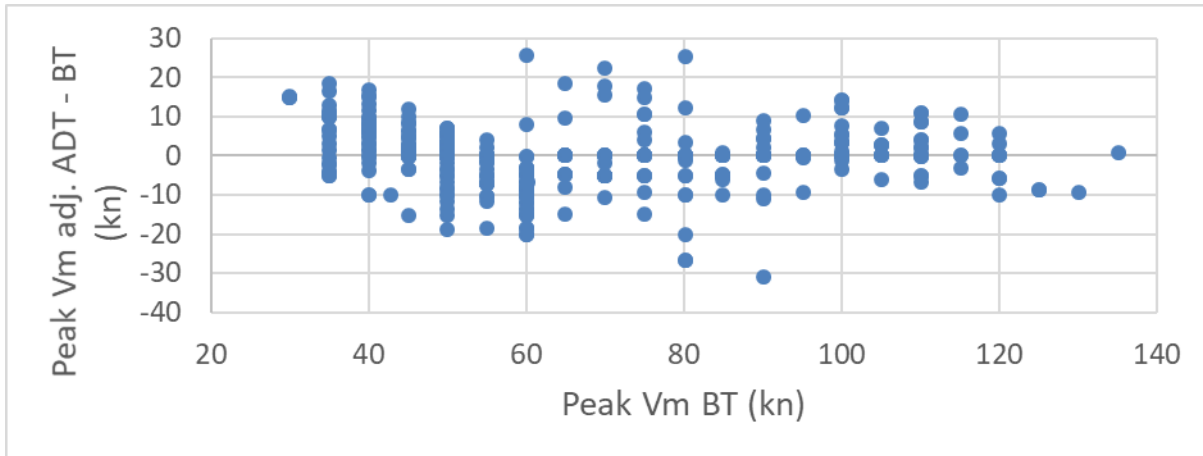
Figure 12 b. Difference in peak v_m, between BT and adjusted ADT by intensity.
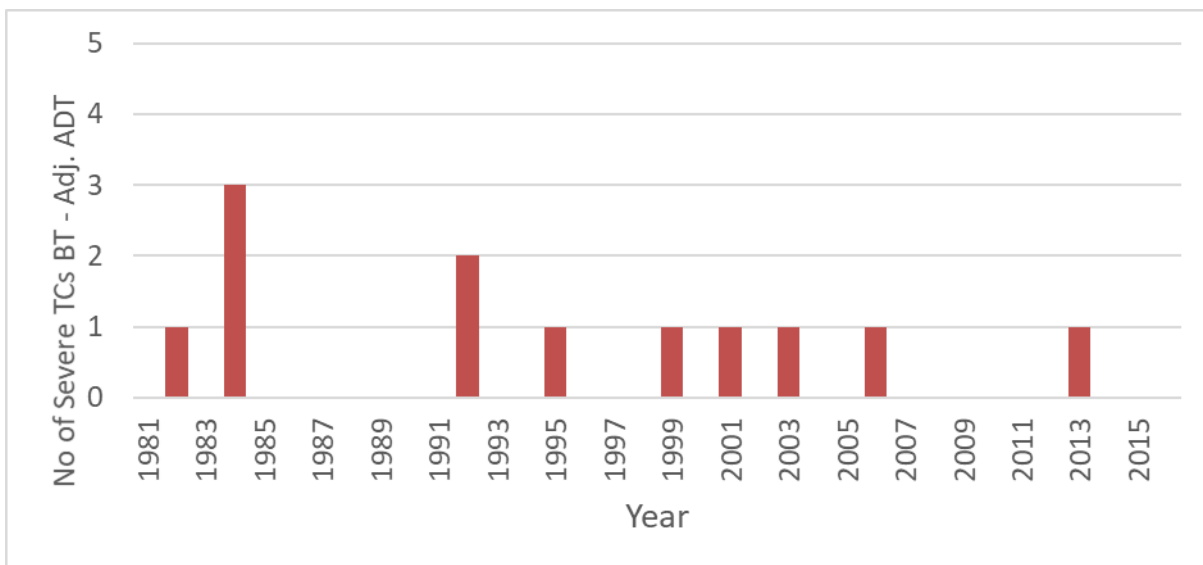
Figure 12 c. Difference in the number of Severe TCs between BT and Adj. ADT

5. Deviation Angle Variance (DAV) Model

5.1 Background

The DAV technique was originally devised to objectively determine the intensity utilising digital brightness temperatures from infrared satellite imagery (Piñeros et al., 2008; Ritchie et al. 2012). More recently the technique has been extended to objectively measure the symmetry of a TC and wind radii parameters for TCs (Dolling et al., 2016). Values of DAV were correlated to wind radii for a NATL TC dataset that had consistent aircraft reconnaissance inputs (21 TCs from 2004-10). A multiple linear regression model was created using DAV, and sea surface temperatures (SST), V_m and TC age to determine wind radii in both axisymmetric and by-quadrant models. The asymmetric ("by-quadrant") regression model had MAE of 51, 47, 37 and 56 km for the NE, SE, SW and NW R34 quadrants respectively. For cases when the intensity is less than 70 kn, there is about a 10-30 km positive bias (model higher than observed) while for stronger cases in the range of 70-100 kn there is about a 10-30 km negative bias (model lower than observed).

5.2 Application to the Australian region

The DAV technique was run on IR imagery over the Australian region. DAV was tested using different configurations and was trained on the 2004–2016 BT wind radii to derive new regression coefficients. A comparison of these with the NATL version of the model indicated the Australian version was more appropriate for the Australian region. Because the technique was being run in hindcast mode rather than predictive mode, this allowed the model to use averaging that was centred on the fix concerned, which improved results.

This approach made the following assumptions:

   i.   The NATL predictors (SST, TC age, V_m) were valid for the Australian region.
  ii.   The 2004–2016 BT wind radii was appropriate to use for the training set (refer to Appendix 3.3 for comments on the BT).

To address the issue of large BT R34 values often associated with the surrounding environment and not the TC circulation, the training set excluded cases when the BT R34 exceeded 300 km. To counter the effects of land effects on the regression coefficients, all cases when TCs were within 150 km of land were excluded. Although the BT R34 is biased to certain values: 30, 60, 90, 120, 150 nm (refer Fig. 7) this was not considered significant to affect the overall distribution of wind radii.

Four issues were noted with the DAV outputs for this study:
   i.   Inconsistencies between V_m and wind radii, i.e. ensuring there are R34 values when V_m exceeds 34 kn, R48 values when V_m exceeds 48 kn and R64 values when V_m exceeds 64 kn.
  ii.   The high degree of asymmetry especially for R64 values. This includes null values in quadrants. R64 radii are expected to be axisymmetric in most systems.
 iii.   The low spread in output compared to BT.
  iv.   The low correlation with BT (2004–2016).

Varying the DAV thresholds improved the first two issues considerably. The final two points were more difficult to overcome.

The technique has been run across the entire 1981–2016 dataset. The technique interpolates the DAV values across the missing intervals. However, even with this approach, the results from 1981–1988 should be used with high degree of caution due to the impact of missing imagery.

5.3 Results

Table 10 shows the basic statistics of the technique separated into three different periods: 1981–1988; 1989–2003; and 2004–2016.

Comparative statistics prior to 2004, are provided for reference but should be largely ignored, especially for the 1981–1988 period. The BT values are unrealistically high prior to the scatterometry era, there are some errors with BT R64 values prior to 2000 and missing images - especially in the 1980s - distorts DAV output.

 For the 2004–2016 period, the bias is close to zero as the algorithm was trained on this period using a bootstrap technique. The MAE for R34 were 38-41 km.

For the 2004–2016 reference period, the correlations with BT are quite low, as shown on the scatterplot diagrams for R34 quadrants in Fig. 13. The highest correlation is 0.12 for R34 in the northwestern quadrants while all other correlations are less than 0.1.

The box and whisker plots by quadrant in Fig. 17 a and cumulative probability distributions in Fig. 17 b show that the DAV model spread is lower than BT, even though the medians are similar, albeit slightly higher than BT. The spread is particularly low for southern quadrants where the DAV model does not have R34 values less than about 120 km on the southern side.

These disappointing results, particularly the low correlations with the 2004-2016 BT wind radii values, indicates that the DAV algorithm is not yet suitable for use an objective diagnostic for wind radii.

Table 10. Bias statistics for DAV (BT-DAV) (Excluding BT > 300 km).

|		1981 to 1988				1989 to 2003				**2004 to 2016**			
		NE	SE	SW	NW	NE	SE	SW	NW	NE	SE	SW	NW
R34	Bias (km)	-61.6	-50.0	-44.1	-62.4	-15.3	-8.8	-1.0	-14.8	**0.0**	**0.0**	**-0.6**	**-2.0**
	MAE (km)	79.9	72.0	70.7	80.8	47.4	49.0	51.6	48.2	40.7	39.6	41.1	37.6
	Mean DAV - (km)	125	134	139	125	125	133	139	126	125	129	135	125
	Mean BT (km)	185	185	185	185	141	141	141	140	126	130	137	128
R48	Bias (km)					1.6	6.4	13.3	-3.9	-1.5	-1.7	-1.2	-1.3
	MAE (km)					5.2	7.3	13.6	10.6	23.0	23.9	24.9	20.7
	Mean DAV (km)	71.4	72.1	73.1	68.1	72.9	73.3	75.0	71.0	71.9	71.5	73.4	69.5
	Mean BT (km)					67.2	66.5	66.7	66.0	70.2	69.1	70.7	66.7
R64	Bias (km)	-22.6	-23.2	-25.4	-22.8	-11.9	-11.9	-11.5	-11.2	-0.1	0.0	0.1	0.1
	MAE (km)	25.8	26.4	27.8	25.0	22.7	23.0	23.0	22.5	9.6	10.4	11.2	9.4
	Mean DAV (km)	40.4	41.2	41.4	40.5	41.2	41.3	41.9	42.0	40.7	40.6	41.3	41.0
	Mean BT (km)	65.5	65.5	65.5	65.5	52.8	53.1	53.0	52.8	41.1	41.3	41.6	41.0
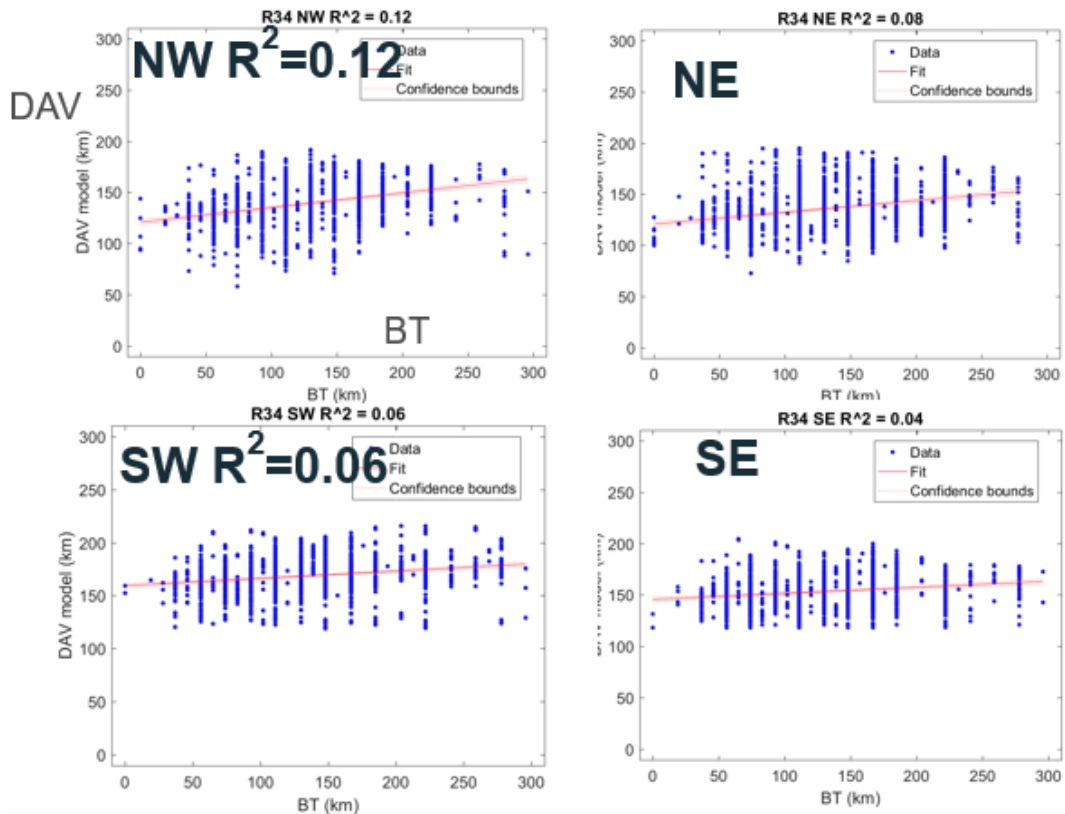
Figure 13 a. Scatter plot of R34 DAV Vs BT, 2004-2016 (excluding cases when BT R34 >300 km)
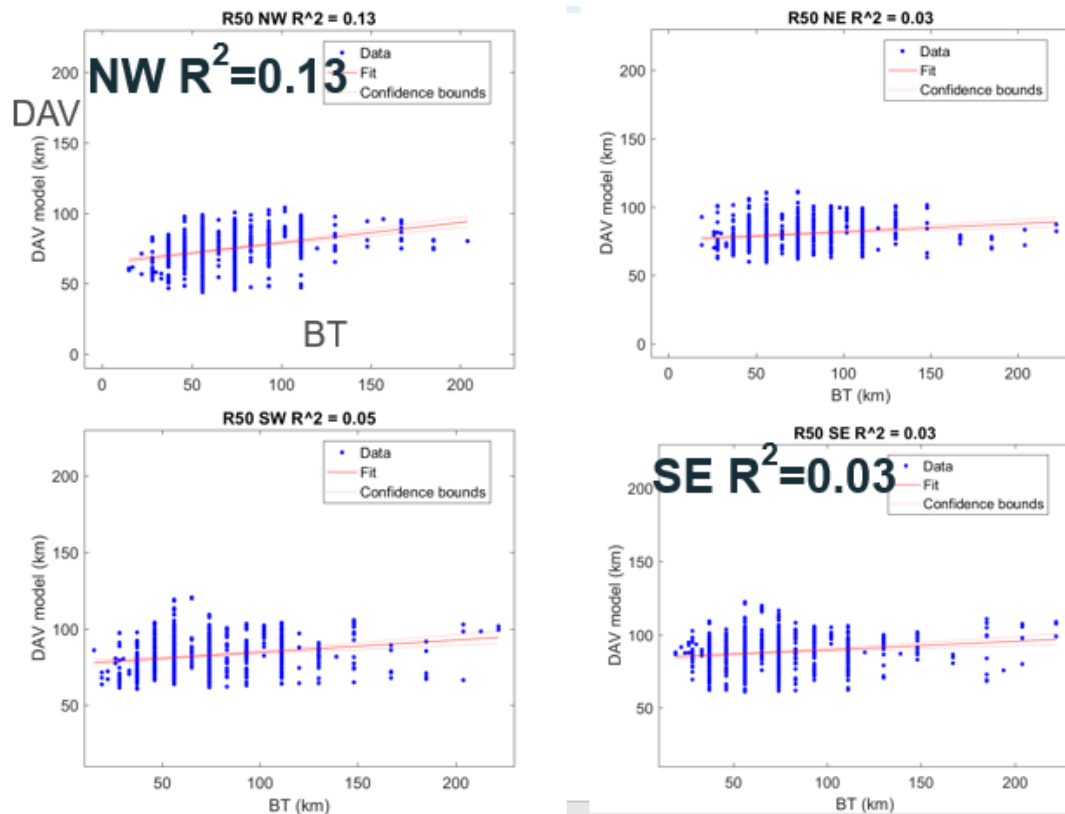

Figure 13 b. Scatter plot of R48 DAV Vs BT, 2004-2016 (excluding cases when BT R34 >300 km)
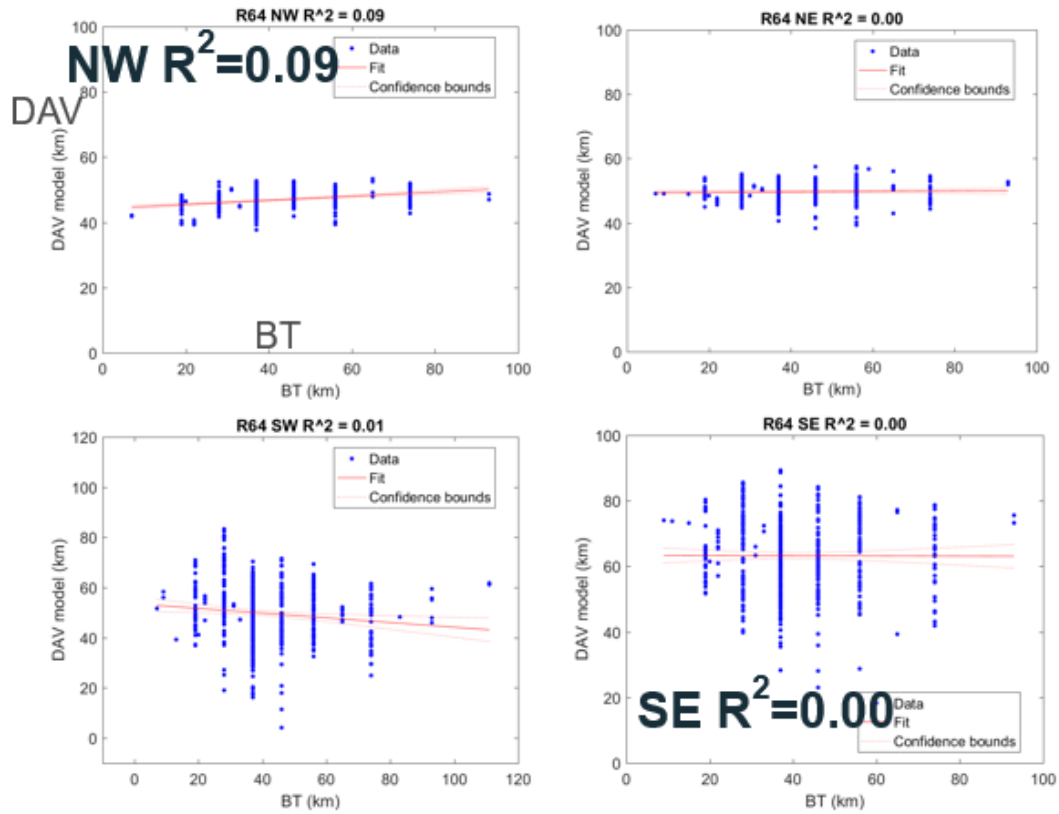
Figure 13 c. Scatter plot of R64 DAV Vs BT, 2004–2016 (excluding cases when BT R34 >300 km).

6. The 'Lok' dataset

6.1 Background

As part of a study on the BT reanalysis, Lok et al. (2013) developed algorithms to estimate radius of gales (R34) by quadrants (NE, SE, SW, NW), radius of outer closed isobar (ROCI), POCI and radius of maximum winds (RMW) for TCs in the BT for the period 1979-2012.

The estimations are based on:
    a. wind analyses from the European Centre for Medium-Range Weather Forecasts Interim Reanalysis (ERA-interim);
    b. a dynamical vortex specification technique to estimate structure from CP and objective ROCI estimates; and
    c. Australian BT positions.

Values of R34 were calculated from a multiple regression with following 6 TC parameters:
- Latitude (Φ)
- RMW estimated by the vortex specification of ACCESS-TC following Chan and Williams (1987) vortex profile;
- ROCI and POCI estimated from ERA-interim reanalysis using the BT centre position;
- Translational speed calculated from the BT;
- 10m wind (v), spatially averaged between TC centre and ROCI in the reanalysis;
- Average 10m wind of quadrant (Vq), same as V but only averaged over the quadrant.

The regression model was fitted with NATL Extended Best Tracks and ERA-Interim Reanalysis dataset. There were 6368 6-hourly fixes from 333 TC events. The scatter plot is shown below. The MAE was 62 km. The model was tested against NE Pacific and NW Pacific cases where the MAE was 43 km and 62 km respectively (Fig. 14). The model was tested against the multiplatform TC surface wind analysis (MTCSWA) from CIRA including in the Southern Hemisphere where the MAE was 74 km.

Estimates for CP were also included based upon the CKZ WPR (Courtney and Knaff, 2009) which uses V_m (BT), POCI, R34, latitude and translation speed (see also Appendix 3.6 and Section 9.1).
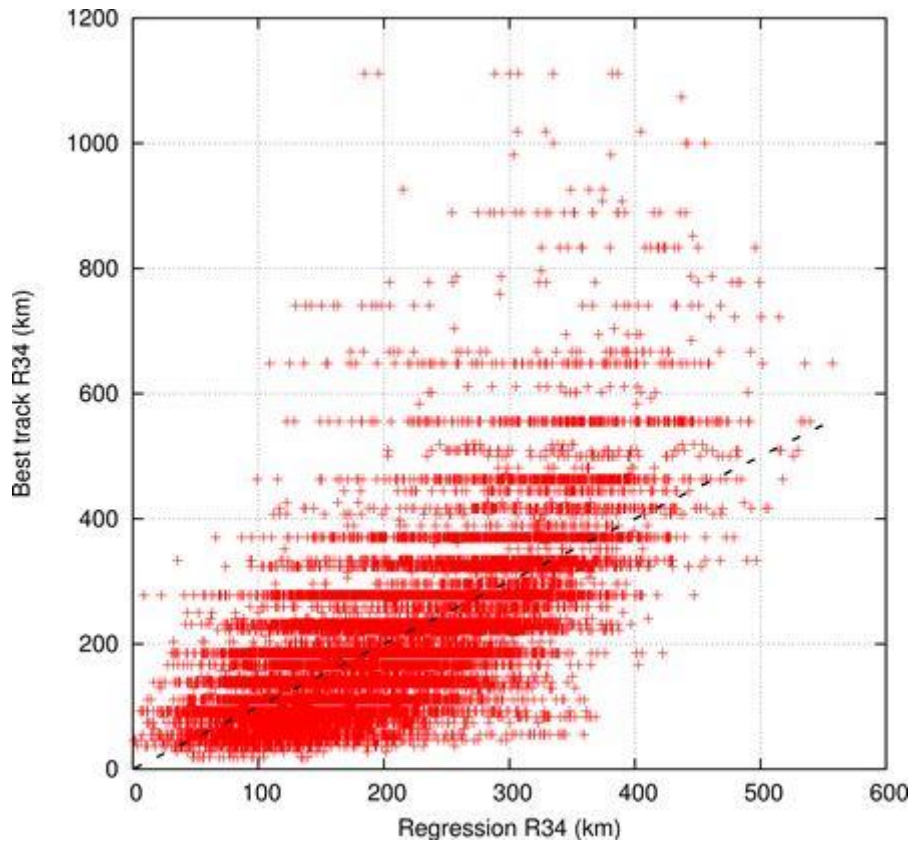
Figure 14. Comparison of Lok objective R34 (x-axis) and NATL best track estimates (Lok et al. 2013). The MAE is 62 km.

6.2 Results in the Australian region.

The Lok dataset was compared to the BT R34. Table 11 shows the bias, MAE, and RMSE. The bias and errors increase significantly in the pre-2003 era highlighting issues in the BT archive as discussed in Appendix 3.3. Over the reliable BT period of 2003–2012, Lok has lower R34 than BT by about 30-40 km on average (Mean Bias), and a MAE of 45-53 km.

The results improve if cases when the BT radii exceeds 300 km are excluded (Mean Bias: 23-35 km; MAE: 41-48 km). As discussed in the previous section, there are some large BT R34 values that occur when gales from the cyclonic flow merge with gales from the synoptic flow, typically strong monsoon flow to the north and/or enhanced trade winds to the south associated with a strong sub-tropical ridge. Lok R34 do not exceed 230 km and would appear to exclude the synoptic flow. Possibly this reflects a difference between the NATL and Australian regions. TCs in the NATL are not typically embedded in strong synoptic flow.

The bias is higher for western quadrants (30-35 km) than eastern quadrants (23 km). This may reflect the differences in wind radii characteristics of the NATL and Australian regions. The MAE (41-48 km) are lower than in the NATL (62 km) and NW Pacific (62 km) and similar to NE Pacific (43 km).

Table 12 shows the breakdown by region. Notably, the bias for northern quadrants is lower in the Western Region (18 km) than the Coral Sea (44 km). The bias is lowest for the Northern and Gulf Region, however the low number of cases and the smaller TC size may contribute to this.

The scatterplots for each quadrant in Fig. 15 show correlation coefficients varying from 0.23 (NW quadrant) to 0.32 (NE quadrant). For BT R34 less than about 75 km Lok has a high bias when compared to BT 2003-2012, but for BT R34 greater than or equal to 100 km, Lok demonstrates a low bias (28-40 km).

This is consistent with the lower spread of Lok R34 evident in the box and whisker quartile plots of Fig. 17a.

Table 11. Statistics for Lok R34 (BT-Lok).

BT-Lok R34; All BT radii.												
	All years				pre 2003				2003–2012			
	NE	SE	SW	NW	NE	SE	SW	NW	NE	SE	SW	NW
Mean Bias (km)	65.2	62.3	67.2	70.8	77.9	74.9	78.1	84.4	30.8	28.4	39.5	34.6
Median Bias (km)	47.0	45.0	50.0	54.0	59.0	55.0	60.0	65.0	25.0	21.0	33.0	31.0
RMSE (km)	112.3	109.3	111.6	114.5	124.7	121.8	124.2	128.2	68.2	64.2	69.6	65.8
MAE (km)	79.4	76.0	78.8	82.4	91.1	87.4	89.2	94.9	48.1	45.5	52.5	49.4
No. samples	3416	3442	3471	3420	2496	2509	2496	2485	920	933	975	935
BT-Lok R34; Excluding BT > 300 km												
	All years				pre 2003				2003–2012			
	NE	SE	SW	NW	NE	SE	SW	NW	NE	SE	SW	NW
Mean Bias (km)	41.4	39.1	44.9	48.3	49.0	45.8	49.2	56.1	23.2	23.1	35.2	29.8
Median Bias (km)	39.0	35.0	40.0	45.0	45.0	45.0	45.0	53.0	23.0	21.0	32.0	28.0
RMSE (km)	71.5	68.1	72.1	76.2	78.2	73.7	76.5	83.0	51.8	52.3	61.2	56.9
MAE (km)	57.1	54.2	57.6	61.1	63.9	59.9	61.7	68.0	41.1	40.7	48.4	45.0
No. samples	3029	3065	3096	3046	2143	2156	2144	2138	886	909	952	908

Table 12. Lok analysis of R34 by region, 2003–2012, excluding BT >300 km.

|	2003-2016 Excluding BT > 300 km											
	west of 125°E (Western Region)				Long. between 125 - 143°E (Northern and Gulf)				Longitudes east of 143°E (Coral Sea)			
	NE	SE	SW	NW	NE	SE	SW	NW	NE	SE	SW	NW
Mean Bias (km)	17.9	24.6	38.2	28.8	10.6	7.3	13.9	12.5	44.0	28.0	38.6	41.9
Median Bias (km)	18.0	23.0	37.0	28.0	8.0	6.0	10.0	15.0	37.0	20.0	28.0	41.5
RMSE (km)	47.7	54.7	63.0	57.5	39.7	38.8	41.6	41.6	66.2	52.2	65.4	62.7
MAE (km)	38.6	43.1	51.2	45.2	32.4	31.8	31.8	34.3	52.6	38.9	49.9	50.4
Standard Dev.	32.8	30.5	34.1	34.5	34.2	32.2	32.2	36.5	40.7	41.4	42.4	35.5
No. samples	549	582	620	572	123	117	121	120	214	210	211	216
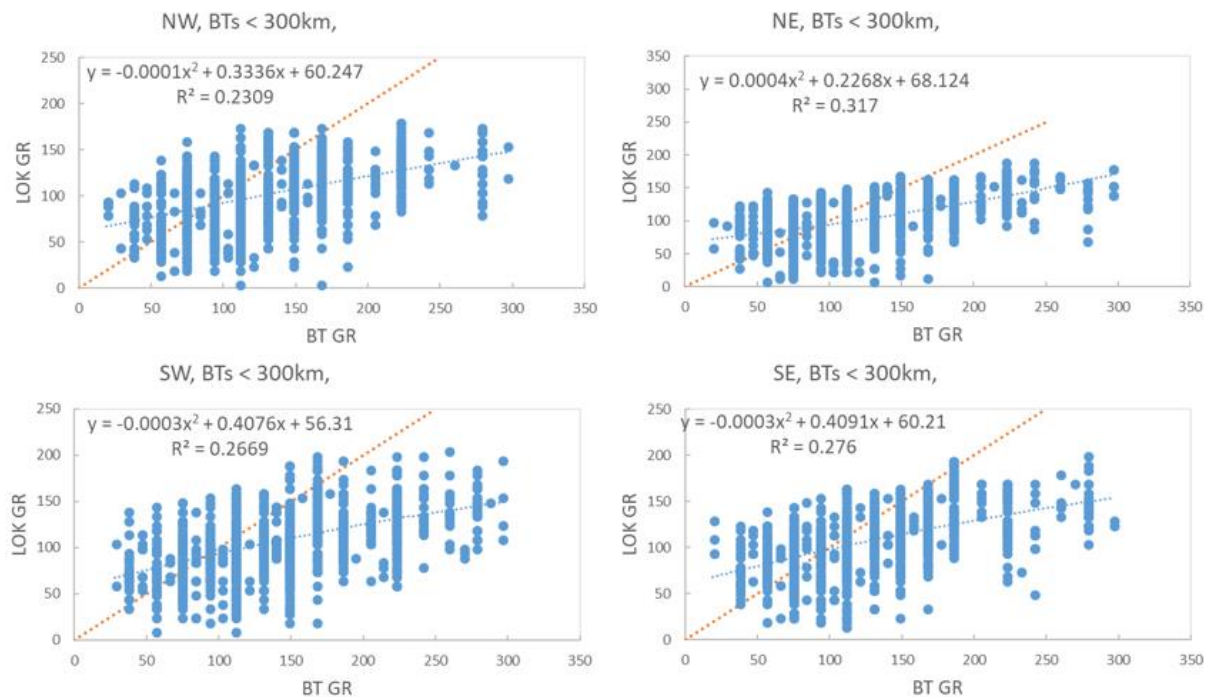
Figure 15. Scatter plot of R34 Lok Vs BT, 2003–2016 (excluding cases when BT R34 >300 km)

7. The 'Knaff' dataset

7.1 Background

A dataset of wind radii was compiled using the technique described in Knaff et al. (2016). This technique uses location, motion, intensity and TC size as predictors; where TC size is derived from a satellite (IR) method. It also assumes that TCs are largely symmetric, with asymmetries arising only from TC motion and location. Wind radii are based on a multiple regression of these factors using BT from the North Atlantic and Northeast Pacific from 1995 to 2012.

The RMW is determined from a North Atlantic climatological relationship using a combination of V_m and latitude.

7.2 Results in the Australian region

Wind radii (R34, R48, R64)

CIMSS ran the Knaff algorithm using the adjusted V_m (ADT) over the entire 1981–2016. Table 13 shows the statistics for R34 by quadrant. Unlike Lok and DAV the bias is negative (Knaff higher than BT) and is actually best when not restricting BT values to be less than 300 km. The bias ranges from -7 to -39 km for 2003–2016 increasing to -11 to -43 km when excluding BT >300 km cases. Some erroneously high values above 750 km during TC *Daryl* (1995) were removed. The MAE ranges from 53 to 69 km being lowest in northern quadrants.

The scatterplots in Fig. 16 show fairly low correlations (less than 0.2) with the BT. The box and whisker quartile plots in Fig. 17 show the Knaff R34 has higher values and the spread is slightly higher than BT R34, especially in the SE quadrant. It is notable that the actual values and the spread is higher than for DAV model or Lok.

RMW

There were only 249 values for RMW in the entire 1981–2016 record limiting its usefulness for this study. It is not known why so few records were generated, but these values corresponded to strong systems (average V_m =94kn). However, the average of this sample is 25 km; only slightly higher than the RMW Lok average of 23 km, and slightly lower than the RMW BT average of 28 km (82 cases) within this sample.

Table 13. Statistics for Knaff R34 validated against BT (2003–2016); (BT- Knaff).

	All BT values											
	All years				pre 2003				2003-2016			
	NE	SE	SW	NW	NE	SE	SW	NW	NE	SE	SW	NW
Mean Bias (km)	-1.6	-17.1	3.0	20.3	11.0	-4.7	14.7	35.1	-24.0	-39.4	-17.4	-5.8
Median Bias (km)	-9.5	-27.4	-7.4	9.1	-1.9	-16.7	-0.1	18.7	-27.5	-37.2	-18.2	-8.9
RMSE (km)	94.9	97.9	97.0	93.5	103.9	103.0	104.0	104.6	76.3	87.9	83.4	69.5
MAE (km)	69.3	74.0	70.3	65.2	75.5	77.0	74.1	72.6	58.2	68.5	63.7	52.0
Std Dev. (km)	69.4	71.9	67.5	59.3	71.8	72.7	67.2	60.4	65.0	70.4	67.9	57.3
No. samples	3655	3709	3607	3469	2338	2384	2297	2218	1320	1328	1313	1253
	Excluding BT > 300 km											
	All years				pre 2003				2003-2016			
	NE	SE	SW	NW	NE	SE	SW	NW	NE	SE	SW	NW
Mean Bias (km)	-19.4	-33.5	-13.8	3.7	-13.1	-27.7	-8.7	12.6	-29.7	-43.2	-22.1	-10.7
Median Bias (km)	-18.6	-31.9	-13.0	0.4	-11.4	-27.4	-9.4	8.9	-27.9	-45.9	-18.6	-9.3
RMSE (km)	78.3	85.8	79.6	71.2	82.7	86.5	80.6	72.9	70.6	84.6	78.1	68.3
MAE (km)	58.9	60.3	60.3	53.3	61.2	65.7	60.0	55.5	55.0	66.9	60.8	49.8
Std Dev. (km)	73.9	76.0	72.4	62.1	79.5	80.2	75.3	63.1	63.7	68.7	67.3	60.2
No. samples	3370	3441	3348	3211	2089	2140	2064	1987	1281	1301	1284	1224

NW, BTs < 300km 2004-16
$y = -0.0014x^2 + 0.749x + 72.967$
$R^2 = 0.096$

NE, BT < 300km, 2004-16
$y = -0.0002x^2 + 0.5387x + 93.961$
$R^2 = 0.1832$

SW, BT < 300km, 2004-16
$y = 0.0005x^2 + 0.1769x + 123.83$
$R^2 = 0.0762$

SE, BT < 300km, 2004-16
$y = 0.0004x^2 + 0.2944x + 128.72$
$R^2 = 0.1063$
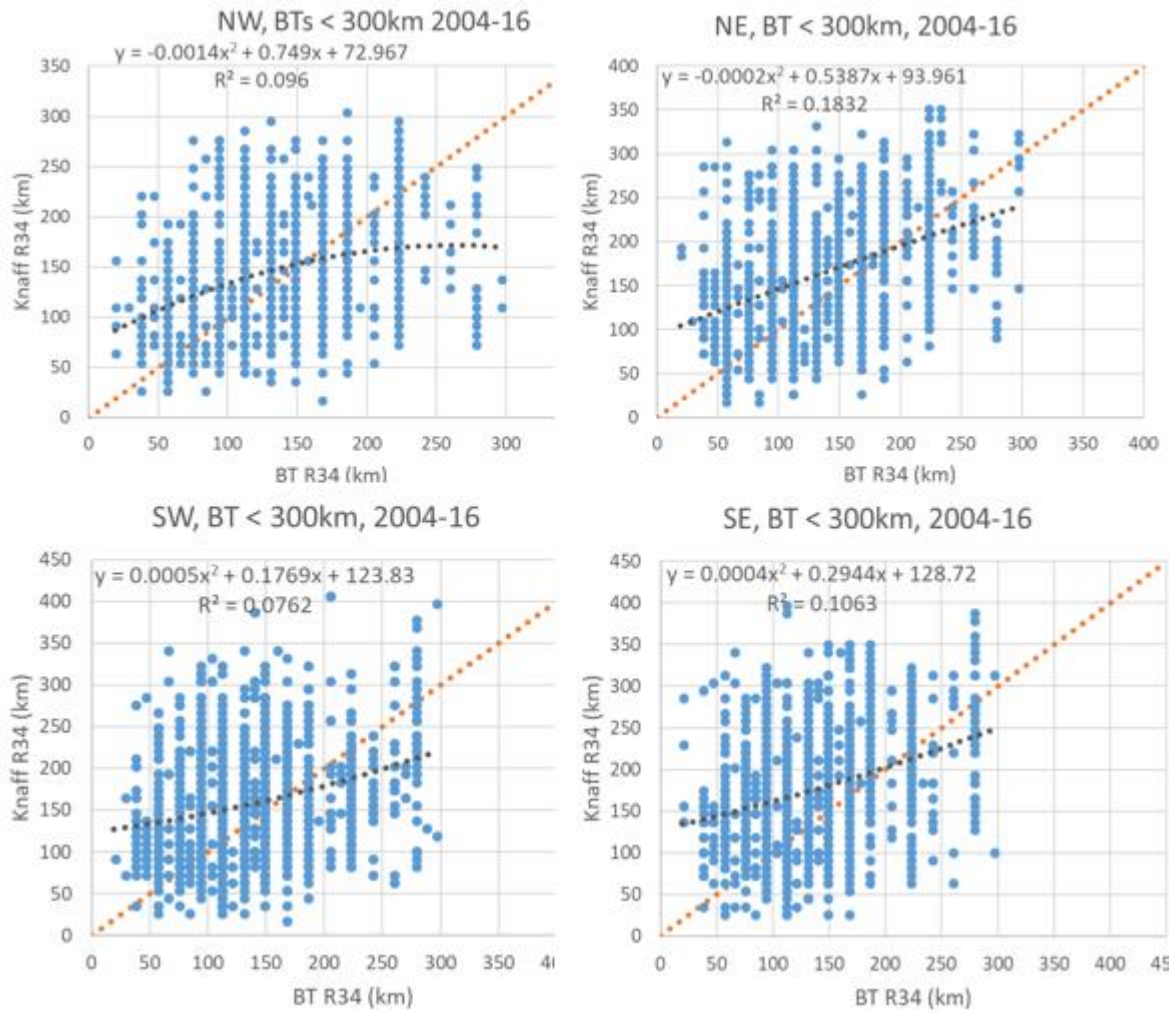
Figure 16. Scatter plot of R34 Knaff Vs BT, 2003–2016 (excluding cases when BT R34 >300 km) by quadrant.

8. Comparison DAV/Lok/Knaff/BT wind radii

The three objective techniques all display a low correlation when compared to the BT for the post 2003 period. As DAV was trained on this dataset there is a near zero bias, whereas Lok has a low bias (BT >Lok) while Knaff has a high bias. DAV and Lok have a low spread compared to the BT, but Knaff has a comparable spread (refer Fig. 17). As described in Appendix 3.3, the BT values prior to 2003 have some unrealistically very high values. This is thought to have arisen through the analyst's inclusion of gales that should properly be attributed to the impinging synoptic flow. This practice also extends to part of the post-2003 era and accounts for some of the high values in that period. The sample comparison for *Zelia* in Jan. 2011 in Table 14 shows a common situation where Lok is lower than BT, Knaff is higher and DAV is somewhat mixed.

Each dataset is incomplete for the period 1981–2016: Lok extends to 2012 only, while DAV and Knaff have missing values.

The low correlations using multiple independent wind radii datasets could suggest an issue with the quality of the BT. However, comparisons between Knaff, Lok and DAV in Table 15 demonstrate the independence of the three methods by the low correlations. The provision of multiple independent wind radii datasets creates an opportunity to derive improved wind radii estimates through a combination of the datasets.

A combination of the three data sources was considered to see if additional accuracy could be obtained through a consensus approach. Averaging the non-null values of Lok and Knaff, and then all three were investigated. While this improves the bias compared to Lok and Knaff, the correlation with the BT for the period 2003–2012 (Table 16) is degraded in two quadrants (and unchanged in the other two).

The Lok dataset appears the best of the three objective datasets though it still has relatively poor correlation (0.23-0.32), is under-spread and has a low bias (28-40 km). Consideration was given to methods of transforming the Lok data (assuming a Gaussian distribution) to better match the BT 2003–2016 distribution. The transformation followed the standard approach for normalising a Gaussian distribution (subtract the mean and divide by the standard deviation); after which the mean and standard deviation of the BT dataset were applied. Given that the BT distribution of R34 is clearly non-Gaussian, it is perhaps not surprising that the resulting distribution was clearly not a good match to the BT distribution ((not shown).

In further considering the problem of statistical transformation of the objective datasets it becomes apparent that the optimal transformation is likely to be application dependent. Even if the chosen transformation yields a distribution that is similar to BT in the bulk statistics, that does not guarantee that relationships found in the BT data between R34 and other parameters (e.g. V_m or latitude) will be reflected in the transformed objective dataset. Indeed, with such relatively low correlation between the datasets it is unlikely the objective datasets will reflect those relationships regardless of statistical transformation.

Disappointingly then, we arrive at the conclusion that none of the objective methods reviewed in this project has sufficient skill to extend the reliable record of R34.

Table 17 provides a summary of the strengths and weaknesses of each dataset with respect to R34.

Table 14. Example of *Zelia,* 00 UTC 16 Jan 2011. Knaff values are highest while Lok values are lowest.

Method	R34 NE (km)	R34 SE (km)	R34 SW (km)	R34 NW (km)
Best Track	**185**	**111**	**111**	**185**
DAV	142	137	126	137
Lok	145	80	70	125
Knaff	231	185	120	222
Combined(K/L/D)	173	134	106	162
Lok (normalised)	191	86	78	164

Table 15. Comparisons between Lok and Knaff, Lok and DAV (1981–2012) and Knaff and DAV (1981–2016) by quadrant. Correlations are low between the techniques.

	Knaff-DAV				DAV-Lok				Knaff-Lok			
	NE	SE	SW	NW	NE	SE	SW	NW	NE	SE	SW	NW
Bias (km)	32.0	37.8	12.3	8.5	20.4	26.2	37.0	26.6	51.2	60.8	46.7	37.2
Correlation	0.35	0.16	0.08	0.19	0.04	0.08	0.06	0.07	0.23	0.20	0.11	0.17
Count	4391	4456	4284	4191	4508	4574	4710	4649	3230	3291	3127	3063

Table 16. Combined Lok, Knaff, DAV R34 against BT by quadrant (2003–2012).

	R34 NE	R34 SE	R34 SW	R34 NW
Bias (km)	-1.1	6.4	-6.0	-7.8
Correlation	0.32	0.21	0.22	0.23
Count	695	717	721	671

Table 17. Summary of the strengths and weaknesses of the datasets for R34.

Dataset	Strengths	Weaknesses
BT	Data for July 2003 onwards considered to be the only dataset of sufficient accuracy and completeness.	Incomplete prior to early 2004. Some values too large (include synoptically-forced gales not directly associated with the TC circulation). Bias to use certain values: 60, 90, 120, 150 nm.
DAV	Satellite method trained on BT 2003-2016.	Very low correlation with BT 2003–2016. Under-spread. Missing images in 1980s affects output. Does not account for friction over land.
Lok	Model based algorithm Complete for the period 1979–2012. Consistent with the BT max winds. R34 by quadrants, (no axisymmetric value produced).	No data beyond 2012. Relatively poor correlation with BT 2003–2016 Under-spread Algorithm trained on NATL data. May struggle with weak systems as not well represented in ERA-interim dataset. No incorporation of satellite information. Not consistent with adjusted ADT V_m.
Knaff	Independent dataset matched to adjusted V_m. Has R34, 48, 64 by quadrant.	Poor correlation with BT 2003-2016 Trained on North Atlantic/NE Pac. High bias. Assumes asymmetry arises only from motion.

BT 2004–2016 is recommended as the only reliable and accurate dataset for R34 for the Australian region. However, some further quality control of high values in this dataset is needed, and until that is completed users of this data should consider excluding larger values (>300 km) evident in the BT.

**BT 2004-2016 is also recommended as the only suitable record of R48 and R64 in the Australian region.**
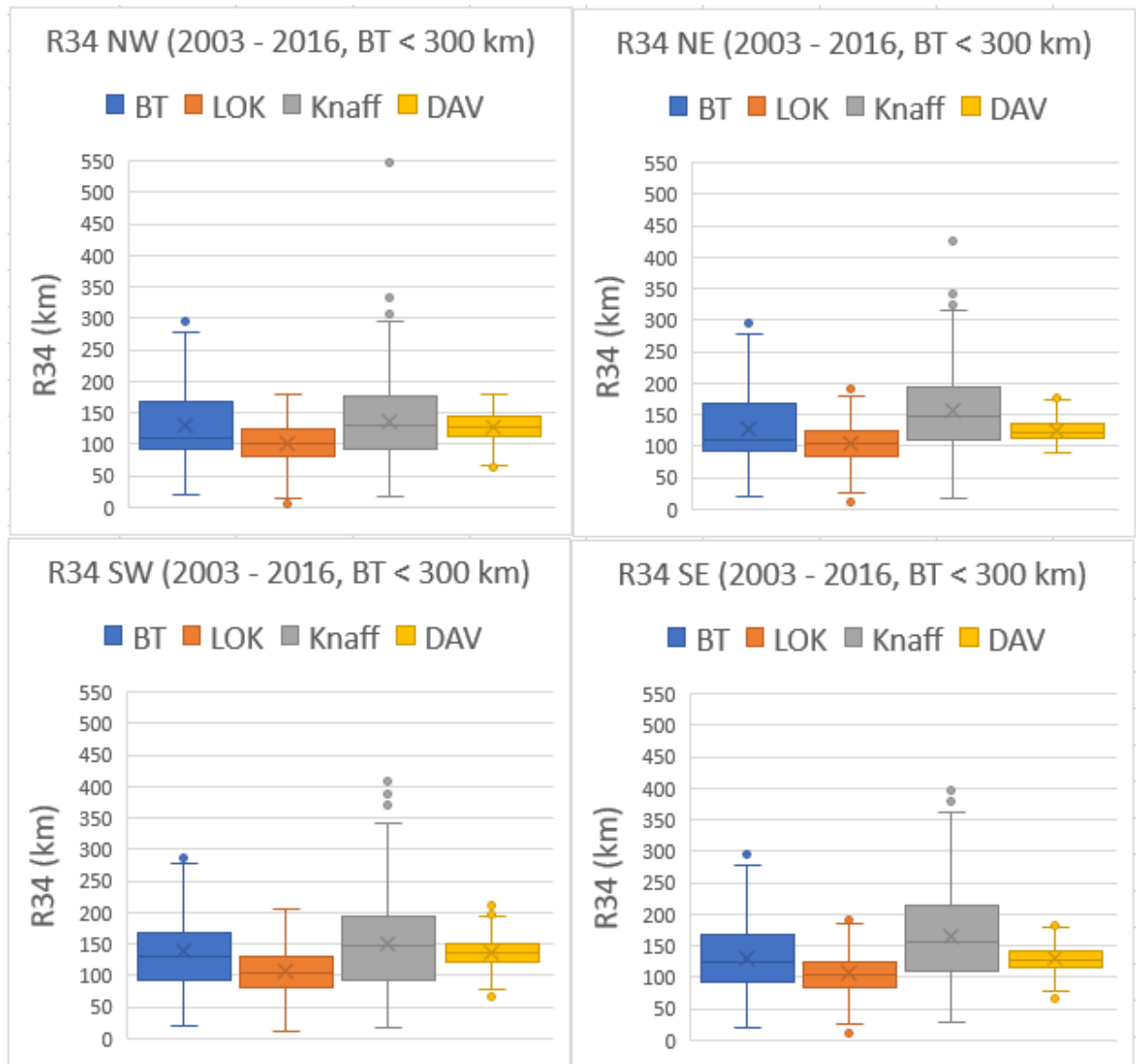
Figure 17 a. Frequency distribution ('box and whisker') plot of R34 by quadrant, BT, DAV, Lok, Knaff, 2003–2016 (excluding cases when BT R34 >300 km).
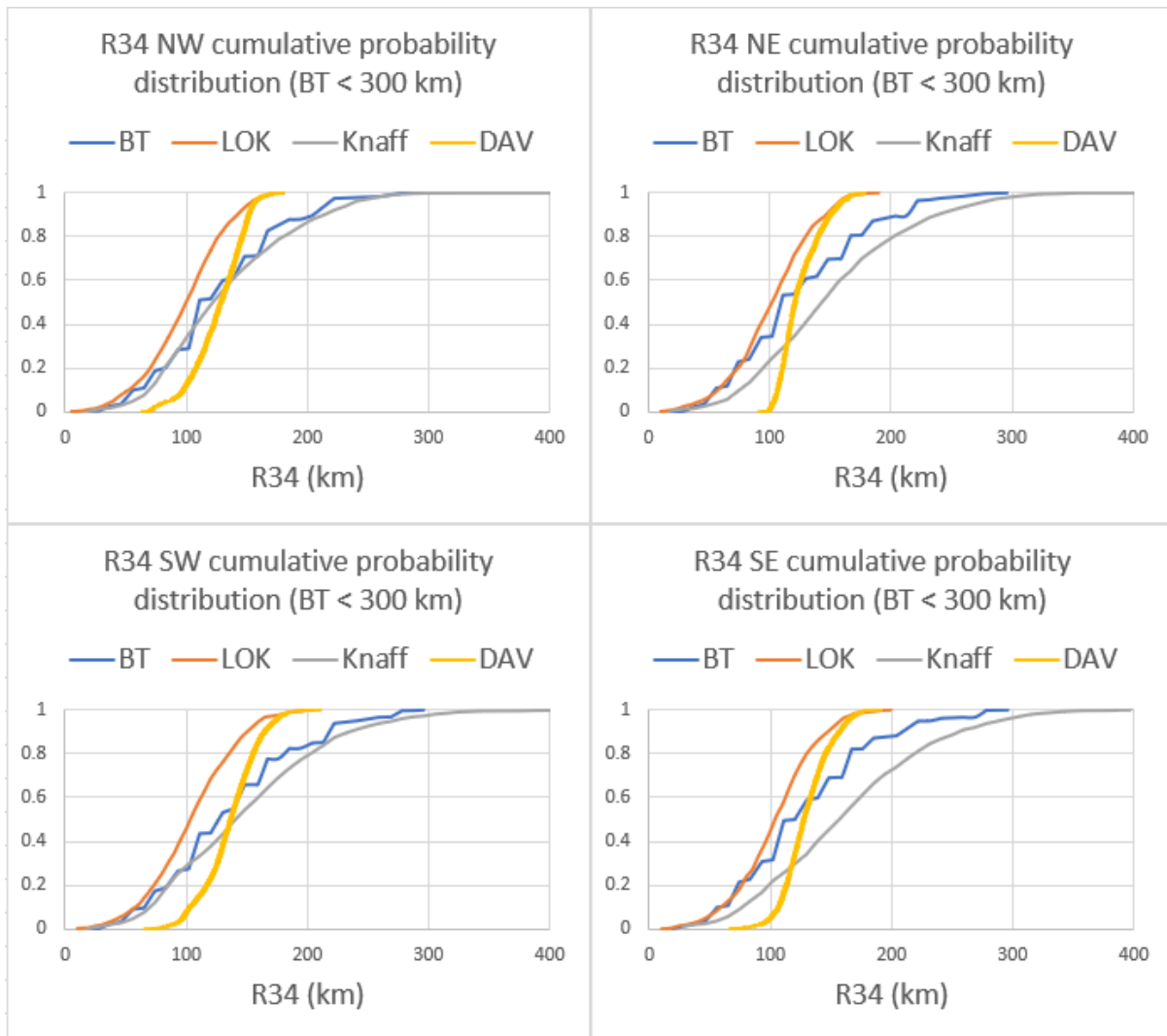
Figure 17 b. Cumulative probability distribution (CPD) for R34 by quadrant: BT, Lok, Knaff, DAV; 2004–2016 (excluding cases when BT R34 >300 km).

9. Other parameters

9.1 Central pressure

As discussed in Appendix 3.7, another metric for intensity of a TC is the CP. In the absence of direct measurement, which is rare, the estimation of CP is via a WPR. BT CP values are derived from a number of different WPRs resulting in an inhomogeneous record (Courtney and Knaff, 2009; Harper, 2002). The current operational WPR is the CKZ method (Knaff and Zehr 2007; Courtney and Knaff, 2009). This is an algorithm based upon the V_m, latitude, motion, R34 and the POCI or environmental pressure (Pe). Values for CP were calculated using the adjusted ADT V_m, and POCI (Lok) for 1981–2004 then P_e BT for 2004–2012 (see below for discussion of P_e and POCI).

As noted above, R34 is an input to the CKZ WPR; however, we have determined that none of the objective R34 methods has sufficient skill to be directly used in parametric modelling studies, (i.e. at least not without some carefully applied statistical transformation that will be application dependent). This presents an issue for extending the homogeneous record of CP. It is encouraging to note that the CKZ WPR has a reasonably low sensitivity to R34 for the variations in the dataset. The CP was calculated using each of the R34 methods, their combined average, and the R34 Lok normalised against the BT R34. Using the reference period 2007-12, the comparison between the BT and values using CKZ with inputs of Lok R34 (averaged over the four quadrants) and POCI, and BT V_m had a bias of 3.5 hPa (BT lower) and a correlation of 0.94, as shown in Fig. 18. The difference in using POCI instead of the BT P_e contributes 1.6 hPa to this bias, otherwise some of this difference is because of observations being an additional input to the BT CP. These results would indicate that the use of Lok R34 and POCI are appropriate to use as inputs to estimates of CP for the purposes of this study. The provided CP dataset uses the adjusted ADT V_m and only when the V_m exceeds 34 kn.

It is recommended that the BT CP be used if using the data for the period 2007–2016. If using the adjusted ADT V_m then the accompanying CP (CKZ using adj. ADT V_m, Lok R34 and Lok POCI) dataset could be used if required.
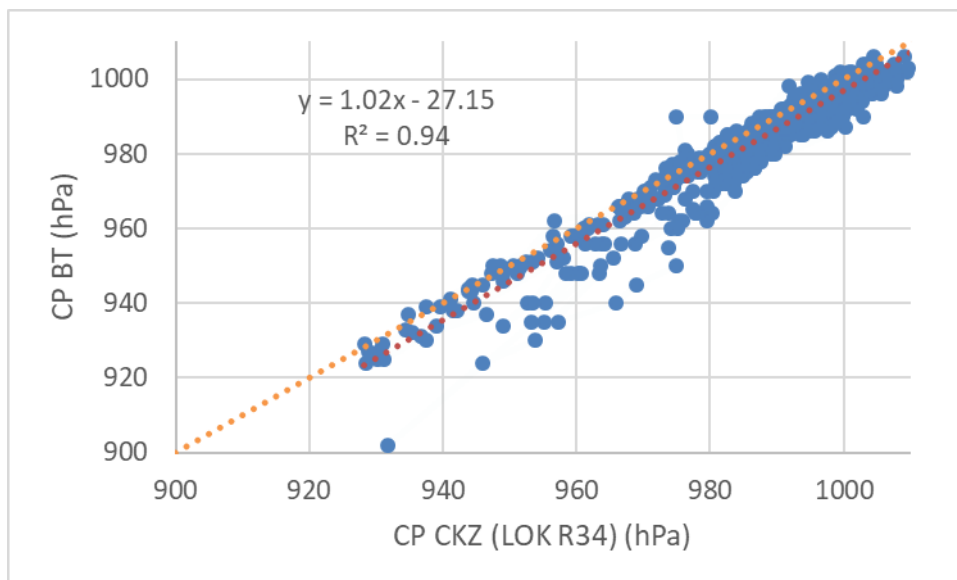
Figure 18. CP Scatterplot: BT against calculated CKZ with inputs of LOK (R34, POCI), BT V_m for 2007-12. The correlation is 0.94 and the bias was 3.5 hPa (BT lower).

9.2 Pressure of outermost closed isobar (POCI), environmental pressure Pe, and radius of outermost closed isobar (ROCI)

The Lok dataset has estimates of POCI and ROCI from 1979 to 2012 derived from the ERA-interim model. The process is described in Lok et al 2013, and has the following approach:

1. Compute all isobars on a polar grid of 0.5 km x 0.625 degree, from the best track centre to a radius of 1500 km. An isobar with a numerical value present in all radial legs is a closed isobar. An iterative approach, which removes radial legs larger than one standard deviation

from the mean radius of the innermost non-closed isobar, is applied until convergence when no closed isobar is found.

2. Take the geometrical centre of the innermost closed isobar as the TC centre. If the new centre is farther than 500 km from the BT position, the symmetric vortex centred at the new centre is removed and the estimation restarts.
3. Calculate the mean radial distances of each closed isobar from the new centre.
    ROCI is the outermost radial distance calculated.
4. The next inner closed isobar is selected if:

*   Geometrical centres of the innermost and outermost isobars are more than 97 km away
*   Ratio of the concave component of the outermost closed isobar to the convex component is larger than 0.4
*   Ratio of the asymmetric Fourier amplitude of the outermost closed isobar to the symmetric amplitude is larger than 0.5.

POCI and Pe

The BT contains values for P_e which equates to the estimated POCI + 2 hPa. The derivation of POCI and the BT P_e are discussed in Appendix 3.5. Values of P_e are in the BT on a consistent basis from about 2004. The subjective nature of the estimation of POCI for the BT is likely to result in variations although the record from about 2008 to about 2014 should be the most consistent data reflecting a systematic change to lower values as there was an operational decision to bias towards the outermost <u>circular</u> isobar. Otherwise there is nothing to indicate a systematic bias in the BT P_e estimates.

A comparison of POCI(Lok) against POCI (BT P_e - 2) in the overlap period (2004 to 2012) indicates a correlation coefficient of 0.61 and a bias of 3.0 hPa (POCI (Lok) higher than BT (P_e -2). Prior to 2004, when there were much fewer cases, the bias was 1.6 hPa with a correlation of 0.67. The change in bias possibly reflects a change in practice in the late 2000s in determining the BT to use the more circular outer closed isobar which would be a lower pressure than the value derived from the Lok method. The scatterplot for 2004-12 is shown in Fig. 19.

Although the BT P_e is derived from POCI by adding 2 hPa, given the small bias and the subjective variability in deriving BT P_e, it is reasonable to compare the Lok POCI with the BT P_e effectively reducing the bias to 1.0 hPa in the 2004-12 period. These values are an input to the calculation of CP as discussed in Section 9.1 above.
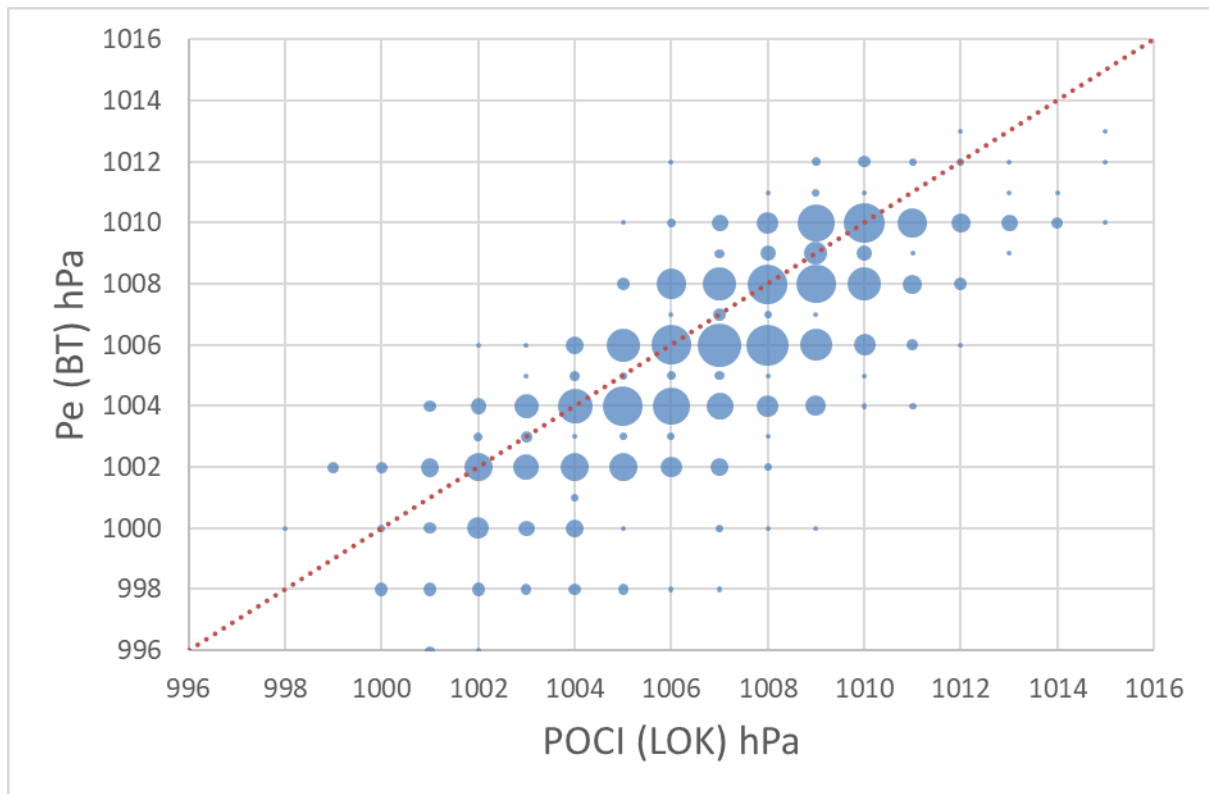
Figure 19. Scatterplot of P_e BT against POCI (Lok) for 2004-2012 period.

ROCI

The derivation of ROCI in the BT is discussed in Appendix 3.5. BT estimates of ROCI are available for earlier periods (early 1990s being the earliest) than for POCI, although not consistently across all basins. ROCI estimates from BT tend to be much higher than the model derived Lok values as illustrated in Fig. 20. For the period 2004-12, the bias is -162km (Lok lower than BT) and the correlation is just 0.19.
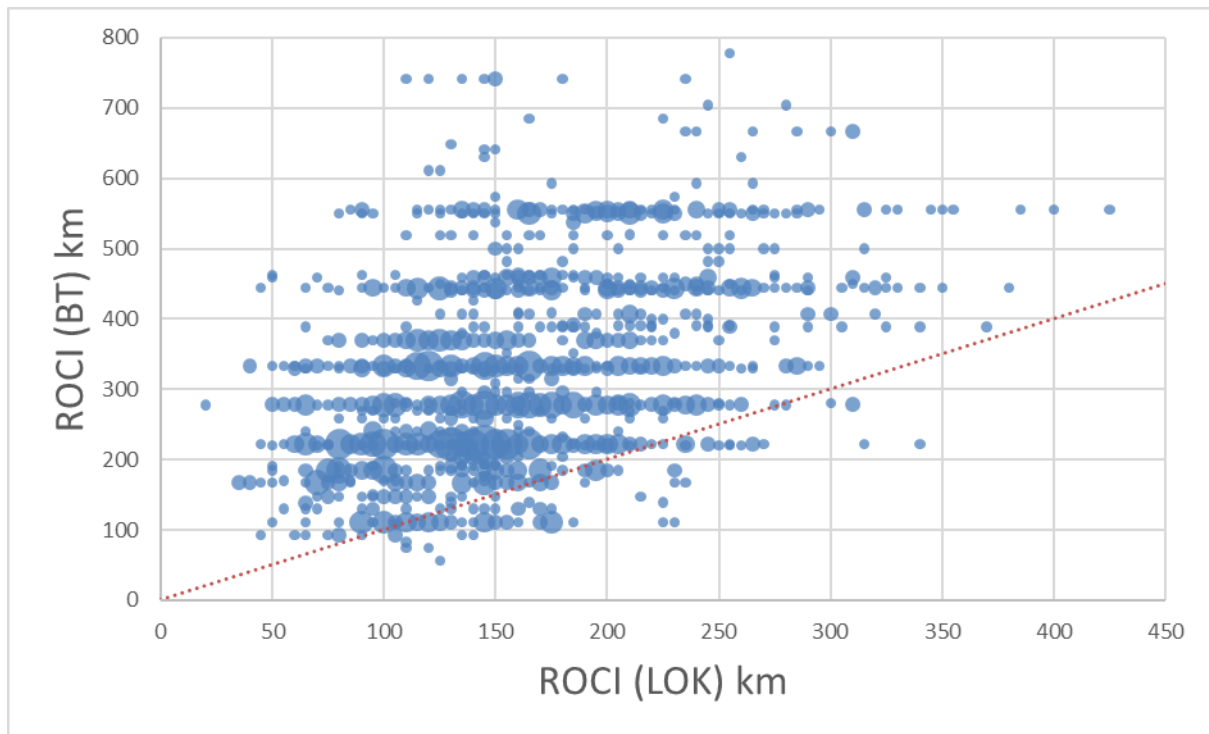
Figure 20. Scatterplot of ROCI from BT against ROCI from Lok for 2004–2012 period.

Fig. 21 a is a comparison of the manual MSLP analysis against the ERA analysis for TC *Vance* at 00UTC 21 March 1999. The BT P_e and ROCI were 1002 hPa and 700 km compared to the Lok values of 1004 hPa and 200 km; a difference of 500 km in the ROCI. The ERA analysis was collated independently of the Lok and although there is no scale available in the analysis, the 1004 hPa isobar in this figure is estimated to be approximately 500 km from the centre.

For TC *Olivia* on 10 April 1996 the BT ROCI was and 448 km compared to the Lok value of 270 km (POCI of 1005 hPa). The analyses in Fig. 21 b would suggest a much higher radius than the Lok 270 km estimate.
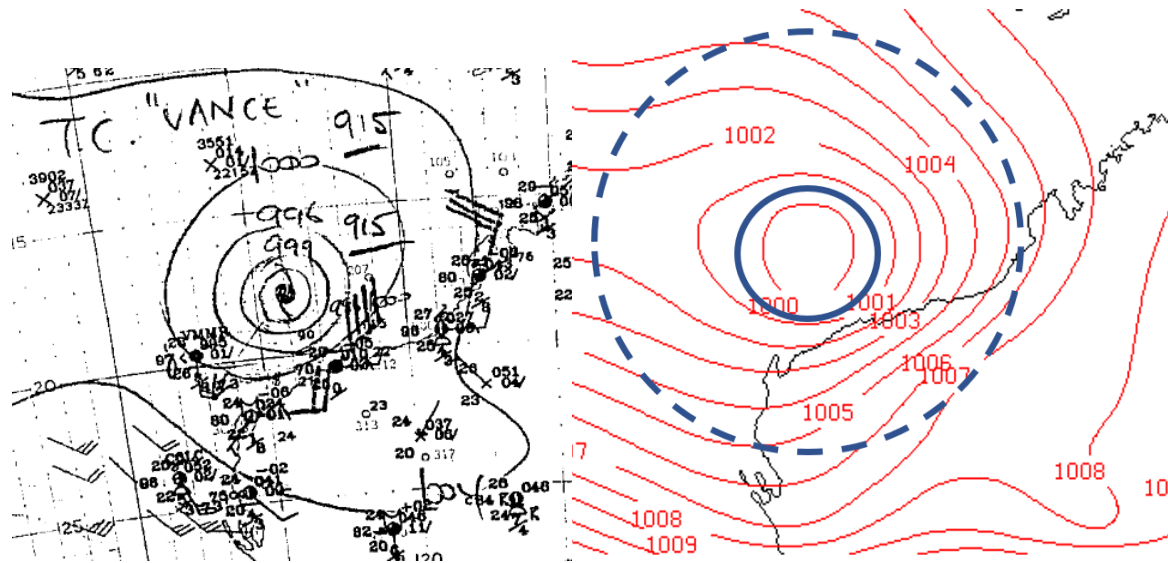
Figure 21 a. MSLP analysis for TC Vance 00UTC 21 March 1999 from a. BoM manual analysis and b. ERA model. The solid ring at 200 km is the ROCI (Lok) and the dashed ring at 700 km is the ROCI (BT).
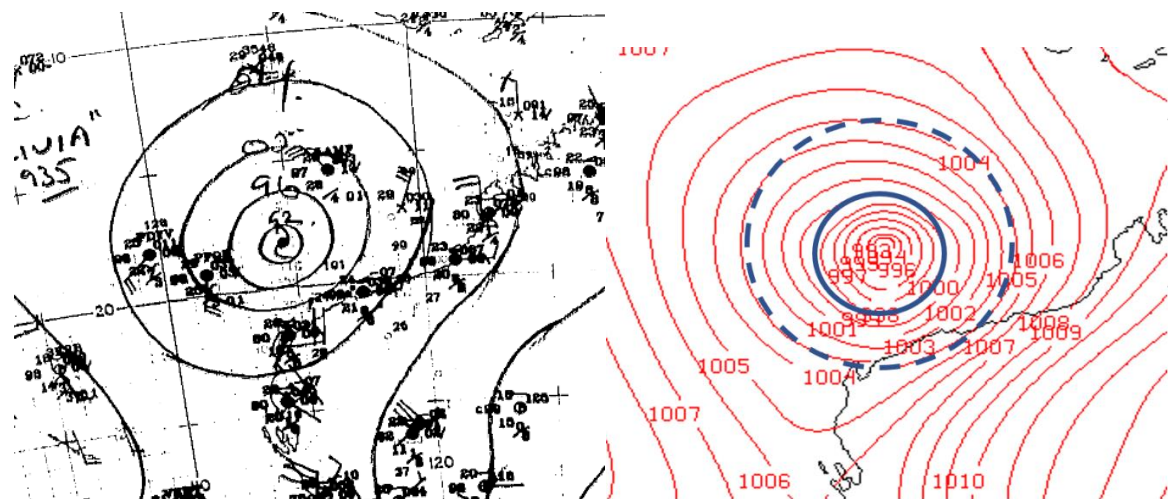
Figure 21 b. As in Fig. 21 a but for TC Olivia, 00 UTC 10 April 1996. The solid ring at 270 km is the ROCI (Lok) and the dashed ring at 448 km is the ROCI (BT).

That ROCI (Lok) has a low bias relative to ROCI (BT) contrasts with the finding that POCI (Lok) has a high bias relative to P_e (BT). The lack of correlation in ROCI is also somewhat surprising considering the POCI results. While it is tempting to dismiss ROCI (BT) given the subjective nature and use the objectively derived values, the few cases examined such as Vance and Olivia would indicate that the ROCI (Lok) are underestimates.

It is recommended that ROCI (Lok) are NOT used. Where possible R34 should be used as a size parameter in preference to ROCI. Where ROCI is required BT values should be used with caution.

9.3 Radius of Maximum Winds (RMW)

Values of RMW exist in the BT on a consistent basis since about 2004 as discussed in Appendix 3.4.

The RMW Lok data was estimated using the vortex specification of the model ACCESS-TC following the Chan and Williams (1987) vortex profile. Values are estimated to the nearest 5 km.

The RMW comparison between Lok and BT for the 2004-12 period is shown in Fig. 22 a. The BT is higher than Lok by 10.3 km on average (average RMW BT=36 km) and the correlation is only 0.19.

It should be noted that the classical parametric models of radial wind profiles in TCs; which depict an axisymmetric V_m near the centre of the circulation, are less representative of weak TCs that have more poorly organised wind circulations, often with maxima at large distances. For this reason, we compared Lok and BT for higher intensity TCs. For cases when V_m is at least 48 kn (595 cases) the bias decreases to 8.3 km (average RMW BT=32 km) and the correlation is 0.24 (Fig. 22 b). For cases when V_m is at least 64 kn (288 cases) the difference decreases further to 7.3 km (RMW BT=27 km) and the correlation increases to 0.37 (Fig. 22 c).

As mentioned in Appendix 3.4, RMW BT values are estimated to the nearest 5 nm (9 km) and are usually assigned to be one of 10, 15, 20, 25, or 30 nm. It is possible that the BT values have a high bias but there is insufficient information to be conclusive. There are cases with observational evidence of RMW less than 10 nm (e.g. *Heidi*, 2012 RMW=6 km) that without such evidence would have been given a higher RMW estimate. The independent RMW from the Knaff dataset lay between that of the BT and Lok for strong cases but as discussed in Section 7.2, there are only 249 values in the entire record.

For eyewall replacement cycle (ERC) cases that occur in strong TCs above 80 kn, the RMW abruptly increases. An inspection of a few cases (*Esau* 28/2/1992, *Drena* 5/01/1997 and *Thelma* 8/12/1998) generally suggests that RMW Lok aren't indicative of appropriate variations during an ERC. There are fluctuations between 25 and 50 km during *Esau* but for *Thelma* the RMW remains at 10 km throughout the ERC; which is unrealistic.

RMW values are relatively small compared with other size parameters. Hence there is potential for the errors in estimation to be a large as a proportion of the true value. This is one of the factors reducing confidence in RMW estimates. However, the RMW BT values 2004-2016 are still considered to be the best available estimates of RMW for this region and hence, it is recommended that the RMW BT is used from 2004 onwards. The comparison of BT RMW values against Lok RMW identified outliers in the BT record. These were investigated and as a result several (*Emma* (2006), *Ikola* (2015), *Uriah* (2016)) BT values have been adjusted downwards.

It is not recommended to use Lok RMW, either as a sole data source, or in combination with BT 2004-2016 without addressing the statistical differences between the two distributions including considering cross-correlations with other parameters.
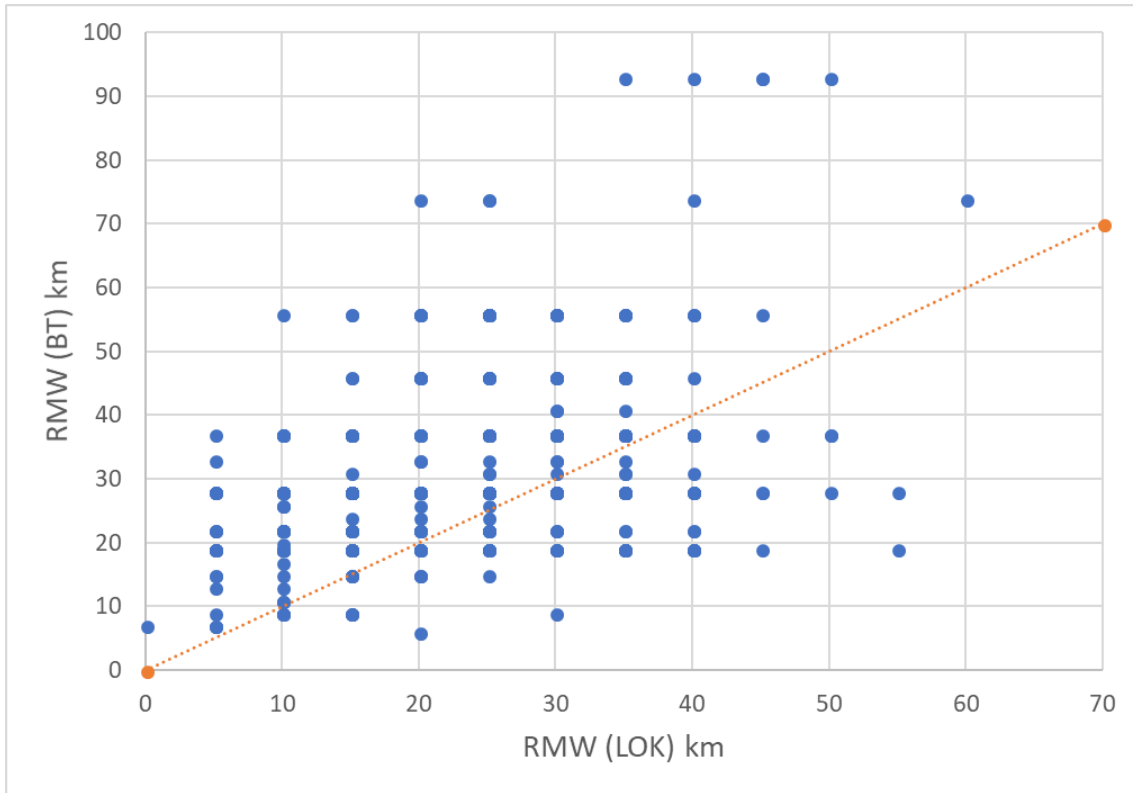
Figure 22 a. Scatterplot of RMW Lok against BT, 2004-2012.
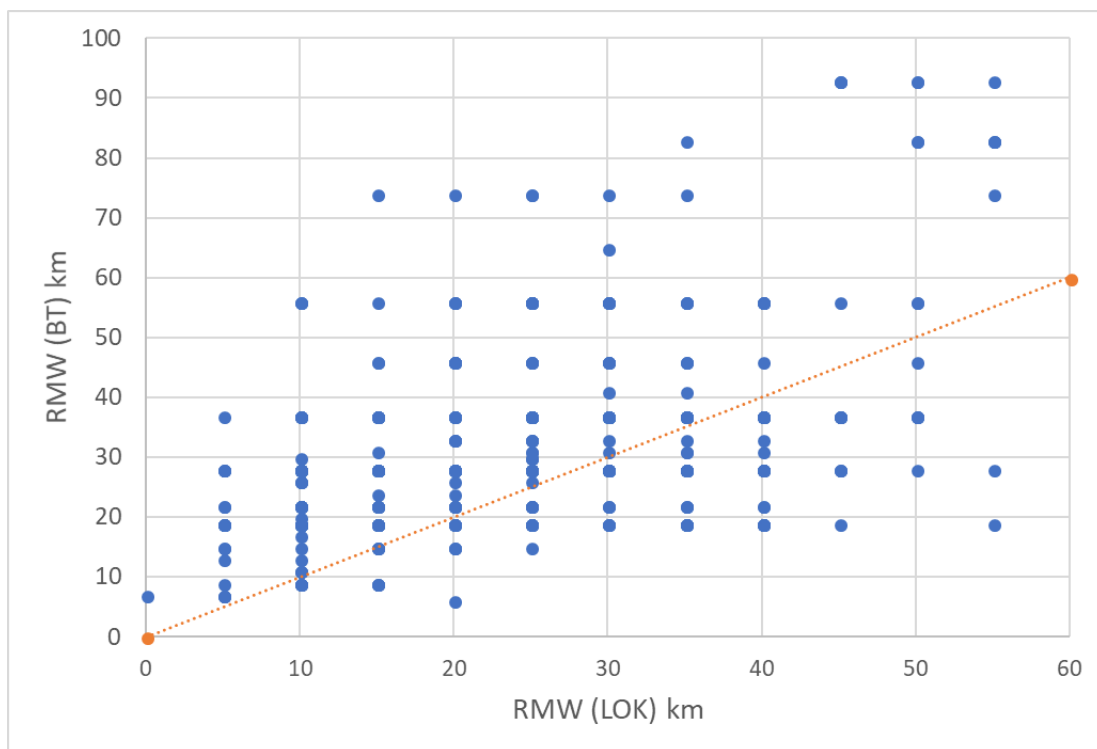
Figure 22 b. Scatterplot of RMW Lok against BT, 2004-2012 when V_m is 48kn or more.
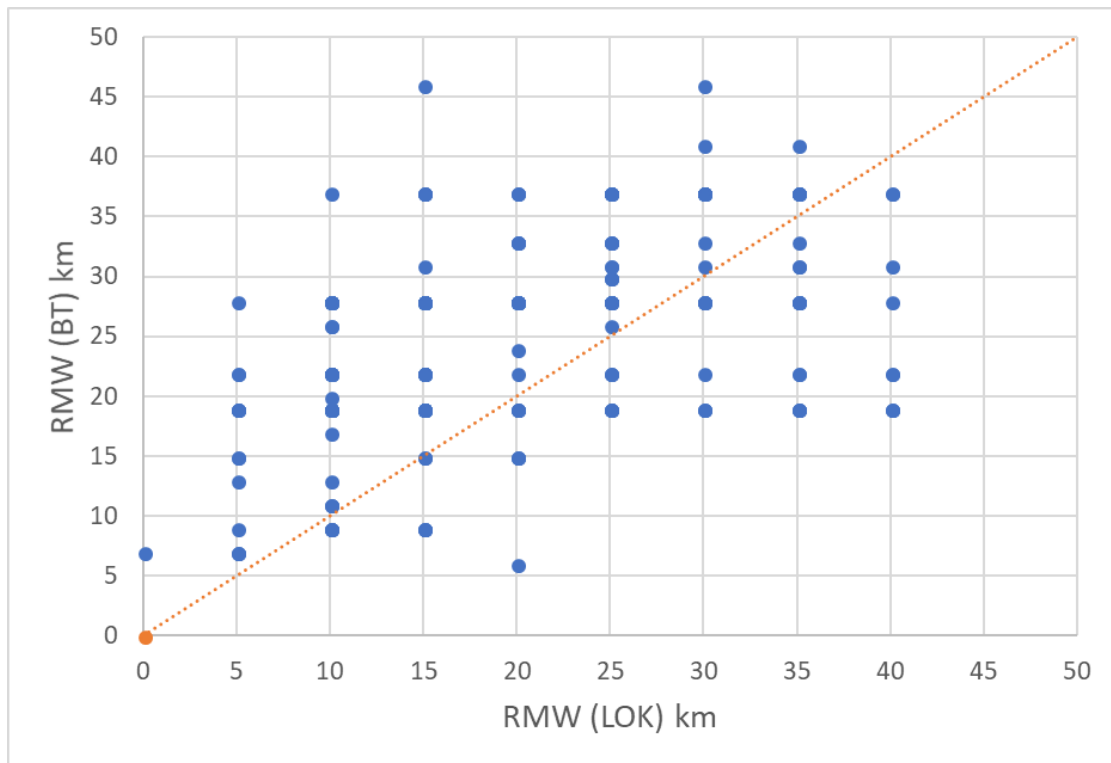
Figure 22 c. Scatterplot of RMW Lok against BT, 2004-2012 when V_m is 64kn or more.

9.4 Eye Radius

Appendix 3.6 describes details of the BT eye radius, available since December 1984. None of the objective techniques provide eye radius estimates, hence the BT is the only available dataset. As noted in Appendix 3.6, there are likely to be some variations historically due to the subjective approaches from one analyst to the next and from the different characteristics of available sources of guidance (radar, IR, Vis, and 37 or 85-92GHz PMW). It is interesting to note that the time series analysis in Fig. A3.8 b indicates little trend in the data over time.

Weak TCs do not have an eye. Given the close relationship between eye size and RMW for intense TCs, and the greater availability of RMW estimates, **it is recommended that RMW is used in preference to eye size whenever possible.**

Hence it is recommended to avoid using eye size if possible, but otherwise use BT values from 2004-2016 if required.

10.   Discussion

There were 375 TCs in the Australian region between 1981 and 2016. For each of these events objective algorithms derived values for V_m, R34, RMW and POCI. After close consideration of the factors affecting the TC record, it was decided that the BT from 2003–2016 provided a suitable benchmark to evaluate objective outputs. **Hence for any analysis for which 13 years of record presents a large enough sample size, it is recommended that BT 2003-2016 be used. The exception to this is CP, for which the highest quality BT period is limited to March 2007 onwards.**

For applications involving analysis of a particular tropical cyclone, the situation is more complex. In general, for any tropical system occurring after July 2003, the BT record represents the most accurate available record. For systems prior to July 2003 the BT record will often, but not always, still represent the best available record. Even where the BT record represents the most accurate record, it is recommended that application-dependent quality control is performed. Here "application-dependent" refers to the sensitivity of a specific type of diagnostic modelling, to errors in the various parameters. For example, some applications will require accurate R34, whereas others may be relatively insensitive to that parameter. Therefore, it is recommended that for critical applications pertaining to a specific tropical cyclone, the input data be quality controlled by an experienced tropical cyclone analyst whenever feasible.

A significant outcome from the project has been the creation of an improved satellite dataset that will support future work on objective estimation of TC parameters. The importance of correcting image navigation errors was identified during project planning, as objective algorithms can produce large errors when working on poorly navigated imagery. The aim of this initial part of the project was to provide a consistently formatted, long, high quality time series of infrared (1981–2015) and visible (1989–2015) imagery from geostationary satellites in the Australian region, having corrected these observations for navigational and, where practicable, calibration issues. However, from 1981 to 1988 (during the 3-hourly era), there was an average 20 per cent unavailability due to missing images and navigation errors that were unable to be corrected. This compromised the quality of the objective techniques for that period and has limited the success of the project in extending the length of reliable homogeneous records.

10.1 Intensity

The ADT algorithm was run in PMW and non-PMW modes and compared to the BT over the reference period 2004-2016. The ADT PMW data verified very well for the 2003–2016 period, but this dataset diminishes prior to then because of a decreasing availability and quality of microwave imagery, so can't provide a complete dataset from 1981.

The objective non-PMW ADT output had a number of weaknesses, requiring it to be adjusted to achieve a reduction in the bias with the BT 2003–2016 to near zero. These weaknesses included: inability to produce estimates for systems over land (8 per cent), missing values requiring interpolation or extrapolation (12 per cent) as well as a low bias under certain conditions (13 per cent). In total,32 per cent of fixes required systematic adjustment of the objective ADT output, or interpolation/extrapolation of V_m values.

The resulting dataset reduced the bias against the BT 2003–2016 period from 3.3 kn to 0.1 (MAE=5.3 kn). This encouraging result is taken to indicate that the systematic corrections (applied a priori based on documented weaknesses in non-PMW ADT) were appropriate in scope and magnitude. The bias for the 1981–2003 period was 3.2 kn. This is attributed to the BT being too high during the weakening phase for this period of record, and to the adjusted ADT dataset being too low especially for the lower quality satellite era from 1981–1988.

One of the objectives of this project was to create the longest possible homogeneous record of V_m suitable for infrastructure design studies. As previously noted, the BT records from 2004-2016 are considered to be the best available TC record for this region. For the period 1989–2003, the adjusted

ADT V_m provides a more homogeneous record than the BT; however for any individual TC it is likely that the BT will provide a more accurate record. **Users requiring a longer period of homogeneous record may find value in using the adjusted ADT V_m over the period 1989-2016, but this is likely to involve some loss of accuracy, particularly in the period 2003–2016**.

Future work on the BT may produce a more accurate V_m dataset for 1989-2016 by adjusting for issues identified in this study including:

- applying the 6-hour weakening rule prior to 2003,
- systematic application of early microwave data and
- reviewing cases where there were significant differences between the BT and ADT estimates.

While the homogeneity of such a dataset will be inferior to the adjusted-ADT V_m, the improved accuracy may be more highly valued.

10.2 Wind radii

As with other parameters, BT 2003–2016 is recommended as the most reliable and accurate dataset for R34, R48 and R64. The availability of scatterometer data over this period improves confidence in the estimated R34 and R48 values. Confidence in the BT values for this period is further improved by independent validation against scatterometer data (Chan and Chan 2015).

Disappointingly, we conclude that none of the objective algorithms considered in this study currently has sufficient skill to produce wind radii suitable to be used as an input to parametric wind modelling.

10.3 Other parameters

Central pressure: BT 2007–2016 provides the most reliable and homogeneous record of CP due to confidence in the input parameters for this period and the consistent application of the CKZ WPR. If using the adjusted ADT V_m over the extended period then the accompanying CP (CKZ using adj. ADT V_m, Lok R34 and Lok POCI) dataset could be used.

RMW: RMW values are relatively small compared with other size parameters. Hence there is potential for the errors in estimation to be a large as a proportion of the true value. This is one of the factors leading to relatively low confidence in RMW estimates. However, the RMW BT values 2004-2016 are still considered to be the best available estimates of RMW for this region.

If RMW values are required over a longer period it may be possible to derive estimates from the Lok dataset. However, it is not recommended to use Lok RMW, either as a sole data source, or in combination with BT 2004-2016 without addressing the statistical differences between the two distributions including considering cross-correlations with other parameters.

Features such as eyewall replacement cycles are not handled in any of the objective datasets and are not reliably handled in the BT.

Eye radius: None of the objective techniques provide eye radius estimates, hence the BT is the only available dataset. As noted in Appendix 3.6 there are likely to be some variations historically due to the subjective methods employed and the differences in available sources from radar, IR, Vis, and 37 or 85-92GHz PMW.

Some outliers occur at lower intensities so filtering for intensities of at least 65 kn would provide a more robust dataset. Given the close relationship between eye size and RMW and the greater availability of RMW (since weak TCs do not exhibit an eye), it is recommended that RMW is used in preference to eye radius in applications where that is possible.

POCI: Values from the Lok dataset are reasonably consistent with the BT P_e so can be used to fill the missing BT records prior to 2004.

11. Conclusions

The initial objectives of the Project were to produce a TC database for the Australian region (southern hemisphere between longitudes 90E and 160E) covering the period from 1981 onwards, that has the following attributes:

5. Provides a complete record of position, intensity and wind structure (eye size, radius to maximum winds, radius to gales, storm and hurricane force winds in quadrants);
6. Has improved homogeneity compared to the existing Australian Tropical Cyclone Database;
7. Is fit-for-purpose for use in the assessment of historical tropical cyclone risk in the Australian region; and
8. Demonstrates an objective tropical cyclone reanalysis methodology that can be applied globally.

The Project had partial success with achieving the first two objectives. A new record of TC intensity (V_m and CP) was created for the period post-January 1989. This new intensity dataset has improved homogeneity compared to the BT (Objective 2). However, the project was unable to provide a complete objective record for wind structure parameters for the same period (Objective 1). The project was also unable to produce a reliable TC database for periods before January 1989; due to a high proportion of missing or poorly navigated imagery in the early satellite record.

The resulting dataset is suitable for some risk analyses (Objective 3), but the absence of a reliable extended dataset for wind structure parameters will limit its application without the use of alternative sources of data for wind structure parameters.

The Project has successfully demonstrated a methodology that can be applied globally (Objective 4). The methodology used, and lessons learnt in the project will be shared with the global community via the publication of a scientific paper.

Two other significant benefits have arisen from the Project.

Firstly, the creation of a quality-controlled satellite image dataset will make it easier to engage in future work with objective algorithms in the Australian region.

Secondly, close examination of the BT record over the course of the Project has:
- facilitated a better understanding of the strengths and weaknesses of the BT record,
- documented (for the first time) periods of reliable record for specific parameters, and
- generated ideas for future work to improve the BT record.

It is hoped that the publication of the scientific paper will encourage others to engage in similar projects in other parts of the globe, thus advancing the science of objective TC analysis.

12.   Recommendations

Table 18 presents a summary of the recommendations for which data sources to use for each parameter according to the historical period. It is not recommended to combine different data sources without giving close consideration to whether the covariances/cross-correlations between parameters that are evident in the BT are preserved in the resulting dataset.

Table 18. Summary of recommendations.

Parameter	Period	Recommended source	Comments
All parameters except CP	Jul 2003 onwards	BT	Refer to report
V_m	Jul 2003 onwards	BT	
V_m	Jan 1989 – Dec 2016	Adjusted non-PMW ADT Vm	Provides a longer period of homogeneous record but with some loss of accuracy, particularly in the period 2003-2016.
CP	Mar 2007 onwards	BT	Consistent use of CKZ with reliable inputs
CP	Jan 1989-2016	Derived from CKZ using adjusted ADT Vm and Lok R34 and POCI	Consistent use of CKZ, but with less accurate inputs. Provides a longer homogeneous record but with some loss of accuracy, particularly in the period 2003-2016. Labelled in the dataset as CP(CKZ(LokR34, LokPOCI,adj.V_m), hPa)
R34, R48, R64	Jul 2003 onwards	BT	Sole reliable source. Further quality control advised to exclude R34 values over 300 km
RMW	Jul 2003 onwards	BT	RMW values are relatively small and hence errors in estimation have potential to be large as a proportion of the true value.
Eye size	Jul 2003 onwards	BT	Use RMW in preference to eye size whenever possible
P_e	Jul 2003 onwards	BT	
P_e	Jan 1989 – Jun 2003	Lok	Use Lok(POCI) as a proxy for Pe to extend the period of reliable record. Values across the datasets are reasonably consistent once the bias is adjusted (by using POCI for P_e).

Diagnostic modelling for specific systems

For applications involving analysis of a particular tropical cyclone, the situation is more complex. In general, for any tropical system occurring after July 2003, the BT record represents the most

accurate available record. For systems prior to July 2003 the BT record will often, but not always, still represent the best available record. Even where the BT record represents the most accurate record, it is recommended that application-dependent quality control is performed. Here "application-dependent" refers to the sensitivity of a specific type of diagnostic modelling, to errors in the various parameters. For example, some applications will require accurate R34, whereas others may be relatively insensitive to that parameter. Therefore, it is recommended that for critical applications pertaining to a specific tropical cyclone, the input data be quality controlled by an experienced tropical cyclone analyst whenever feasible.

11.1 Future work

This section outlines ideas for future work that may yield improved outcomes. While the results from the objective algorithms for size parameters were not as accurate as had been expected, this work has broken new ground in international efforts to improve the global tropical cyclone record. The lessons learnt from this project will be communicated to the scientific community through a scientific paper

Image navigation

As noted in Section 2, a significant effort was undertaken to quality control the satellite imagery, particularly for navigation errors. Renavigation was done algorithmically, and while it significantly improved the availability of high quality images, there was a proportion of images with gross errors that the algorithm was not able to correct. Older satellites generally produced a higher proportion of gross errors and together with a higher proportion of missing imagery this reduced the period of high quality record. A citizen-science approach could be used to improve the navigation of images where the algorithmic outputs failed quality checks. The citizen scientist would be represented with a satellite image with the map visible. The citizen scientist would be instructed to click on a notable coastline feature evident in the image, an on the corresponding point on the map of the coast. This would need to be repeated several times for each image, then a correction could be applied to the image navigation. The citizen science approach is recommended here due to the large number of candidate images.

The project team noted that objective reanalysis efforts previously reported in the scientific literature (in other tropical cyclone basins) do not appear to have performed quality control for image navigation, despite the sensitivity of many algorithms to centre location. The scientific paper that will be submitted to a peer-reviewed journal will recommend that future work with objective algorithms pay attention to quality control of image navigation.

Retuning algorithms

The Knaff objective algorithm for wind radii was tuned on North Atlantic data. Improved results may be obtained by retuning the algorithm for Australian conditions.

The project demonstrated the quality of the ADT intensity estimates when PMW data is available; and the importance of systematic adjustments to ADT estimates where PMW data is unavailable. Examination of the systematic corrections applied to counter the lack of PMW suggests that ADT is likely to produce better intensity estimates if it was refactored to run in a hindcast mode. In a

hindcast mode ADT could use knowledge of the future state of the system (for example the later emergence of an eye) to improve its estimates.

Using both satellite imagery and NWP as inputs

In the course of this project we examined three different objective algorithms for wind radii estimation. Two of these (DAV and Knaff) relied on satellite imagery. The other (Lok) relied upon numerical weather prediction (NWP) reanalysis data. It is likely that superior skill could be obtained with a technique that used both satellite imagery and NWP fields as inputs. It is recommended that any future work give close consideration be given to exploring this prospect. This recommendation will be included in the accompanying scientific paper with the hope of influencing future work in this field.

Expert analyst approach

This project has explored opportunities to use objective algorithms to extend the period of homogeneous record. While objective algorithms produce homogeneous outputs, this study has shown that this is sometimes at the expense of accuracy. Inhomogeneity arises in the BT record partly as a result of the range of analysts, each with their own bias, applying techniques that have changed over time. An alternative approach would be to use an expert tropical cyclone analyst to consistently analyse the entire period of record from 1989 onwards (or earlier if the completeness of the satellite record can be improved). By using a consistent methodology across the period of high quality satellite record the homogeneity should be improved. While a single analyst is likely to exhibit some bias, the bias should be small and will be consistent across the record. Furthermore, it should be possible to correct for the analyst's bias if and when the nature and magnitude of the bias is identified.

Acknowledgements

References

Australian Bureau of Meteorology (BOM). Previous Tropical Cyclones: The Australian Tropical Cyclone Database. Accessed 20 December 2017 at http://www.bom.gov.au/cyclone/history/

Bell, G.D., M.S. Halpert, R.C. Schnell, R.W. Higgins, J. Lawrimore, V.E. Kousky, R. Tinker, W. Thiaw, M. Chelliah, and A. Artusa, 2000: Climate Assessment for 1999. *Bull. Amer. Meteor. Soc.,* 81, S1–S50, https://doi.org/10.1175/1520-0477(2000)81[s1:CAF]2.0.CO;2

Chan, J. C. L., and R. T. Williams, 1987. Analytical and numerical studies of the beta effect in tropical cyclone motion. I: Zero mean flow. *J. Atmos. Sci.,* 44, 1257-1265.

Chan, K. T. and Chan, J. C. 2015. Global climatology of tropical cyclone size as inferred from QuikSCAT data. *Int. J. Climatol.*, 35: 4843-4848. 10.1002/joc.4307

Cooperative Institute for Meteorological Satellite Studies (CIMSS) tropical cyclone ADT web page: Accessed on April 28, 2018 http://tropic.ssec.wisc.edu/misc/adt/

Courtney, J., and J. A. Knaff, 2009: Adapting the Knaff and Zehr wind–pressure relationship for operational use in tropical cyclone warning centres. *Aust. Meteor. Oceanogr. J.*, 58, 167–179.

Demuth, J.L., M. DeMaria, and J.A. Knaff, 2006. Improvement of Advanced Microwave Sounding Unit Tropical Cyclone Intensity and Size Estimation Algorithms. *J. Appl. Meteor. Climatol.,* 45, 1573–1581, https://doi.org/10.1175/JAM2429.1

Dolling, K., E.A. Ritchie, and J.S. Tyo. 2016. The Use of the Deviation Angle Variance Technique on Geostationary Satellite Imagery to Estimate Tropical Cyclone Size Parameters. *Wea.Forecasting,* 31, 1625-1642.

Dvorak, V.F. 1984 Tropical cyclone intensity analysis using satellite data. NOAA Technical Report NESDIS 1984; 11, 1–47.

Dvorak, V.F. 1995. Tropical clouds and cloud systems observed in satellite imagery: Tropical cyclones. Workbook Vol. 2., 359 pp. [Available from NOAA/NESDIS, 5200 Auth Rd., Washington, DC, 20333.]

Harper, B. A., 2002: Tropical cyclone parameter estimation in the Australian region—Wind–pressure relationships and related issues for engineering planning and design—A discussion paper. Systems Engineering Australia Pty Ltd (SEA) for Woodside Energy Ltd, SEA Rep. J0106-PR003E, 83 pp. [Available from http://www.systemsengineeringaustralia.com.au/download/Wind-Pressure%20Discussion%20Paper%20Rev%20E.pdf. accessed 13 July 2018]

Harper, B. A., Stroud, S. A., McCormack, M., and West, S. 2008. A review of historical tropical cyclone intensity in northwestern Australia and implications for climate change trend analysis, *Aust. Met. Mag*, 57, 121–141.

Holland, G. 1981. On the quality of the Australian tropical cyclone database, *Aust. Met. Mag*, 29, 169–181.

Kimball, S.K. and M.S. Mulekar, 2004. A 15-Year Climatology of North Atlantic Tropical Cyclones. Part I: Size Parameters. J. Climate, 17, 3555–3575, https://doi.org/10.1175/1520-0442(2004)017<3555:AYCONA>2.0.CO;2

Knaff, J.A., C.J. Slocum, K.D. Musgrave, C.R. Sampson, and B.R. Strahl, 2016. Using Routinely Available Information to Estimate Tropical Cyclone Wind Structure. *Mon. Wea. Rev.,* 144, 1233–1247, https://doi.org/10.1175/MWR-D-15-0267.1

Knaff, J.A. and Zehr, R.M. 2007. Re-examination of tropical cyclone wind pressure relationships. *Weath. Forecasting*, 22, 71–88.

Knaff, J. A., S. P. Longmore, and D. A. Molenar, 2014. An objective satellite-based tropical cyclone size climatology*. J. Climate*, 27, 455–476, https://doi.org/10.1175/JCLI-D-13-00096.1.

Knapp, K.R., C.S. Velden, and A.J. Wimmers, 2018. A Global Climatology of Tropical Cyclone Eyes. *Mon. Wea. Rev*., 146, 2089–2101, https://doi.org/10.1175/MWR-D-17-0343.1

Kossin, J.P., T.L. Olander, and K.R. Knapp, 2013. Trend Analysis with a New Global Record of Tropical Cyclone Intensity*. J. Climate,* 26, 9960–9976, https://doi.org/10.1175/JCLI-D-13-00262.1

Landsea, C. W., B. A. Harper, K. Hoarau, and J. A. Knaff, 2006. Can we detect trends in extreme tropical cyclones? *Science*, 313, 452–454.

Lok C., Foley, G., Shaik, H.. Weber, H.C. 2013. Estimating Tropical Cyclone Structure from Global Reanalysis Data, AOGS conference, Brisbane. http://asiaoceania.org/aogs2013/

Lourensz, R. S. 1981. Tropical Cyclones in the Australian region: July 1909 to June 1980, Melbourne, 94 pp.

Olander, T.L. and Velden, C.S. 2007. The advanced Dvorak technique: continued development of an objective scheme to estimate tropical cyclone intensity using geostationary infrared satellite imagery. *Wea. Forecasting*, 2007; 22, 287–298.

Piñeros, M. F., E. A. Ritchie, and J. S. Tyo, 2008: Objective measures of tropical cyclone structure and intensity change from remotely-sensed infrared image data*. IEEE Trans. Geosci. Remote Sens.,* 46, 3574–3580.

Ritchie, E.A., Valliere-Kelley, G., Piñeros, M.F., and Tyo, J.S. 2012. Tropical cyclone intensity estimation in the North Atlantic basin using an improved deviation angle variance technique. *Wea. Forecasting*, 2012; 27, 1264–1277.

Takagi, M., 2003. Precise geometric correction for NOAA and GMS images considering elevation effects using GCP template matching and affine transform. In: Proceedings of SPIE, Vol. 5238, Conference on Remote Sensing, Image and Signal Processing for Remote Sensing IX, Barcelona, Spain, pp.132-141.

Taylor, P. K, Kent, E. C, Yelland, M. J and Moat, B. I. 1994. The Accuracy of Wind Observations from Ships. Proceedings of the International COADS Wind Workshop. 31 May-2 June 1994, Kiel, Germany. pp.132–155. Kiel: Institut. fur Meereskunde/ChristianAlbrechts-Universitat.

Trewin, B. 2008. An enhanced tropical cyclone data set for the Australian region. *20th Conf. Clim. Var. Chang*., available at: https://ams.confex.com/ams/88Annual/techprogram/paper_128054.htm (last access: 31 July 2018).

Velden, C.S., Olander, T.L., and Zehr, R.M. 1988. Development of an objective scheme to estimate tropical cyclone intensity from digital geostationary satellite infrared imagery. *Wea. Forecasting*, 13, 172–186.

Velden, C., B. Harper, F. Wells, J.L. Beven, R. Zehr, T. Olander, M. Mayfield, C.". Guard, M. Lander, R. Edson, L. Avila, A. Burton, M. Turk, A. Kikuchi, A. Christian, P. Caroff, and P. McCrone, 2006. The Dvorak Tropical Cyclone Intensity Estimation Technique: A Satellite-Based Method that Has Endured for over 30 Years. *Bull. Amer. Meteor. Soc*., 87, 1195–1210, https://doi.org/10.1175/BAMS-87-9-1195

Velden, C., T. Olander, D. Herndon, and J.P. Kossin, 2017. Reprocessing the Most Intense Historical Tropical Cyclones in the Satellite Era Using the Advanced Dvorak Technique. *Mon. Wea. Rev*., 145, 971–983, https://doi.org/10.1175/MWR-D-16-0312.1

Appendix 1. Description of the data files.

1.1 Australian Tropical Cyclone Best Track (BT) dataset.

The latest BT dataset is available online at: http://www.bom.gov.au/cyclone/history/

BT data supplied in these data files are from the version downloaded 20 December 2017.

A description of the file is available here:

http://www.bom.gov.au/cyclone/history/database/TC_Database_Structure_Oct2011.pdf

File provided

BT_adjusted_180831.csv

Contains BT with additional columns inserted after latitude and longitude columns: the adjusted ADT Vm in kn; CP (hPa) that uses CKZ with inputs adj. ADT Vm, Lok R34; and Lok POCI for P_e (hPa). Other units of columns conform to SI standards outlined in pdf above. This file was extracted 20 December 2017 and has been edited to contain only the TCs relevant for this study.

```
NAME,DISTURBANCE_ID,TM,TYPE,DATA_SRC,SURFACE_CODE,CYC_TYPE,LAT,LON,
POSITION_METHOD, POSITION_UNCERTAINTY,Adj Vm (kn),CP(CKZ(LokR34,
LokPOCI,adj.Vm),hPa),POCI (Lok, hPa),DVORAK_DATA_T_NO,
DVORAK_MODEL_T_NO, DVORAK_PATTERN_T_NO, DVORAK_FINAL_T_NO,
DVORAK_CI_NO,CENTRAL_PRES,CENTRAL_PRES_UNCERTAINTY,CENTRAL_PRES_METH
OD,PRES_WIND_RELATION_USED,ENV_PRES,ENV_PRES_UNCERTAINTY,MN_RADIUS_O
UTER_ISOBAR,MN_RADIUS_GF_WIND,MN_RADIUS_GF_SECNE,MN_RADIUS_GF_SECSE,
MN_RADIUS_GF_SECSW,MN_RADIUS_GF_SECNW,MN_RADIUS_SF_WIND,MN_RADIUS_SF
_SECNE,MN_RADIUS_SF_SECSE,MN_RADIUS_SF_SECSW,MN_RADIUS_SF_SECNW,MN_R
ADIUS_HF_WIND,MN_RADIUS_HF_SECNE,MN_RADIUS_HF_SECSE,MN_RADIUS_HF_SEC
SW,MN_RADIUS_HF_SECNW,MN_RADIUS_MAX_WIND,MN_RADIUS_MAX_WIND_METHOD,M
N_RADIUS_GF_WIND_METHOD,MN_RADIUS_SF_WIND_METHOD,MN_RADIUS_HF_WIND_M
ETHOD,MAX_WIND_SPD,MAX_WIND_SPD_UNCERTAINTY,MAX_WIND_SPD_METHOD,MAX_
WIND_GUST_PER,MAX_WIND_GUST,Gust
(kn),MAX_WIND_GUST_METHOD,MN_EYE_RAD,MN_EYE_RAD_UNCERTAINTY,MN_EYE_R
AD_METHOD,MAX_REP_WIND_SPD,MAX_REP_WIND_DIR,MAX_REP_WIND_METHOD,MAX_
REP_WIND_LON,MAX_REP_WIND_LAT,MAX_REP_WAV_HT,MAX_REP_WAV_METHOD,MAX_
REP_WAV_LON,MAX_REP_WAV_LAT,MAX_REP_SWL_HT,MAX_REP_SWL_DIR,MAX_REP_S
WL_PER,MAX_REP_SWL_METHOD,MAX_REP_SWL_LON,MAX_REP_SWL_LAT,MAX_REP_TI
DE_ANOM,MAX_REP_TIDE_ANOM_UNCERTAINTY,MAX_REP_TIDE_ANOM_METHOD,MAX_R
EP_TIDE_ANOM_LON,MAX_REP_TIDE_ANOM_LAT,
```

1.2 DAV data.

DAVwindradiidata_180531.csv

Date/time in dd/mm/yyyy hh:mm format in UTC.

Times in standard six hourly time-steps: 00, 06, 12, 18.

All wind radii in km.

```
ID,Date time,R34 NE,R34 SE,R34 SW,R34 NW,R48 NE,R48 SE,R48 SW,R48
NW,R64 NE,R64 SE,R64 SW,R64 NW
```

1.3 Knaff data

Knaffwindradiidata_180531.csv

Date/time in dd/mm/yyyy hh:mm format in UTC.

Times not at standard hours.

All wind radii in nm.

```
ID,Date Time (UTC),Spd (kn),Dir deg,Vm (kn),RMW nm,R34 NE (nm),R34
SE (nm),RR34 SW (nm),R34 NW (nm),R48 NE (nm),R48 SE (nm),R48 SW
(nm),R48 NW (nm),R64 NE (nm),R64 SE (nm),R64 SW (nm),R64 NW
(nm),Lat,Lon
```

1.4 Lok data

Lokwindradiidata_180531.csv

Date/time in dd/mm/yyyy hh:mm format in UTC.

Times in standard six hourly time-steps: 00, 06, 12, 18.

All wind radii in km.

```
ID,Date Time (UTC),Name,Lat,Long,Cp (hPa),Vm (kn),Rm (km),POCI
(hPa),ROCI (km),R34 NE (km),R34 SE (km),R34 SW (km),RS34 NW (km)
```

1.5 ADT non-PMW 1981-2003

ADT_nonPMW_1981-2003_180531.csv

Date/ time in UTC. Times not at standard hours.

Wind speeds in knots.

Title and sample row displayed below.

```
ID,Date,Time (UTC),CI,MSLP,Vm (kn),FT,Adj Raw,Ini Raw,Constraint
Limit,Wkng Flag,Rpd Wkng,Cntr Region,Mean Cloud,Scene Type,est RMW
(km),MW Score,Lat,Lon,FixMethod,Sat,VZA,Comments
198081_10,1981MAR01,332,6.0,960,101,6.0,6.0,6.0,NO LIMIT,OFF,OFF,-
45.03,-64.86,UNIFR,N/A,N/A,-17.11,-104.88,COMBO,GMS5,0,
```

1.6 ADT non-PMW 2004-2016 (note starts June 2003)

ADT_nonPMW_2004-2016_180531.csv

Date yyyyMONdd.

Time in UTC Times not at standard hours.

Wind speeds in knots.

Title and sample row displayed below.

```
ID,Date,Time (UTC),CI,MSLP,Vm (kn),FT,Adj Raw,Ini Raw,Constraint
Limit,Wkng Flag,Rpd Wkng,Cntr Region,Mean Cloud,Scene Type,est
RMW (km),MW Score,Lat,Lon,FixMethod,Sat,VZA,Comments
200203_09,2003JUN05,25,2.4,1006,30,2.4,2.4,2.4,NO
LIMIT,OFF,OFF,22.04,21.36,SHEAR,N/A,N/A,-7.37,-
154.02,BEST,GOES9,0,
```

1.7 ADT PMW 1981-2003

ADT_PMW_1981-2003_180531.csv

Date/ time in UTC. Times not at standard hours.

Wind speeds in knots.

Title and sample row displayed below.

```
ID,Date,Time (UTC),CI,MSLP,Vm (kn),FT,Adj Raw,Ini Raw,Constraint
Limit,Wkng Flag,Rpd Wkng,Cntr Region,Mean Cloud,Scene Type,est
RMW (km),MW Score,Lat,Lon,FixMethod,Sat,Sat,VZA,Comments
198081_10,1981MAR01,332,,948.3,101,6,6,6,NO LIMIT,OFF,OFF,-
45.03,-64.86,UNIFR,N/A,N/A,-17.11,-104.88,COMBO,GMS5,GMS5,0,
```

1.8 ADT PMW 2004-2016 (note starts June 2003)
ADT_PMW_2004-2016_180531.csv
Date/ time in UTC.
Times not at standard hours.

Wind speeds in knots.

Title and sample row displayed below.

```
ID,Date,Time (UTC),CI,MSLP,Vm (kn),FT,Adj Raw,Ini Raw,Constraint
Limit,Wkng Flag,Rpd Wkng,Cntr Region,Mean Cloud,Scene Type,est RMW
(km),MW Score,Lat,Lon,FixMethod,Sat,VZA,Comments
200304_01,2003DEC06,1800,2.4,1008,30,2.4,2.4,2.4,NO LIMIT,OFF,OFF,-
45.66,-71.62,UNIFR,N/A,N/A,-7.5,-95.2,BEST,MET5,0,
```

1.9 Master sheet
OTCR_alldata_180831.csv
This file has data from the above files on the one sheet except that only rows that match the BT fix times are included. The matching process takes the nearest fix within 2 hours of the BT fix. The derived fields pertinent to this study are in the columns after the BT position fields: the adjusted ADT V_m in kn; CP (hPa) that uses CKZ with inputs adj. ADT V_m, Lok R34; and Lok POCI for P_e (hPa). These CP fields are only included when the adjusted V_m exceeds 34 kn. A value of adjusted V_m is not included with every fix.

Times are in UTC but are not necessarily at a standard hour. For most of the overall period the standard hours adhere to 00, 06, 12, 18 UTC. There are periods when the standard at the time was 01, 07, 13, 19 or 23, 05, 11, 17 UTC. Intermediate fixes are included for some other significant times, for example, at landfall.

The file has columns in the following order (Refer to 1.1 to 1.8 for formats):
BT_adjusted; ADT non-PMW 1981; ADT PMW 1981; ADT PMW 2004; ADT non-PMW 2004; Lok; KNAFF; DAV.
The dataset is referenced in the ID column e.g. ID (Lok).

Appendix 2. Details of satellite availability and correction process

Fifteen meteorological geostationary missions were positioned over the target region in the period 1977-2015 as detailed in Table A2.1. Of these, seven were operated on behalf of JMA[1] (GMS-1 to -5, MTSAT-1R and MTSAT-2). Seven were operated on behalf of CMA[2] (FY-2A to -2G) however imagers are known to have significant calibration issues so have been excluded from this analysis. One mission, GOES-9, was operated by NOAA.

The JMA missions provide a near-continuous record from 1977-2015, with each mission having a sub-satellite point located between 140 and 145 E. In 1999, the rocket carrying MTSAT-1, the successor to GMS-5, failed on launch resulting in the loss of the mission. In 2002, GMS-5 experienced an anomaly resulting in a reduction in the number of observations. NOAA GOES-9 platform was brought out of stasis and repositioned over 155 E to operate as a replacement for GMS-5, until MTSAT-1R was operational (2005).

Table A2.1. Overview of meteorological geostationary missions considered.

Mission	Launch Date yyyy-mm-dd	Decommission Date yyyy-mm-dd	Central Longitude	Operator
GMS-1	1977-07-14	1989-06-30	140.0	JMA
GMS-2	1981-08-11	1987-11-20	140.0	JMA
GMS-3	1984-08-03	1995-06-22	140.0	JMA
GMS-4	1989-09-06	2000-02-24	140.0	JMA
GMS-5	1995-03-18	2005-07-21	140.0	JMA
FY-2A	1997-06-10	1998-04-08	105.0	CMA
FY-2B	2000-06-25	2006-02-01	105.0	CMA
GOES-9*	2003-05-22	2006-07-24	155.0	NOAA
FY-2C	2004-10-19	2009-11-23	123.5	CMA
MTSAT-1R	2005-02-26	2015-12-04	140.0	JMA
MTSAT-2	2006-02-18	-	145.0	JMA
FY-2D	2006-12-08	2015-07-15	123.5	CMA
FY-2E	2008-12-23	-	86.5	CMA
FY-2F	2012-01-13	-	112.5	CMA
FY-2G	2014-12-31	-	105.0	CMA

*GOES-9 was launched 1995-05-23, positioned over 135 W, but began operations at 155E on 2003-05-22

Each of the missions in Table A2.1 carried a meteorological imager as detailed in Table A2.2. Each imager has a visible channel centred in the range 0.62-0.73 um, hereafter referred to as the VIS channel. The spatial resolution of the VIS channel across the missions ranged between 1000-1250 m.

Table A2.2 also shows that there was variation in the available infrared channels: VISSR-1 to -4 each had one infrared channel, VISSR-5 had 3 infrared channels, while the GOES-9 IMAGER, JAMI and MTSAT-2 IMAGER each had four infrared channels. All missions had an infrared channel centred in the 10.7-11.5 um range, hereafter referred to as the IR11 channel. The IR11 channel of the VISSR instruments had a spatial resolution of 5000 m at the sub-satellite point, while the GOES-9 IMAGER, JAMI and MTSAT-2 IMAGER were finer (4000 m).

---

[1] JMA in coordination with Japan Aerospace Exploration Agency and Japanese Civil Aviation Bureau
[2] CMA in coordination with National Remote Sensing Center of China

The spectral response function for VIS and IR channels differ significantly across sensors. This can result in sensor dependant performance of the objective techniques, including navigation correction algorithms.

Table A2.2. Details of imaging instruments carried by missions in Table A2.1.

Imager	Visible Channels		Infrared Channels	
	Central Wavelength (µm) [and Channel Number]	Resolution[1] (m)	Central Wavelength (µm) [and Channel Number]	Resolution[1] (m)
VISSR-1	0.62 [1]	1250	11.4 [2]	5000
VISSR-2	0.62 [1]	1250	11.0 [2]	5000
VISSR-3	0.64 [1]	1250	11.5 [2]	5000
VISSR-4	0.63 [1]	1250	10.9 [2]	5000
VISSR-5	0.73 [1]	1250	10.8 [2], 11.5 [3], 6.9 [4]	5000
IMAGER	0.64 [1]	1000	10.7 [2], 12.0 [3], 6.8 [4], 3.9 [5]	4000[2]
JAMI	0.72 [1]	1000	10.8 [2], 12.0 [3], 6.75 [4], 3.78 [5]	4000
IMAGER	0.68 [1]	1000	10.8 [2], 12.0 [3], 6.75 [4], 3.75 [5]	4000

[1]Approximate spatial resolution at the sub-satellite point. [2]There seems to be some uncertainty around the resolution of these bands (Band 3 == 5000 m, Band 4 == 8000).

There has been a significant improvement in computational capability over the period of these satellite missions. From 1977-1989 the Australian Bureau of Meteorology stored GMS imagery as High Resolution Facsimile (HR-FAX) images. In 2005, the HR-FAX images were scanned and stored as digital TIFF images. The resulting images include annotations (overlayed coastlines and navigation marks) and artefacts, and provide little/no calibration information.

From 1989-2000, the Bureau used McIDAS AREA format to store digital copies of the GMS data. For the period May 1999 through to May 2003 GMS-5 data was stored in both S-VISSR and AREA format. The Bureau also used the McIDAS AREA format to store the GOES-9 data (2003-05). It should be noted that the GOES-9 GVAR broadcast was received by NOAA at Fairbanks, Alaska, and that this GVAR data was processed (brightness-enhanced, de-striped and stretched) and reformatted into S-VISSR format, before being rebroadcast.

In 2010, JMA provided the Bureau with a digital version of the infrared observations for the period March 1981 through to 23 January 1989 (~31,000 observations), substantially improving the GMS infrared data record.

Table A2.3 provides details of the Bureau's data holdings. Combining the period of observation and the expected number of full disk images per day the total number of expected observations for the period of interest can be calculated. The result is that there are over 260,000 observations of the target region from March 1981 through to 6 June 2015. Approximately 155,000 of these observations are made by the GMS series, GOES-9 made ~18,000 observations, while the MTSAT series made ~85,000.

Table A2.3. Details of geostationary missions considered.

Data Start yyyy-mm-dd	Data End yyyy-mm-dd	Mission	Central Long.	Instrument	Images per Day[1]	IR Format[2]	VIS Format[2]
1977-09-08	1979-11-30	GMS-1	140	VISSR-1	8	-	-
1979-12-01	1981-02-28	GMS-1	140	VISSR-1	8	TIFF	TIFF

1981-03-01	1981-12-20	GMS-1	140	VISSR-1	8	VISSR[3]	TIFF
1981-12-21	1984-01-20	GMS-2	140	VISSR-2	8	VISSR[3]	TIFF
1984-01-21	1984-06-29	GMS-1	140	VISSR-1	8	VISSR[3]	TIFF
1984-06-30	1984-09-26	GMS-2	140	VISSR-2	4	VISSR[3]	TIFF
1984-09-27	1987-03-26	GMS-3	140	VISSR-3	8	VISSR[3]	TIFF
1987-03-27	1989-01-23	GMS-3	140	VISSR-3	21	VISSR[3]	TIFF
1989-01-24	1989-12-03	GMS-3	140	VISSR-3	21	AREA	AREA
1989-12-04	1995-06-12	GMS-4	140	VISSR-4	24	AREA	AREA
1995-06-13[5]	1999-04-30	GMS-5	140	VISSR-5	24	AREA	AREA
1998-03-09	2001-07-19	FY-2A	105	S-VISSR	24	S-VISSR	S-VISSR
1999-05-01[5]	2003-05-21	GMS-5	140	VISSR-5	16	AREA[4]	AREA4
2000-10-15	2005-01-09	FY-2B	105	S-VISSR	24	S-VISSR	S-VISSR
2003-05-21	2005-06-27	GOES-9[6]	155	IMAGER	24	AREA	AREA
2005-01-09	2009-12-01	FY-2C	123.5	S-VISSR	24	S-VISSR	S-VISSR
2005-06-28	2010-06-30	MTSAT-1R	140	JAMI	24	HRIT	HRIT
2007-06-27	2015-09-05	FY-2D	123.5	S-VISSR	24	S-VISSR	S-VISSR
2009-11-25	-	FY-2E	86.5	S-VISSR	24	S-VISSR	S-VISSR
2010-07-01	2016-03-21	MTSAT-2	145	IMAGER	24	HRIT	HRIT
2011	-	FY-2F	112.5	S-VISSR	24	-	-
2015-09-05	-	FY-2G	105	S-VISSR	24	S-VISSR	S-VISSR

[1]Approximate observation schedule.

[2]Some gaps in data holdings exist due to errors in archiving.

[3]VISSR and McIDAS AREA.

[4]S-VISSR and McIDAS AREA.

[5]GMS-5 had degraded imaging capability from 2001.

[6]GOES-9 was re-positioned to 155.0 E in 2002.

The quality of imagery can be adversely affected by a number of issues including, but not limited to, sensor anomalies, sensor design (e.g. stray light effects), and data encoding and transmission. These issues manifest themselves in imagery as missing or erroneous data.

Navigation correction

A key element of the satellite QC process was to correct for navigation issues. Satellite data contains navigation information to enable the calculation of the latitude and longitude of each on-Earth observation (i.e. geo-location). Different missions provide this information in different forms. Unfortunately, these geo-location methods do not fully account for the slight variations in platform position and, consequently, sensor pointing geometry. As such, there can be errors in the geo-location of observations on the order of tens or hundreds of kilometres. Errors are expected to be greater for earlier missions.

It is assumed that once the standard navigation technique is applied, the geo-location errors are under < 250 km in magnitude. However, this assumption may not hold for platforms with large errors in orbital parameters (e.g. FY-2C) or erroneous scanner characteristics (e.g. spin rate). Additional optimisation may be required to overcome these issues.

The quality of the image geo-location can be assessed by matching coastline features observed within the imagery and the known location of these features. The distance between the observed and ideal location provides the measure of accuracy.

The uncertainty in the navigation/geo-location of well navigated observations is roughly half the spatial resolution in N-S and E-W directions. VISSR IR observations have a spatial resolution (at the sub-satellite point) of approximately 5x5 km. Thus, the uncertainty for VISSR IR imagery is on the order of +/- 2.5 km in the N-S and E-W direction (magnitude of +/- 3.5 km).

The navigation uncertainty requirement of the TC project is on the order of 10 km. Thus, if a VISSR IR is well-navigated, it will meet the uncertainty requirement.

A variation of the coastline-matching technique can be used to automatically correct image navigation (Takagi, 2003). Essentially, imagery is searched for known coastline features (high temperature and reflectance gradient across the land/sea boundary). Once found, the distance between the observed feature and it's known location can be calculated. Given a set of N coastline feature matches (where N > 5 and ~evenly distributed across the image), each with error V, coefficients of an affine transform can be developed to minimise the sum of $|V|$.

The detection of coastline features is hampered by the presence of cloud and poor image quality (i.e. missing lines). The use of reflectance channels is limited to day-time only, while infrared channels can be used at any time. However, at certain times of the day/night the temperature gradient across the land/sea boundary can tend to zero, limiting the applicability of the method.

With these limitations in mind, multiple regions within the image are searched for coastline feature matches. The size of the feature being searched for determines the size of the area to be searched. As these windows get larger, it is more likely for cloud to obscure the feature. As the windows get smaller, the chance for erroneous matches increases, along with computational intensity. Thus, the parameters must be optimised to balance performance and accuracy. Additionally, coastline feature matches must be filtered for spatial consistency.

Another measure of geo-location accuracy is the correlation between one image and the next and/or previous image(s). If the first image is well geo-located, and the correlation with the subsequent image is high, then the second image may, to first order, be considered to have similar uncertainty in geo-location. Such a test can be used to identify image pairs with low correlation, which may indicate a failure of the automated navigation correct and require additional analysis.

Appendix 3. Description of the Best Track

A3.1 How the BT intensity is determined

The intensity of a TC is subjectively estimated using a number of inputs depending upon the situation and availability of information as summarised in Fig. A3.1 and described here:
 http://www.bom.gov.au/cyclone/faq/tc-intensity-faq.shtml

Dvorak Technique: The Dvorak Technique has been the primary method to determine cyclone intensity around the world since the 1970s. The technique is based on analysing cloud patterns in the visible and infra-red (IR) that vary as the cyclone changes intensity. These patterns are then matched to the wind speed. The accuracy varies depending on the pattern type but overall is usually accurate to within 25 kilometres per hour (13 kn). The Dvorak technique has been applied throughout the 1981–2016 period.

Surface Observations: Wind speeds measured by anemometers at observing sites provide reliable records for the site. However, it is unlikely that a single observing site would sample the maximum winds of a cyclone even if the cyclone passes nearby. So while valuable anemometer records need to be used in conjunction with other inputs. In the Australian region it is a rare occurrence for an observing site to reliably measure the intensity of a TC.

Scatterometry: Scatterometers such as the Advanced Scatterometer (ASCAT) and QuickSCAT (QSCAT) measure the roughness of the ocean surface to estimate wind speeds. These are very useful to estimate wind speeds over broad areas to about 50 kn but have trouble resolving higher winds and winds under very heavy rain.

Objective techniques: SATCON is a consensus of several techniques including ADT.
http://tropic.ssec.wisc.edu/real-time/satcon/

Microwave: Microwave imagery shows additional information compared to the standard visible and infrared satellite channels. In particular, microwave imagery has the advantage that it can 'see through' the high cloud that typically obscures the area near the cyclone centre. They can also detect temperatures near the eye region, which are used to infer the intensity of a cyclone.

Numerical Weather Prediction (NWP): surface wind analyses near the centre from computer model output are now being used to assist with maximum wind estimation. For example, surface winds analyses can identify the region of maximum winds to assist in interpreting surface observations and scatterometry.

 The availability of these inputs varies from one point in time to the next. This occurs both within a TC's lifetime and throughout the historical archive. For example, ASCAT scatterometry is available at up to two time periods per day and may miss the circulation resulting in long gaps between useful passes. ASCAT has only been used operationally since November 2007 while QSCAT was used prior to this from 2000. The availability of microwave imagery is discussed in more detail in Section 4.3.2.

Changes in the application of these methods are discussed in the following section.
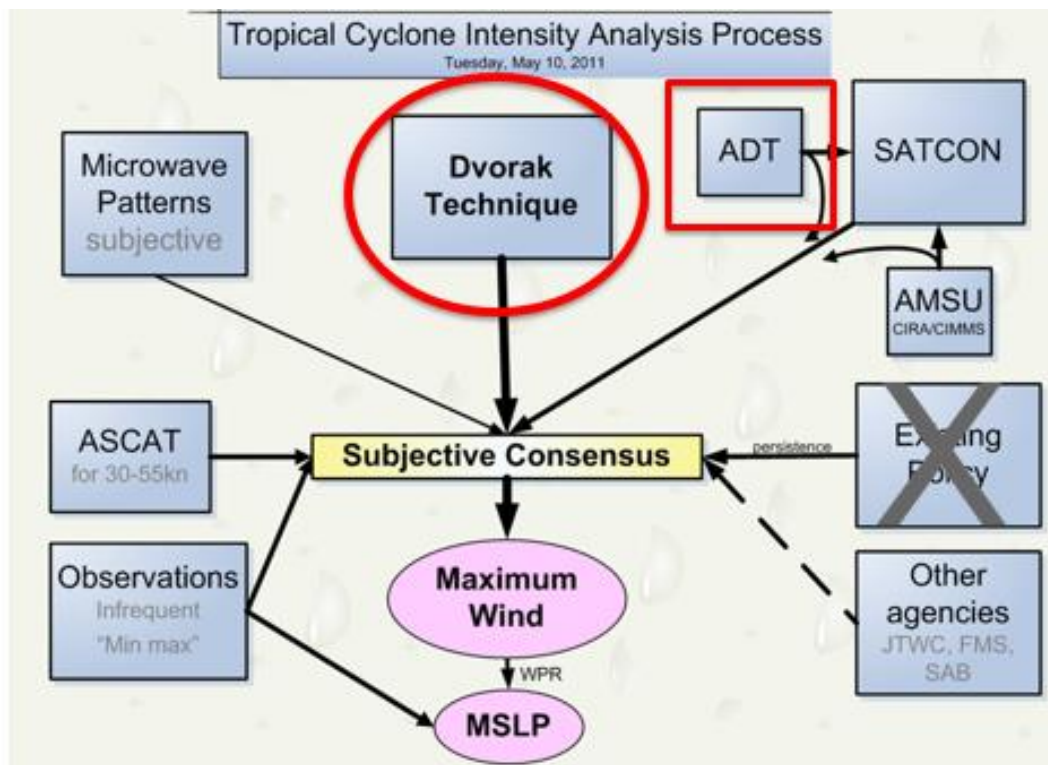
Figure A3.1. Summary of the inputs into determining the intensity of a TC.

A3.2 The level of homogeneity of V_m BT

Variations in the homogeneity of V_m in the BT database occur because of several factors (e.g. Landsea et al. 2006 and Kossin et al. 2013) described below and summarised in Table A3.1.

1. Changing observing capability

Since the advent of satellite imagery in the 1960s through to 1978 forecasters only had access to a few polar orbiting satellites that provided as few as two satellite passes per day. Given that TCs can change intensity rapidly, it is unrealistic to expect that the true peak intensity was able to be detected in this era. Hence, TC intensity estimates for this period are not considered sufficiently reliable to be used for design or trends. Geostationary satellites, initially the GMS series (1978-2005), then MTSAT (2005-2015) then Himawari-8 (2015 to present) provided more frequent coverage allowing for intensity changes to be more accurately detected. From 1978 to 1988 imagery was available every three hours, and then every hour from 1989 until more recently, increasing to every 10 min from Himawari-8. As noted in Velden et al. (2017) in the study of extreme TC intensities, corrections of about 3 kn were made especially for small eyes cases for the lower spatial and temporal resolution era in the 1970s and 80s.

Additional information is provided by passive and active (scatterometery) sensors on polar orbiting satellites. Surface observations have gradually increased over the decades, but these are primarily located over land. It is still a rarity for a TC to pass sufficiently close to an observing site to provide an accurate estimate of the intensity at that time. Indeed, several sites are required to accurately sample the maximum winds near the centre.

2. Changing techniques

The Dvorak technique was initially introduced to Australian Tropical Cyclone Warning Centre (TCWCs) in the early 1970s. The Enhanced IR technique commenced in about 1981 with TC *Brian* and has been applied with a fair degree of consistency to this day. Some of the changes in the application include: altering the weakening rule to use 6 hours not 12 hours as the period to hold the CI before weakening, after the work of Brown and Franklin (2004). This happened in about 2003-2004. This has a net result of lowering the intensity during weakening phase. Dvorak 1995 introduced a more flexible interpretation of the application of the shear technique to allow greater discretion in determining whether the DT should be 2.5, 3.0 or 3.5. This change is not likely to cause a net change in the bias of the intensity. In the 1980s and 90s analysts were more likely to use the embedded centre pattern to arrive at an intensity of 80 kn. Since the early 2000s Dvorak analysts use more discretion and often discount DT estimates using the embedded centre pattern especially for the early stages of development. In the last decade the addition of objective techniques such as ADT and SATCON has an influence, albeit often only as an adjustment to preliminary estimates following the subjective Dvorak technique and analyses of scatterometry, microwave and other observations.

3. TCWCs and forecaster subjectivity

Because of the subjective nature of the analysis there are variations from one analyst to the next. This is perhaps magnified between offices Brisbane, Perth, Darwin but since the early 2000s there has been greater uniformity between these offices and a review process.

Even today there are variations in the intensity characteristics from one TC to the next. A TC that is over the open ocean will only have satellite and model inputs to intensity estimates but one that moves close to land is more likely to have observations and be scrutinised in more detail and at a three-hourly resolution rather than the standard six hours.

For the above reasons it is difficult to quantify the homogeneity of the database.

Additionally, a histogram of V_m BT in Fig. A3.2 shows a bias to use certain wind speeds over adjacent values. There are pronounced relative peaks at 30, 50 and 80 kn and even 90, 100 and 110 kn. There is no physical reason why there should more intensities at 80 kn rather than 75 or 85 kn other than the gradual decrease with higher intensities. The main reason for these is the Dvorak CI to V_m scale. A CI of 3.0 matches to 35-45 kn, 3.5 to 50 kn, 4.0 to 55-60 kn, 4.5 to 65-75 kn; 5.0 to 80-85 kn etc. There are more 50 kn values because there is a single match with 3.5. For CI matching multiple wind speeds, the analyst has discretion but CI values of 3.0, 4.5, 5.0, 5.5, 6.0 and 6.5 directly match 40 kn, 70 kn, 80 kn, 90 kn, 100 kn and 110 kn respectively. Hence there are more values at 70 kn than 65 or 75 kn and more at 80 kn than 85 kn etc. A clustering by 10 kn intervals (not shown) shows a more even distribution.

Table A3.1. Summary of potential influences on creating inhomogeneities in the BT 1981–2016.

Change in Best Track process or input information	Potential impact on bias in intensity
Increase in temporal IR/Vis satellite imagery resolution from 3 hourly (1981–1988) to hourly and then 10min (Himawari-8 post 2015).	Slight decrease in intensity for 1981–1988. Otherwise little change.
Increase in spatial resolution in IR/Vis satellite imagery.	Slight decrease in intensity for 1981–1988 especially for small eye patterns. Otherwise little change.
Variation from one analyst to the next	Nil. While there are variations, there is likely no systematic bias.
Greater discrimination of embedded centre pattern since early 2000s.	Likely slight high bias in the range 70-85 kn prior to 2004.
Application of Dvorak 6 h weakening rule	Likely slight high bias during weakening prior to ~2004.
Availability of scatterometry (QSCAT post 2000; and ASCAT post Nov 2007).	Slight high bias in the 35-50 kn range. For example, more likely to have 35-45 kn when CI is 2.5.
Introduction of microwave imagery ~2001.	Microwave allows for greater discrimination of cloud patterns. This doesn't automatically mean a bias towards higher or lower intensities.
Increased surface observation network and radar coverage.	The presence of observations likely has a positive bias on the intensity – more likely to increase the intensity than not. Although there are more surface observations in the current AWS network, the number of instances when observations have a direct role in changing the estimated intensity is too low to significantly influence the overall bias.
Development of objective guidance ADT/SATCON.	Not likely to change the bias.
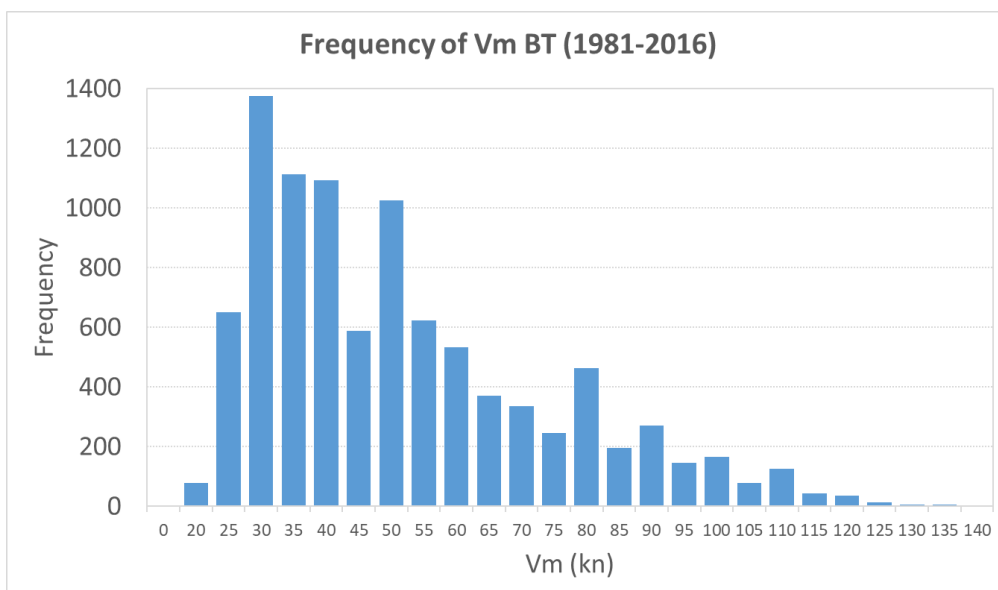
Figure A3.2. Frequency of V_m BT estimates, 1981–2016.

A3.3 Best track wind radii

The BT contains wind radii for gale (R34), storm-force (R48) and hurricane-force (R64) winds as a mean and for northeast (NE), southeast (SE), southwest (SW) and northwest (NW) quadrants. It also has values for RMW. Other size metrics include the ROCI and the radius of the eye. The above parameters have varying degrees of completeness. Until the early 2000s the WMO standard was to record radii for two wind speed thresholds that could be nominated by each fix. Values were R48 were not typically included and quadrant values were also not included.

Beginning with April 2003 (Inigo) the Bureau adopted the new standard to routinely include R34, R48 and R64 and their values by quadrants, with a few exceptions that retained only single (symmetric) estimates (*Erica* 2003, *Fritz* 2004, *Grace* 2004, *Harvey* 2005, *Kerry* 2005, *Ingrid* 2005 (partial), and *Jim* 2006).

The first values of R34 in the BT occurred in the 1984/85 season in the western region and initially on an opportunity basis when a surface observation was available, but then more regularly from about 1988, although there were still incomplete records (e.g. *Ned* 1989, *Alex* 1990, *Errol* 1991).

Estimates of gale radii were heavily biased towards available surface observations including ship observations. Ship observations are known to have a high bias (Taylor et al. 1994) and while the analyst may have used some discretion in interpreting 35-40 kn ship observations, in the absence of any other information this was used to estimate the gale extent. Many of these peripheral observations of gales may be attributed to the prevailing synoptic flow be it monsoonal northwesterly flow to the north of the centre, or southeasterly flow to the south especially in the Coral Sea.

In the absence of observations, estimates were based on the cloud patterns and in particular, the area of cold cloud on IR imagery but the practice may have varied significantly amongst analysts.

The arrival of microwave and scatterometry in the early 2000s heralded a major improvement in the quality of wind radii estimates in the BT. QSCAT along with microwave imagery was incorporated into the BT process in 2001 while ASCAT commenced in November 2007 with TC *Lee*.

A comparison of the two eras shows a reduction in R34 estimates from 173 km (pre-2001) to ~140 km when scatterometry and microwave was available. The decrease agrees with anecdotal evidence from analysts who conducted best tracking in both eras. The recent average is consistent with the study using QSCAT imagery from 1999 to 2009 (Chan and Chan 2015, and pers. comm. 2018) who found the average gale radius in the Australian region was 145 km.

The refinement of gale radii estimates is demonstrated in the time series of BT gale radii (NE quadrant) in Fig. A3.3. There is a downward trend in the 1981–2016 period in Fig A3.3 a. By contrast the record since 2001 shown in Fig. A3.3 b has little or no trend.

This is partly a consequence of being able to discriminate the cyclonic flow region from the prevailing synoptic flow. Prior to scatterometry there are quite a few cases where the gale radius extends beyond 500 km such as *Justin* (1997), *Drena* (1997), *Roger* (1993), *Betsy* (1992) in the Coral Sea and *Billy-Lila* (1986 in the central Indian Ocean), *Damien* (1997 off NW Australia) and *Bessi*

(1990). For these cases the difference between the model-based Lok radii and BT averaged 400 km. Indeed, while the highest values are likely to be based on surface wind observations: 900 km (*Billy-Lila*); 739 km (*Justin*); 700 km (*Damien*); 650 km (*Roger*) they are also likely to be significantly overestimated because of the prevailing synoptic flow. TC *Justin* was described as a large TC that increased in size in part because of a surge in the monsoon that caused damage over PNG well to the north of the centre. The BT gale radius peaked at 739 km at 06 UTC 10 March 1997 based on surface observations that indicated 'gales extended from Cape Moreton (just NE of Brisbane) north to PNG waters' (http://www.bom.gov.au/cyclone/history/pdf/justin.pdf).
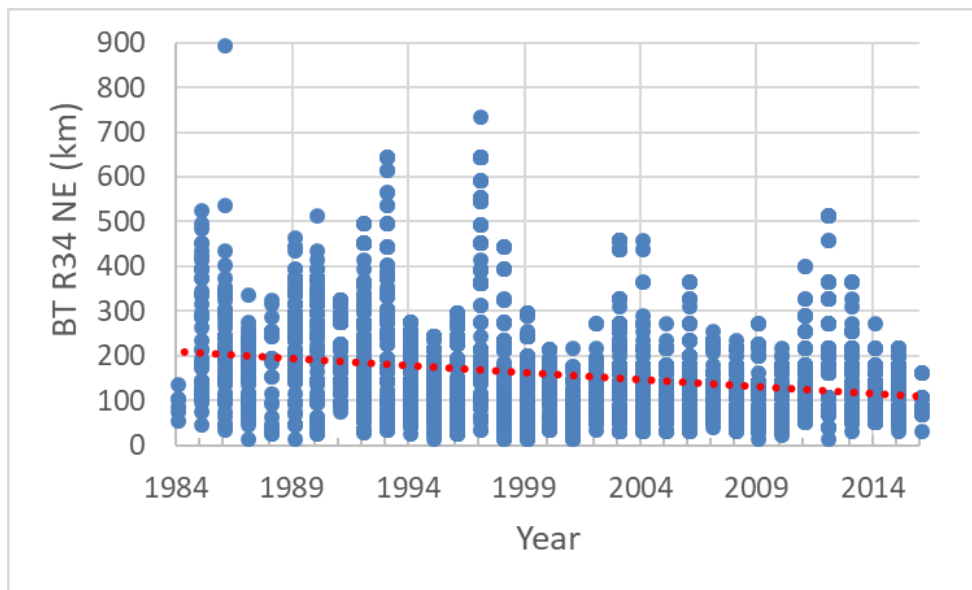
Figure A3.3 a. Time series of BT R34 NE quadrant, 1981–2016 showing a downward trend. High values above 300 km often indicate the influence of the surrounding environment. There are more of these earlier in the record, before scatterometry provided a higher degree of accuracy. Other quadrants show similar results.
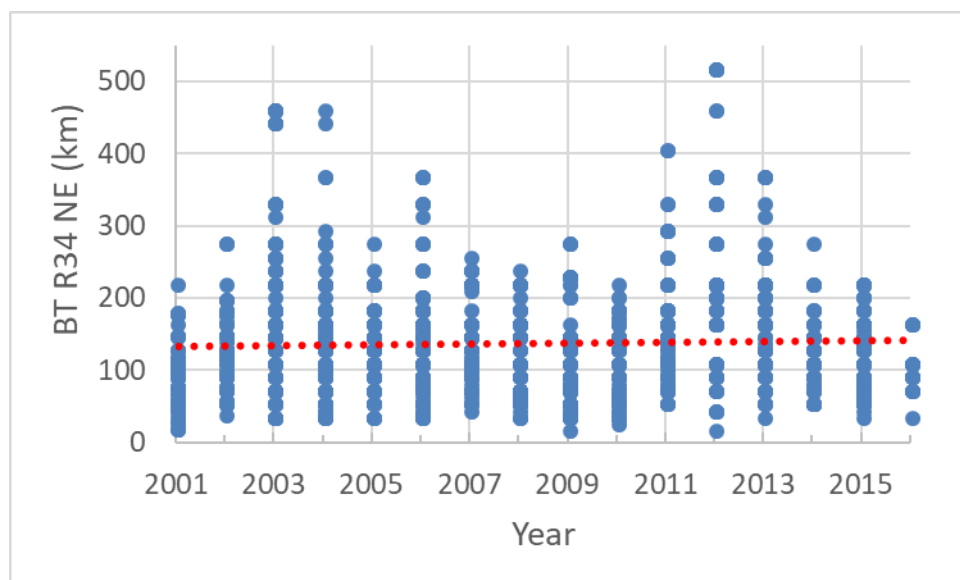
Figure A3.3 b. Time series of BT R34 NE quadrant, 2001–2016 showing little or no trend. Cases such as Lua (max. 519 km in 2012) are outliers. Other quadrants show similar results.

Contrast that with *Ului* (Fig. A3.4) when ASCAT on 18 March 2010 showed gales extending more than 800 km in southern quadrants owing to a strong ridge in the Tasman Sea. The BT estimates during this time on the southwest quadrant reached 250-300 km.
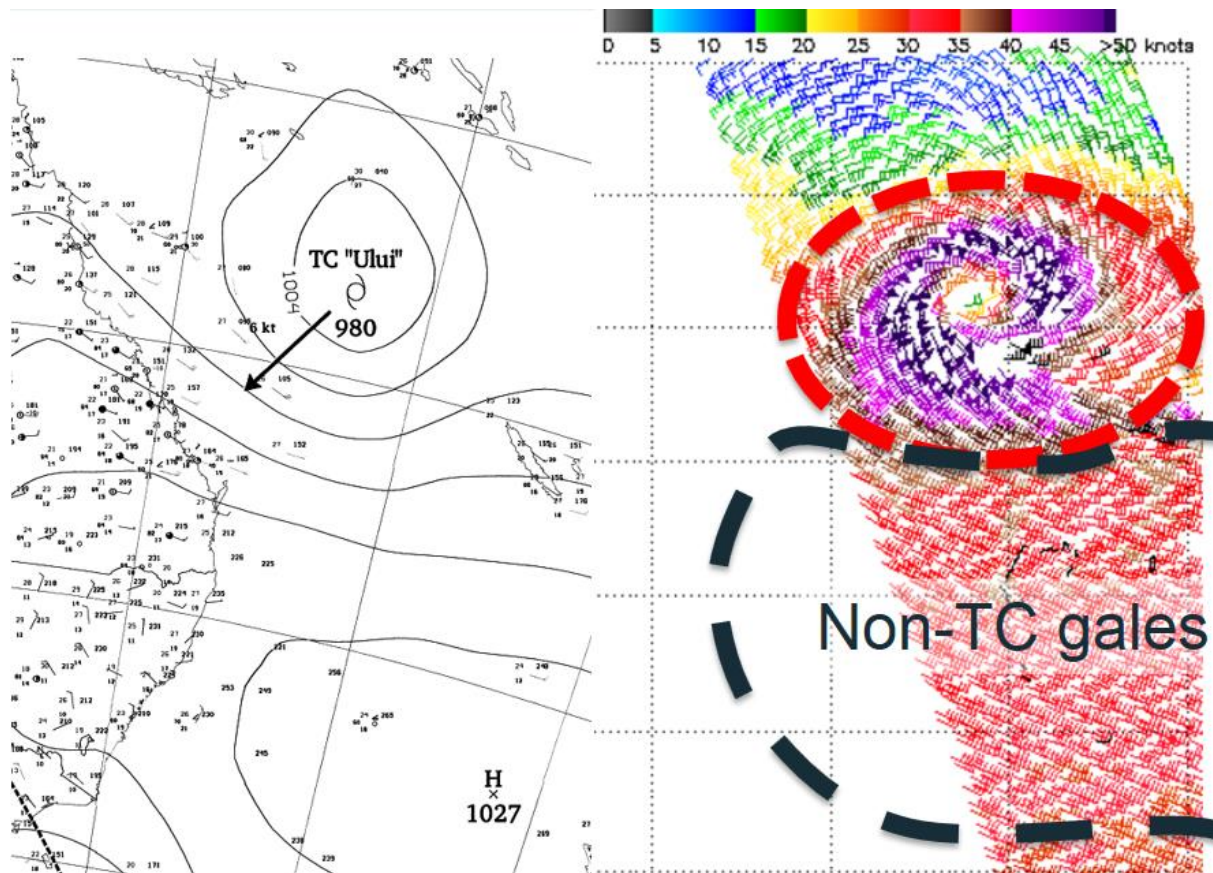
Figure A3.4. ASCAT image during Ului (1131 UTC 18 March 2010) and corresponding MSLP analysis. The BT approach is to separate the cyclonic flow from the synoptic flow in order to determine the R34.

However, even with scatterometry for synoptically enhanced gale scenarios it is often difficult to determine when the cyclonic flow ends and when the synoptic flow begins. When there is a degree of ambiguity, the BT estimates have likely to be conservatively on the large side to encroach into the synoptic flow.TC *Lua* (2012) was a case in the scatterometry era when BT R34 exceeded 500 km in the northeast quadrant as shown in the ASCAT image in Fig. A3.5.
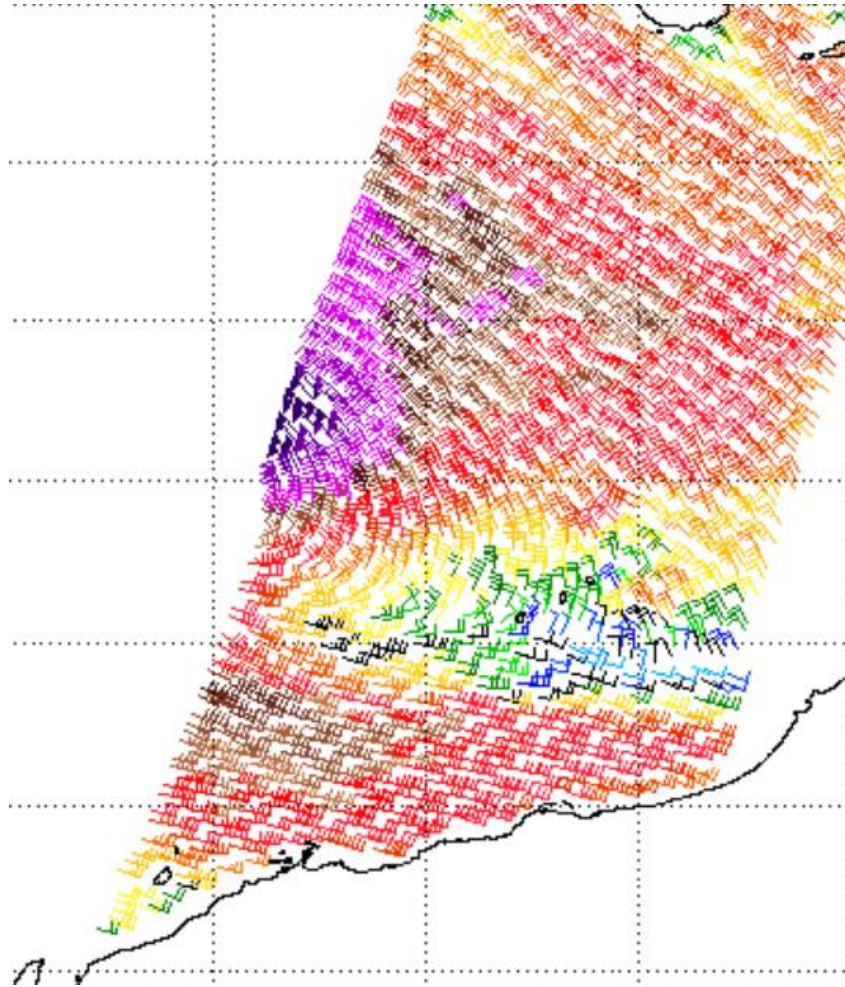
Figure A3.5. ASCAT image during Lua (01 UTC 16 March 2012) when the BT NE gale radius was estimated at 519 km (lat,long gridlines are spaced at 2 degrees).

Since about 2012, BT analysts have also incorporated objective guidance such as MTCSWA and high-resolution NWP.

As was the case for V_m (see Fig. 3), there is a bias to preferred values for BT wind radii as demonstrated in the histogram of BT R34 for the northeast quadrant in Fig. A3.6. The preferred values correspond to 30 nm (50-60 nm), 40 nm (70-80 km), 50 nm (90-100 km), 60 nm (110-120 km), 90 nm (160-170 km) and 120 nm (220-230 km). For R48 and R64 the preferred values are to the nearest 10 nm.
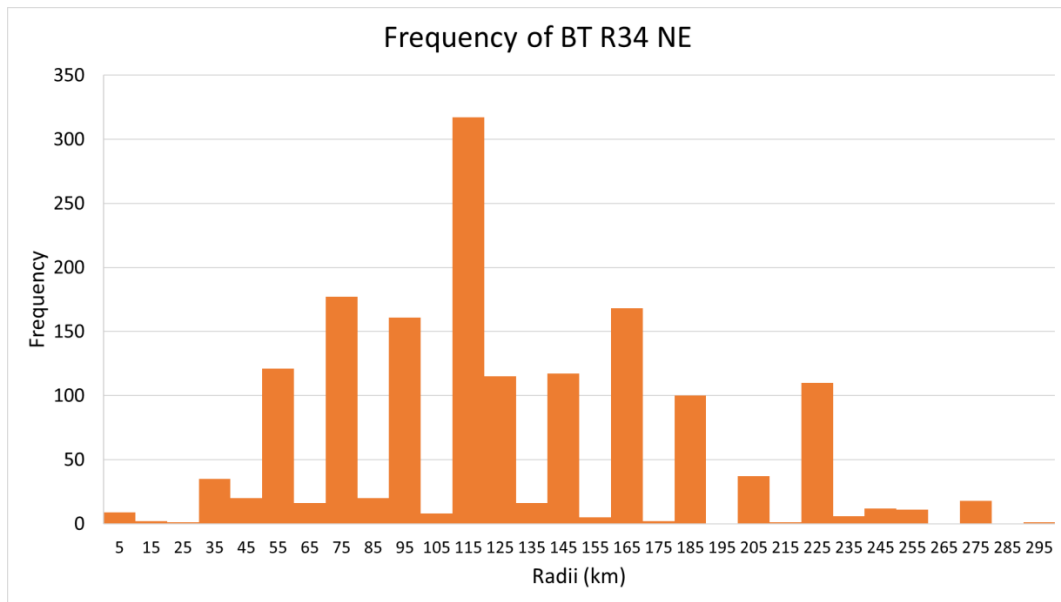
Figure A3.6 a. Histogram of BT R34 NE quadrant, 2003–2016. There is a pronounced peak at 110-120 km corresponding to 60 nm while the next most frequency radii correspond to 40 and 90 nm.

The distribution is similar by quadrant as shown in the box and whisker plot in Fig. A3.6 b (2001–2016) showing the 25-75 percentiles lie between 95 and 160 km. This also highlights the high outliers above 300 km.
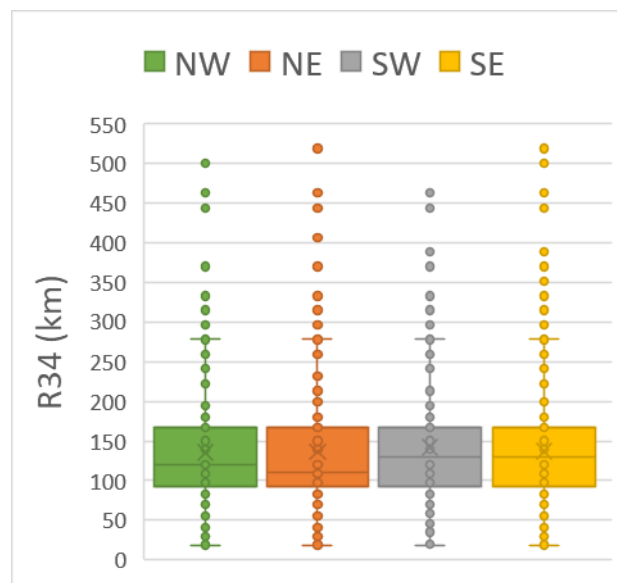
Figure A3.6 b. Frequency distribution ('Box and Whisker') plot of BT R34 by quadrant, 2001–2016.

ASCAT and microwave imagery can also influence estimates of R48. Microwave also has an influence on R64 values. In the absence of observations, R48 and R64 can default towards standard values such as R48 being approximately half trof R34 and R64 being half of R48. Indeed, for the 2003-2016 BT period the ratio of R48 to R34 is 0.48 to 0.49 and the ratio of R64 to R48 is 0.56-0.58.

A3.4 Best Track Radius of Maximum Winds (RMW)

Values of RMW exist in the BT on a consistent basis since about 2004. RMW values are estimated to the nearest 5 nm (9 km) and standard defaults are likely to be 10, 15, 20, 25, 30. The median and mean values are 38 km (20 nm) and 36 km (19 nm) respectively, and the considerable majority of RMW fall between 28 and 46 km (15-30 nm) as shown in Figs A3.7 a and b. Furthermore, half of all RMW estimates are either 15 or 20 nm for cases when V_m is at least 48 kn. There is greater spread in RMW for V_m in the range of 34-47 kn (category 1) and with increasing intensity the RMW is likely to decrease as shown in Fig. A3.7 c. The time series in Fig. A3.7 d shows little trend for the 2003–2016 period.

In the absence of direct observational (surface winds) evidence, the RMW is estimated by radar, microwave and scatterometry. The strongest winds occur in the eye wall which is best seen on either microwave (Fig. A3.7 e) or by radar (Fig. A3.7 f). The RMW appears in the eye wall on 37 GHz microwave whereas at 85-91 GHz frequencies the eye is resolved well above the surface where it is wider and hence the RMW will appear to be just inside the eye.

In the case of eyewall replacement cycles (ERC), the RMW will change abruptly when the V_m changes from the inner eye to the outer eye. Although not analysed in any detail, RMW BT for ERC cases since 2003 are likely to vary according to the interpretation by the analyst.

High values were investigated and all cases above 170 km were amended down in the BT.
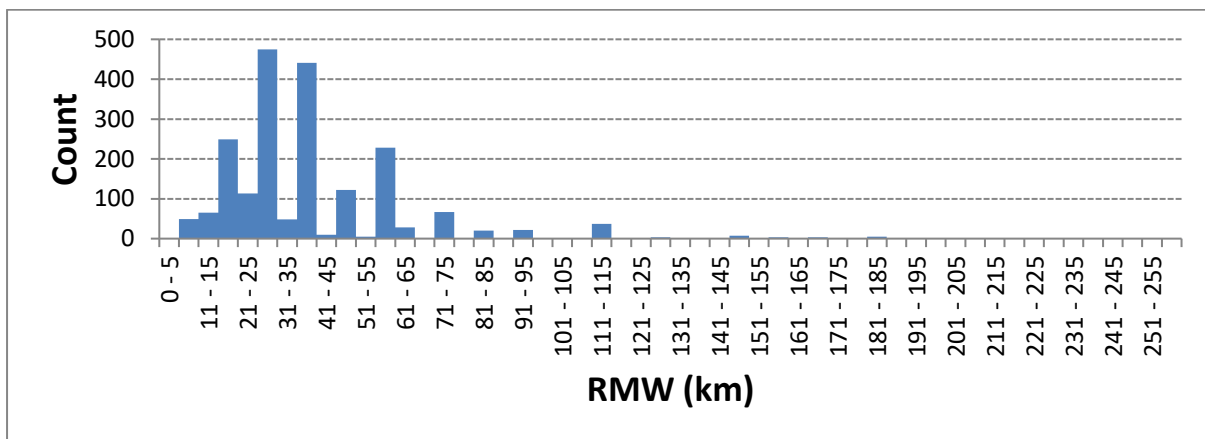
Figure A3.7 a. Histogram of RMW BT. There are pronounced peaks corresponding to 15 nm (26-30 km), 20 nm (36-40 km), 10 nm (16-20 km) and 30 nm (56-60 km).
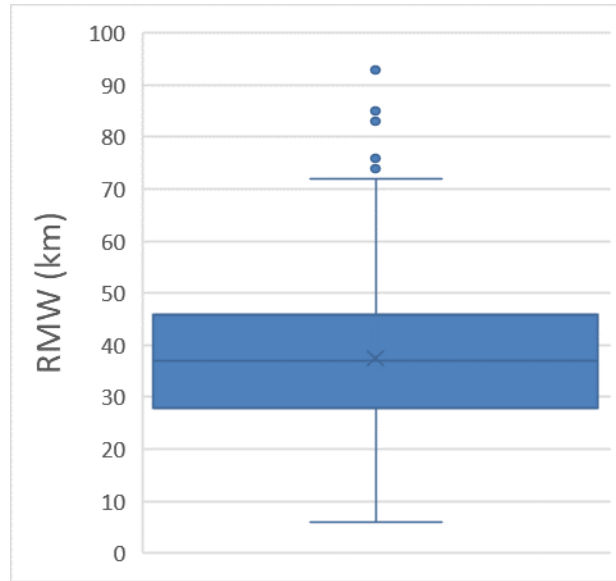
 Figure A3.7 b. Frequency distribution ('Box and Whisker') plot of RMW BT. Some high outliers have been excluded.
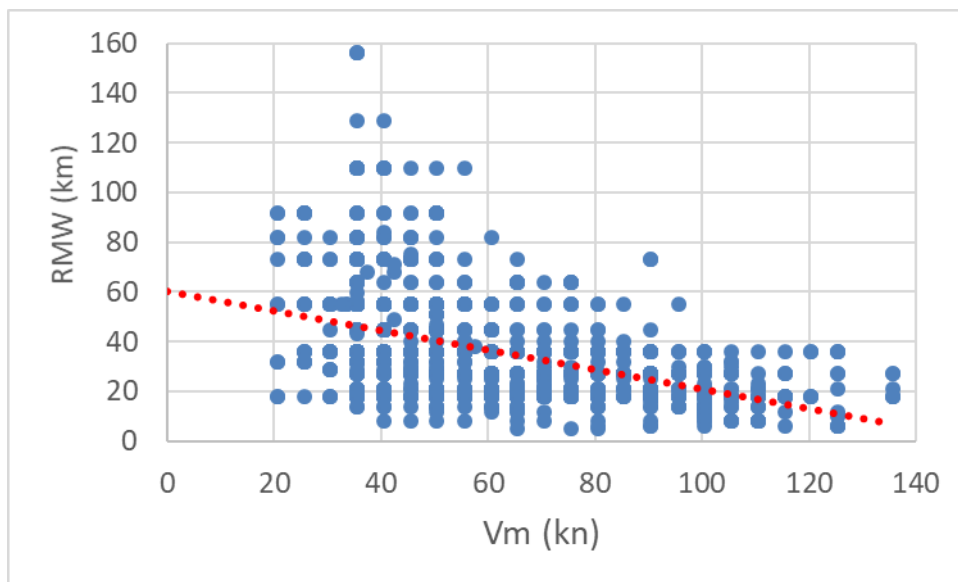

Figure A3.7 c. RMW BT by intensity (V_m).
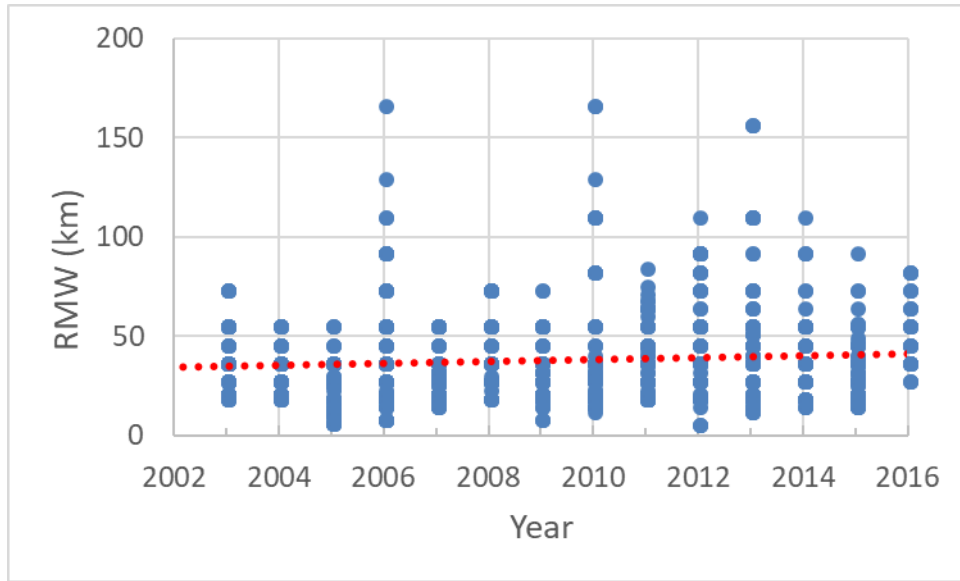
Figure A3.7 d. RMW BT by year (2002–2016). There is little trend.
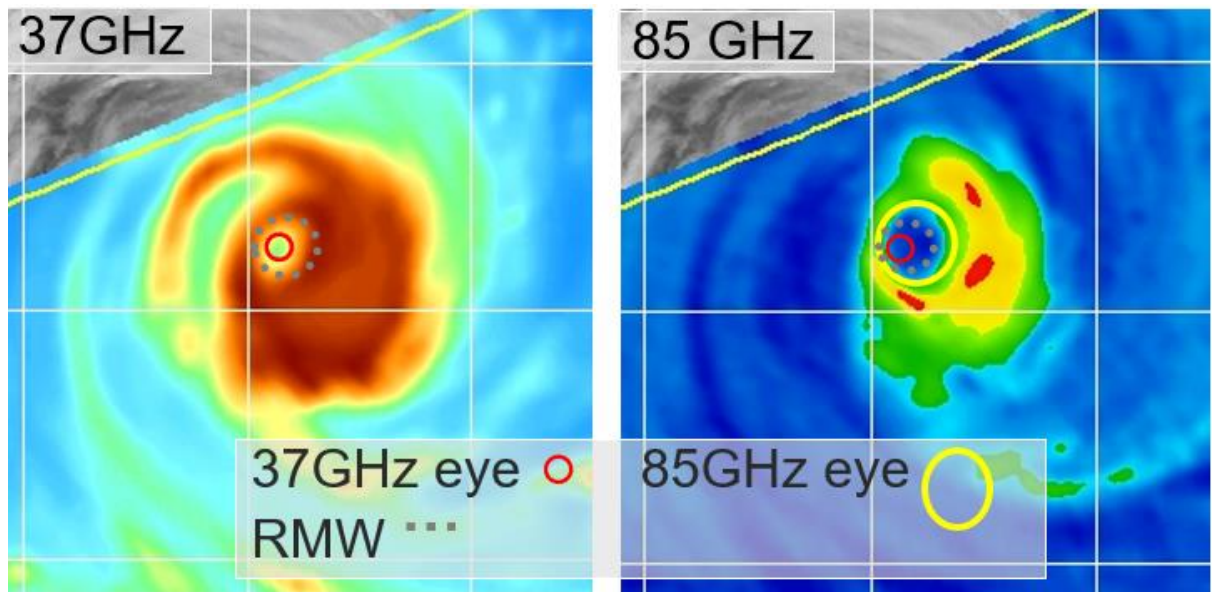
Figure A3.7 e. Schematic of estimation of RMW using microwave imagery (TC *Jasmine*, 2012). The RMW lies between the 37 and 85GHz eye. Note: the eye is offset because of parallax.

Figure A3.7 f. Schematic of estimation of RMW (red dashed circle) using radar (TC Yasi, 2011). The RMW relationship with the maximum reflectivity in the eyewall will vary with distance from the radar requiring some subjective interpretation.

A3.5 Best track ROCI, POCI and Environmental Pressure (P$_e$)

The BT contains the fields ROCI and Pe. Historically the process to estimate ROCI and POCI subjectively has been to identify the last outer isobar to enclose the TC on MSLP analyses. The current approach is to ensure the outer isobar matches the extent of the surface wind circulation and the distance measured to the centre being the ROCI. Fig. A3.8 shows this process for TC Billy (2008). The BT approach for P$_e$ is to add 2 hPa to POCI estimates.

A3.6 Best Track eye size

The BT 'eye radius' (km) is the average distance from the centre to the inner edge of the surface eye wall. The first record in the BT occurs in December 1984 (TC *Frank*). Since the early 2000s microwave imagery has been used to estimate the eye size with the following suggested approach. *The eye radius should be estimated when the eye wall cloud is evident more than half the way around the centre, although discretion is used for transient partial eyes in microwave images. It is suggested to use the 37 GHz frequency rather than 85-91 GHz microwave to measure the eye diameter when available. Radar should also be used, although the distance from the radar should be considered as the radar beam increases in height with distance.*

Prior to the use of microwave imagery, the eye radius was estimated using IR and Vis imagery, and occasionally radar when available. Microwave eyes on 37 GHz will be smaller than 85-91GHz and can occur when not evident on IR/Vis imagery. Fig. A3.7 e is one example indicating the differences between the eye size on the 37 and 85 GHz imagery. The subjectivity also adds a factor to the inhomogeneity of the dataset.

Eye radii in the BT range from 2 to 74 km, but the majority lie between 10 and 20 km as shown in Fig. A3.8 a. This is slightly less than other regions, for example in the NATL which has a mean of 22 km (Kimball and Mulekar 2004) and in the NW Pacific where most are approximately 15-30 km (Knapp et al. 2018). About 90 per cent of TCs have an eye radius less than 40 km (22 nm) with only a very small percentage 50 km (27 nm) or greater. The time series of eye radius in Fig. A3.8 b shows little trend since 1984.

There is a dependency on the intensity, the stronger TCs having a smaller eye size on average as shown in Fig. A3.8 c. Typically eye size estimates occur for TCs of at least 65 kn when the eye may become evident on IR and/or visible imagery but as shown in Fig A3.8 c, there are many cases at lower intensities. These estimates are often based upon radar images, and possibly microwave images. Filtering the eye radius for cases when the intensity is at least 65 kn shows a smaller eye radius.
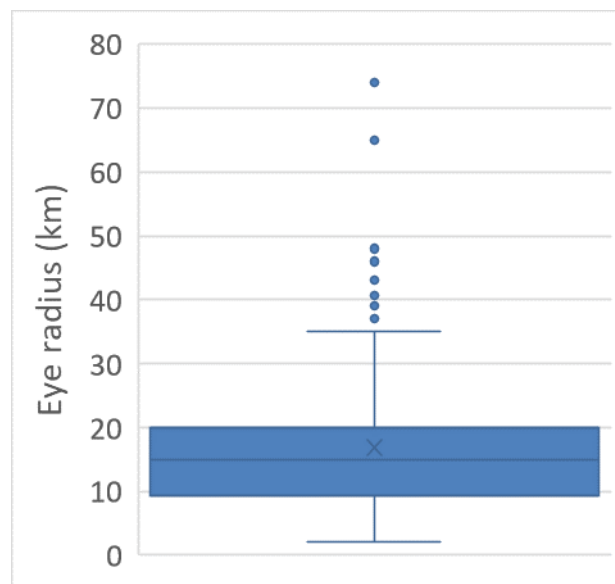

Figure A3.8 a. Frequency distribution ('Box and Whisker') plot of eye radius (1984–2016).
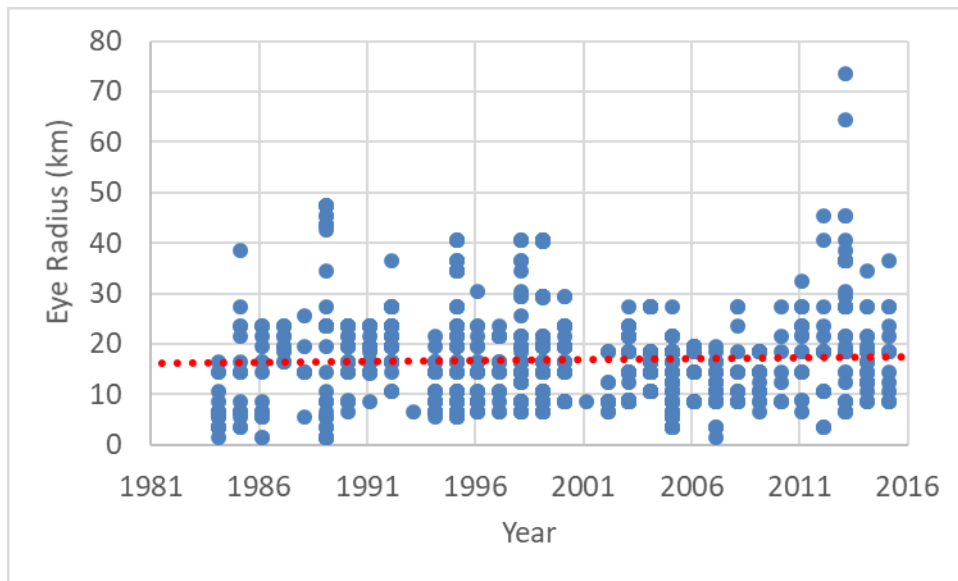
Figure A3.8 b. Time series of eye radius. There is little trend in the data.
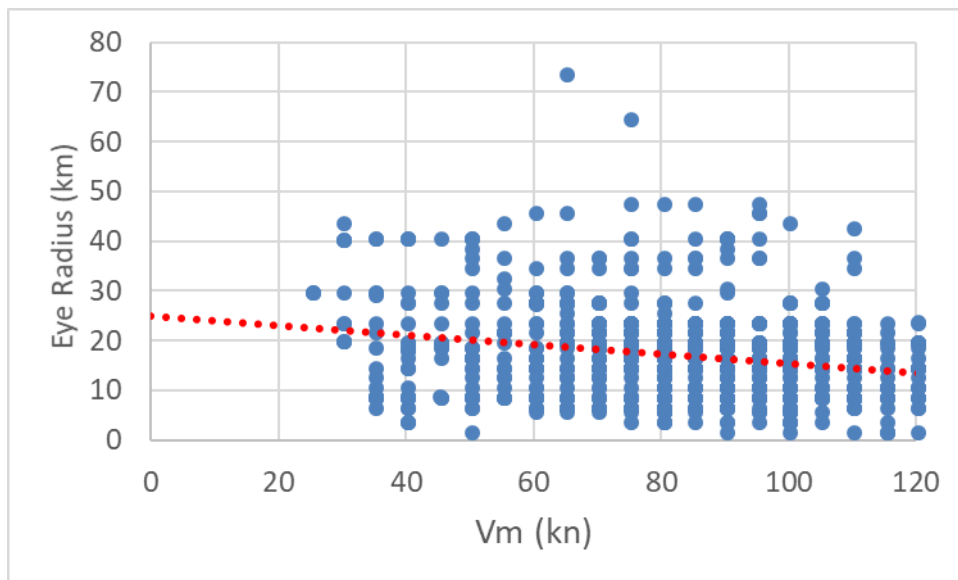
Figure A3.8 c. Eye radius by intensity (BT V_m). Stronger systems will have a smaller eye radius.

A3.7 Best Track Central Pressure

In the absence of direct measurement, which is rare, the estimation of CP is via a WPR. BT CP values are derived from a number of different WPRs resulting in an inhomogeneous record (Courtney and Knaff, 2009; Harper, 2002). The current operational WPR is the CKZ method (Knaff and Zehr 2007; Courtney and Knaff, 2009). This is an algorithm based upon the V_m, latitude, motion, R34 and the POCI or environmental pressure (Pe). The BT CP (hPa) is typically estimated by applying a WPR. Since 2007 the CKZ WPR has been adopted (Courtney and Knaff, 2009) which uses V_m (BT), POCI, R34, latitude and translation speed.